NGU REPORT 2015.018

Crustal structure of continental fragments

GEOLOGY FOR SOCIETY

SINCE 1858

GEOLOGICAL SURVEY OF NORWAY

- NGU -

GEOLOGICAL SURVEY OF NORWAY
- NGU -

REPORT

Geological Survey of Norway
P.O.Box 6315 Sluppen
NO-7491 TRONDHEIM
Tel.: 47 73 90 40 00

Report no.: 2015.018

ISSN: 0800-3416 (print)
ISSN: 2387-3515 (online)

Grading: Confidential until 16.03.2017

Title: Crustal structure of continental fragments

Authors: Joya Tetreault and Susanne J.H. Buiter

Client: Det norske oljeselskap ASA

County:

Commune:

Map-sheet name (M=1:250.000)

Map-sheet no. and -name (M=1:50.000)

Deposit name and grid-reference:

Number of pages: 88 **Price (NOK):** 400
Map enclosures:

Fieldwork carried out:

Date of report:
16 March 2015

Project no.:
347200

Person responsible:

Summary: Continental fragments and microcontinents are blocks of continental crust rifted off of passive margins. These relatively unthinned regions (compared to the surrounding crust) offer a perplexing conundrum as to their tectonic history: why are these blocks relatively undeformed compared to the surrounding regions on the passive margin? In this report we review the crustal structure as revealed from deep crustal seismic studies of modern continental fragments and microcontinents. From this review, it is clear that magmatic underplating or plume and LIP emplacement are not essential to isolating continental blocks during rifting. Many continental fragments have thick crusts (> 20 km) with thin layers of overlying sediments, while other continental fragments are severely thinned (~10 km thick) and exhibit horst and graben topography in the upper crust. The wide variability in crustal thickness and structure of continental fragments and microcontinents suggests that many different tectonic processes can explain these features. Initial widespread intra-continental rifting, active upwelling from back-arc spreading, plume-induced rift jumping, inherited weaknesses in ancient suture zones, and shifting extension directions can all contribute to localizing deformation in the surrounding basins, thus separating continental fragments from the mainland.

Keywords:	Microcontinents	Crust
Seismic refraction	Continental fragments	Passive margins

Contents

1 INTRODUCTION

Continental fragments and microcontinents are bathymetric highs of continental crust on the ocean floor, formed by rift processes. These features vary in thickness, length, and area. Microcontinents are special regions of isolated continental crust, often submerged below sealevel, and completely surrounded by oceanic crust. Much too small in area to be called continents, microcontinents typically are less than 100 km wide, such as Jan Mayen, the Seychelles, and Elan Bank. Continental fragments are similar isolated crustal features on the ocean floor, but are connected to the continental mainland by basins overlying thinned continental crust. Large continental fragments often have ribbon-like geometries, leading to the term "continental ribbon" used by *Peron-Pinvidic and Manatschal* (2010). Continental fragments are found all over the globe and are not confined to volcanic and non-volcanic margins only. Logically, questions arise about their formation and why they exist on some margins and not others.

Tectonically, we can divide continental fragments into two subgroups: those created by passive rifting tectonic processes and those created by active rifting processes. Passive rifting is when extension occurs due to farfield forces, whereas active rifting is driven by active mantle upwelling, such as in cases of plumes and back-arc rifting. Continental fragments have been hypothesized to form by 1) localization of extension in separate regions of a passive margin (*Peron-Pinvidic and Manatschal*, 2010) which could be regions of inherited heterogeneity, 2) back-arc extension above a retreating subduction zone (*Sdrolias et al.*, 2003; *Schellart et al.*, 2006), 3) misalignment of rift axes and their subsequent linkage (*Eagles et al.*, 2002), 4) multiphase rifting, or 5) a rift jump towards a region which has become warm and weak because of an impinging mantle plume (*Müller et al.*, 2001; *Gaina et al.*, 2009). There is so far no general consensus in scientific literature for a "recipe for microcontinent formation" (*Müller et al.*, 2001). Many scenarios crucially depend on stretching factors between the continental fragment and its surrounding basins, the relative timing of rifting in the surrounding basins, and indications for magmatic activity.

Much of our understanding of these submarine features is based on magnetic, gravity, and seismic reflection studies over continental fragments and their surrounding basins. These studies provide us with a wealth of insight on rifting evolution, stratigraphy, volcanic extrusions, and possible sub-basement structures. However, an understanding of the deep crustal structure, including crustal thickness, and the presence or absence of magmatic underplating, really requires wide-angle seismic refraction studies (*Prodehl and Mooney*, 2012; *Hackney et al.*, 2015). Ideally, combined gravity, P-wave, and S-wave studies can even constrain crustal lithologies (*Hackney et al.*, 2015).

In this review of the seismic crustal structure of continental fragments, we report the interpreted models of wide-angle seismic studies covering continental fragments, microcontinents, and the surrounding basins. We include the geological background of the continental fragments and related basins and seas, the tectonic history, and seismic velocities and thicknesses for all layers. In more recent studies, researchers have supplemented the velocity inversions with data from seismic reflection lines or even gravity models, thus constraining crust and sedimentary structures better. In this report, the reviewed studies run the gamut from ship-to-ship source-receiver studies in the 1970s to combined seismic method modelling of reflection and refraction waves. Yet all these studies provide constraints on continental fragments and their formation within our understanding of passive margins. Deep crustal seismic studies detail the crustal shape, thickness, seismic velocities, crustal layers, and anomalous features in the upper mantle and lower

crust.

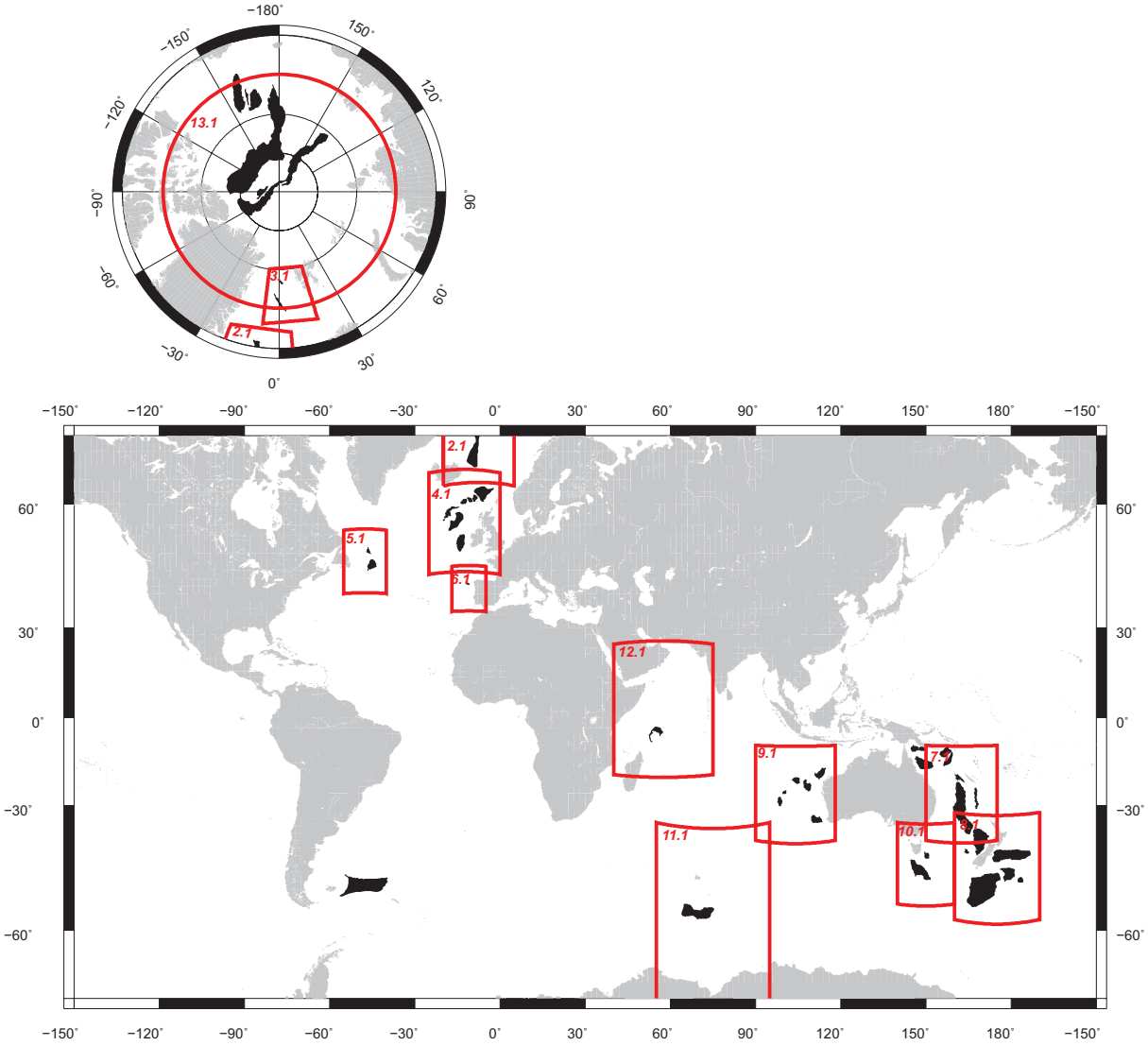

Figure 1.1: Global Map showing the locations of continental fragments (black). Red frames show the locations of map figures in this report, with the figure number in the upper right corner.

2 JAN MAYEN MICROCONTINENT

2.1 Geologic Background

The Jan Mayen microcontinent is located in the North Atlantic ocean, in the center of the Norwegian-Greenland Sea (Figure 2.1). This microcontinent was formed by breaking up first with the Norwegian margin and then with Greenland. Numerous seismic and potential field studies have been performed around Jan Mayen since the 1970's (see *Peron-Pinvidic et al.* (2012a) for a historical review). Since the 1990s and the drastic advancements in methodology and instruments in marine seismic studies, several published seismic refraction studies have focused on the crustal structure of Jan Mayen and the surrounding regions (*Kodaira et al.*, 1998; *Breivik et al.*, 2012; *Kandilarov et al.*, 2012; *Peron-Pinvidic et al.*, 2012a).

The Jan Mayen microcontinent is composed of a main ridge that trends approximately N-S, called the Jan Mayen Ridge, and a southern region extending to the Icelandic shelf, called the southern microcontinent or the southern ridge (Figure 2.1b). The main and southern ridges are separated by the narrow Jan Mayen Trough. The main Jan Mayen Ridge itself is bound to the west by the Jan Mayen Basin and Kolbeinsey mid-ocean ridge and to the east by the Norway Basin and extinct Aegir mid-ocean ridge.

2.2 Tectonic Setting

Potential field and seismic interpretation studies suggest that multiple stages of extension produced the blocky crustal features of the Jan Mayen microcontinent (*Gaina et al.*, 2009; *Peron-Pinvidic et al.*, 2012b). Initial spreading under the Jan Mayen Basin could have initiated during the Mesozoic, suggesting pre-rifting (chron 25) deformational stages in the Jan Mayen Basin and Norway Basin (*Peron-Pinvidic et al.*, 2012b).

Jan Mayen, while still joined with Greenland, began rifting from Norway around 56 Ma (*Talwani and Eldholm*, 1977; *Seton et al.*, 2012). Extension produced the Norway Basin and seafloor-spreading was active from 56 Ma (chron 25y) to 33–30 Ma (chron 13y) at the Aegir Ridge (*Gaina et al.*, 2009; *Seton et al.*, 2012). Seafloor spreading in the later stages of the Aegir Ridge were probably ultraslow (*Jung and Vogt*, 1997; *Gernigon et al.*, 2012). Spreading then jumped to the Kolbeinsey Ridge, to the west of Jan Mayen, corresponding to a large shift in spreading directions between Greenland and Eurasia (from NW-SE to NE-SW) (*Gaina et al.*, 2009; *Gernigon et al.*, 2012; *Seton et al.*, 2012). There is some uncertainty in the timing of the Aegir Ridge cessation and the jump in rifting to the Kolbeinsey Ridge, and whether Aegir Ridge was still active when Kolbeinsey Ridge separated Jan Mayen from Greenland. *Gaina et al.* (2009) model the Mohns Ridge linking with the Kolbeinsey Ridge and the Aegir Ridge expiring at 30 Ma. More recent work by *Gernigon et al.* (2012) suggest that the rift jump from the Aegir to the Kolbeinsey actually occurred around chron 10 (28 Ma), and that the Aegir Ridge did not go extinct until 28 Ma. Break-up of Jan Mayen from Greenland is completed by chron 6o–5o (20-11 Ma) and the Reykjanes Ridge linked to the Mohns Ridge via the Kolbeinsey Ridge (*Gaina et al.*, 2009).

The jump in rift location around Jan Mayen has been attributed to a mantle plume influence (*Müller et al.*, 2001), reactivation of inherited structures and strong Archaean crust, or shifting far-field forces (*Peron-Pinvidic et al.*, 2012a). Plate reconstructions place the Iceland plume near the locus of the Kolbeinsey Ridge around chron 13, when rift jumping is believed to occur (*Gaina et al.*, 2009). However, initial rifting around Jan Mayen is posited to be before 50 Ma,

and the plume locus would be under Greenland at that time (*Gaina et al.*, 2009). After 50 Ma, the influence of the rising plume would most likely affect all ridge systems and the Jan Mayen crust with magmatic underplating. Evidence for plume magmatism is observed in the seaward dipping reflectors (SDRs) on the eastern margin of Jan Mayen. Magmatic underplating on the eastern margin of the Jan Mayen microcontinent is suggested as a possibility based on gradual changes in lower crustal velocities at the COT (*Breivik et al.*, 2012).

2.3 Crustal Structure

The crustal structure of the Jan Mayen microcontinent discussed here is based on seismic refraction studies from eight lines (Figure 2.2). The crustal thickness varies from 7 to 24 km, with the greatest thickness near the non-continental Jan Mayen Island (*Kodaira et al.*, 1998; *Kandilarov et al.*, 2012; *Breivik et al.*, 2012). *Breivik et al.* (2012) identify three crustal layers in the two profiles 7-00 and 8-00, but *Kodaira et al.* (1998) and *Kandilarov et al.* (2012) interpret the crustal structure of the Jan Mayen Ridge to the north with two crustal layers. In the northern part of the Jan Mayen Ridge, *Kodaira et al.* (1998) identify an upper crust with P-wave velocities of 6.0–6.4 km s^{-1} and a lower crust of 6.7–6.8 km s^{-1}. Just 25 km to the south, *Breivik et al.* (2012) identify three basement reflectors and P-wave velocities of 5.5 km s^{-1} for the upper crust, 6.25–6.5 km s^{-1} for the middle crust, and 6.75–7.0 km s^{-1} for the lower crust. It is possible that the middle crust identified in the profiles of *Breivik et al.* (2012) corresponds to the base of the upper crust identified in line L4 of *Kodaira et al.* (1998) because it is highly unlikely that the middle crust would pinch out over such a short distance. The upper crustal signal of *Kodaira et al.* (1998) could be masked by the flood basalts covering the top basement in line L4. Both studies include a thick lower crustal layer (approximately 8–12 km thick) and an asymmetric crustal block shape for the microcontinent (*Kodaira et al.*, 1998; *Breivik et al.*, 2012).

Covering the basement, flood basalts (4.6–4.8 km s^{-1}) are found in the northernmost profile only (*Kodaira et al.*, 1998). Three sedimentary successions are identified on Jan Mayen ridge via seismic reflection data (*Peron-Pinvidic et al.*, 2012a). On the western edge of the L4 profile through Jan Mayen Ridge, a tilted layer with seismic velocities of 5.0–5.5 km s^{-1} covers the basement and is interpreted to be Paleozoic-age deposits (*Kodaira et al.*, 1998). The sediment covering the Jan Mayen Ridge is 2–3 km thick, interpreted to be of Mesozoic to Cenozoic age based on its seismic velocities (*Kodaira et al.*, 1998; *Mjelde et al.*, 2007; *Breivik et al.*, 2012).

2.4 Basin Crustal Structure

The Jan Mayen microcontinent is flanked by the Norway Basin on the east and the Jan Mayen Basin on the west. The Jan Mayen Basin has a crustal thickness of about 3 km and is interpreted to be of continental origin (*Kodaira et al.*, 1998). Compared to the 15 km-thick crust of the Jan Mayen Ridge, *Kodaira et al.* (1998) estimate a stretching factor of 5 for the Jan Mayen Basin. The upper crust of the Jan Mayen Basin has seismic velocities of 5.8 to 6.1 km s^{-1}, and the lower crust has velocities of 6.7 to 6.8 km s^{-1} (*Kodaira et al.*, 1998). Two to five sedimentary layers (including a basalt flow) are imaged in the seismic lines (Lines L3-L6 in Figure 2.2) of *Kodaira et al.* (1998). Seismic lines L4 and L5 (Figure 2.2) include a lowermost sedimentary layer with velocities of 5.0–5.5 km s^{-1} in the western edge of Jan Mayen Ridge that extends slightly into Jan Mayen Basin (*Kodaira et al.*, 1998). The high P-wave velocities and a relatively high Poisson's ration (1.9) are used to infer that these sediments are Paleozoic age (possibly matching the Devonian-Permian on the eastern Greenland margin) and have shale-type lithologies (*Kodaira et al.*, 1998; *Mjelde et al.*, 2007). The main Jan Mayen Basin has a

lowermost sedimentary layer with velocities of 4.0–4.7 km s^{-1} and Poisson's ratio of 2.2 that is interpreted to be of Mesozoic-age shale-dominated lithologies (*Kodaira et al.*, 1998; *Mjelde et al.*, 2007). Above that layer, sediments with velocities lower than 3.5 km s^{-1} are interpreted to be of Cenozoic and younger ages (*Kodaira et al.*, 1998).

To the east of the Jan Mayen Ridge, seismic refraction lines and reflection lines do not image attenuated continental crust flanking the ridge, as in the western margin of the microcontinent. Instead, the Jan Mayen microcontinent abruptly transitions to oceanic crust under the Norway Basin and Eastern Jan Mayen Fracture Zone. The eastern margin of the main Jan Mayen Ridge and southern Jan Mayen microcontinent is imaged in the two seismic refraction lines (7-00 and 8-00) of *Breivik et al.* (2012). In profile 7-00 across the main ridge and into the Eastern Jan Mayen Fracture Zone, four sedimentary layers are resolved (*Breivik et al.*, 2012). The higher velocity sedimentary layers found on the western margin of the Jan Mayen Ridge are not observed here. Extending just to the eastern edge of the Jan Mayen Ridge, a layer with P-wave velocities of about 3.5 km s^{-1} overlies the basement (*Breivik et al.*, 2012). Sedimentary layers extending out into oceanic crust of the Norway Basin have velocities around 2.0 to 2.75 km s^{-1} (*Breivik et al.*, 2012), most likely deposited syn- or post-break up.

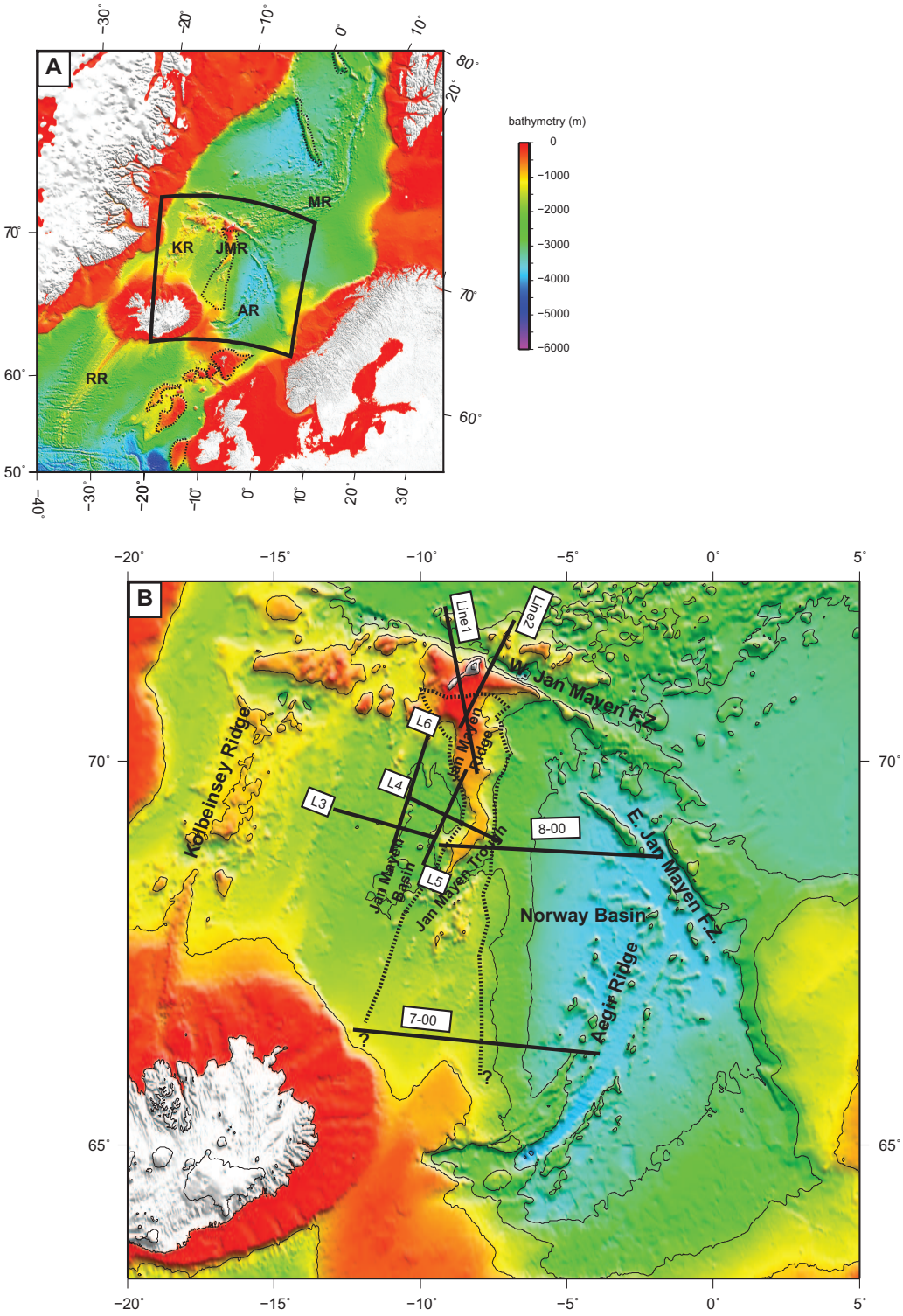

Figure 2.1: Map of the North Atlantic (A) and Jan Mayen Microcontinent (B). The approximate boundaries of the continental fragments are shown in a black dashed line. In the regional map (A), the Jan Mayen microcontinent (JMR) is bounded by the Mohns Ridge (MR), the Aegir Ridge (AR), the Kolbeinsey Ridge (KR). The Kolbeinsey Ridge extends north from the Reykjanes Ridge (RR). The black inset shows the location of map (B): the location map with locations of refractions studies L3-L6 (*Kodaira et al.*, 1998), Line 1-2 *Kandilarov et al.* (2012), and 7-00 and 8-00 (*Breivik et al.*, 2012). The exact southern extent of the Jan Mayen microcontinent is unknown and possibly extends to Iceland. Bathymetry from ETOPO-1 (*Amante and Eakins*, 2009).

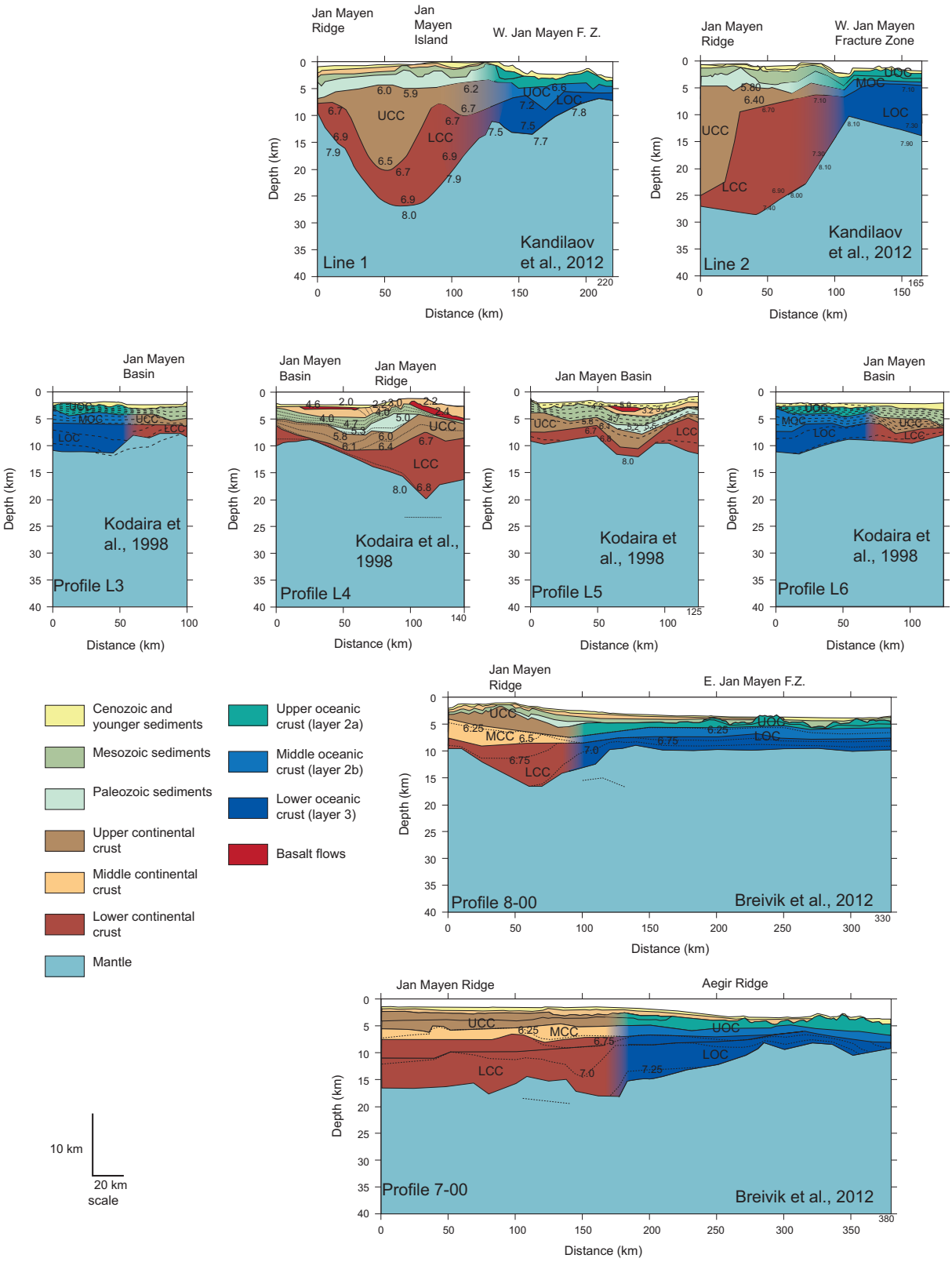

Figure 2.2: Seismic refraction lines across Jan Mayen Microcontinent. Redrawn from *Kodaira et al.* (1998); *Kandilarov et al.* (2012); *Breivik et al.* (2012). UCC = upper continental crust, MCC = middle continental crust, LCC= lower continental crust, UOC = upper oceanic crust, LOC = lower oceanic crust. Numbers are seismic velocities in km s^{-1}. Vertical exaggeration is 4:1.

3 THE NORTHERN ATLANTIC OCEAN-GREENLAND REGION

3.1 Geologic Background

The East Greenland Ridge is a continental sliver on the northeastern margin of Greenland (Figure 3.1). The East Greenland Ridge is continental crust trapped along the Greenland Fracture Zone. Originally considered to be oceanic crust, it was alternatively attributed to have a continental affinity because of the fit to the conjugate Senja Fracture Zone in plate reconstruction models (*Tsikalas et al.*, 2002). Recent seismic reflection/refraction studies confirmed the continental nature of the East Greenland Ridge (*Døssing et al.*, 2008).

To the north is the Hovgård Ridge, a parallel bathymetric high that might also be continental. However, seismic refraction studies that reached the margin of the Hovgård Ridge found the seismic velocities non-conclusive (*Ritzmann et al.*, 2004) (Figure 3.2. Gravity data can only be fit with an oceanic crust, when constraining the crustal thickness with the seismic refraction data (*Engen et al.*, 2008).

3.2 Tectonic Setting

The Norwegian-Greenland Sea opened around chron 24r (54–56 Ma), separating northern Greenland from Lofoten (*Tsikalas et al.*, 2002; *Seton et al.*, 2012). The conjugate Greenland and Senja fracture zones developed this time, as the Greenland Sea opened. Shortly afterward, the Boreas Basin between the Hovgård and East Greenland ridges opened around chron 18 (around 40 Ma), if it is considered to be oceanic (*Engen et al.*, 2008; *Døssing et al.*, 2008). Changes in the plate motion from chron 24 through chron 13 (53–33 Ma) forced a reorganization of the transform system and isolated the continental sliver of the East Greenland Ridge (*Døssing and Funck*, 2012).

3.3 Continental Fragment Crustal Structure

3.3.1 East Greenland Ridge

The East Greenland Ridge is crossed by two wide-angle seismic lines by *Døssing et al.* (2008) (Figure 3.2). The crustal thickness of the continental sliver is only 6–7 km (*Døssing et al.*, 2008). The East Greenland Ridge crust has two layers: an upper crust with velocities of 4.8–5.9 km s^{-1} and a lower crust with average velocities of 6.1–6.6 km s^{-1} (*Døssing et al.*, 2008). In transverse Line B, a region in the lower crust with high velocities (7.3–7.7 km s^{-1}) around 50 km is interpreted as serpentinized mantle (*Døssing et al.*, 2008). Coincident multichannel reflection seismic lines reveal that the upper crust is high faulted (*Døssing and Funck*, 2012).

Above the crust, three sedimentary layers are identified in the seismic refraction and reflection lines. The top layer has velocities of 2.00–2.20 km s^{-1}, the second layer has velocities of 2.40–3.70 km s^{-1}, and the third sedimentary layer has velocities of 4.00–4.80 km s^{-1} (*Døssing et al.*, 2008).

3.4 Basin Crustal Structure

3.4.1 Greenland Basin

Line A of *Døssing et al.* (2008) partly extends over the Greenland Basin (Figure 3.2). Based on clear magnetic anomalies and the crustal velocities, the Greenland Basin is interpreted as having a 6.5 km thick oceanic crust (*Døssing et al.*, 2008). The two crustal layers of the Greenland Basin are correlated to oceanic layers 2 and 3. The upper crust (oceanic layer 2) is about 2 km

thick with velocities of 5.4–6.5 km s^{-1} (*Døssing et al.*, 2008). The lower crust (ocean layer 3) is 4–4.5 km thick with velocities of 6.8–7.4 km s^{-1} (*Døssing et al.*, 2008).

The sedimentary cover the oceanic crust of the Greenland Basin is about 1–2 km thick (*Døssing et al.*, 2008). The three layers of sediments have velocities of 1.85–2.0 km s^{-1}, 2.2–2.7 km s^{-1}, and 3.2–3.5 km s^{-1}, from top to basal sedimentary layer (*Døssing et al.*, 2008).

3.4.2 Boreas Basin

The southern margin of the Boreas Basin where it abuts the East Greenland Ridge is covered by Line A of *Døssing et al.* (2008) and AWI-20090200 line of *Hermann and Jokat* (2013) covers the middle of the basin. This region of the Boreas Basin sampled by Line A is called the NE Fault Province because of the demonstrable amount of horst and graben structures revealed in the seismic reflection data (*Døssing et al.*, 2008). The crustal thickness of the NE Fault Province of the Boreas Basin here ranges from 2 to 9 km and has velocities of 5.67–7.15 km s^{-1} (*Døssing et al.*, 2008). Based on the seismic velocities, faulted upper crust, and corresponding gravity model, *Døssing et al.* (2008) interpret the edge of the Boreas Basin as extremely thinned continental crust. In line AWI-20090200, *Hermann and Jokat* (2013) interpret the crust of the Boreas Basin as oceanic, based on seismic and gravity modeling. The crust of the Boreas Basin in line AWI-20090200 is about 3.2 km thick with velocities with three crustal layers (*Hermann and Jokat*, 2013). The upper layer (oceanic crust 2a) has velocities of 3.4–4.3 km s^{-1}, the middle layer (oceanic crust 2b) has velocities of 4.2–5.4 km s^{-1}, and the lower layer (oceanic crust 2c) has velocities of 5.7–6.3 km s^{-1} (*Hermann and Jokat*, 2013).

The three sedimentary layers across the Greenland Basin and East Greenland Ridge are identified in the NE Fault Province as well. The top two sedimentary layers have velocities of 2.0–2.2 km s^{-1} and 2.4–3.7 km s^{-1} and have nearly continuous thicknesses in this region (*Døssing et al.*, 2008). The third sedimentary layer is mainly restricted to the deep grabens and has velocities of 3.3–4.5 km s^{-1} (*Døssing et al.*, 2008). In the main Boreas Basin, four sedimentary layers are identified in the seismic line AWI-20090200 with seismic velocities ranging from 1.6 km s^{-1} at the top to 3.5 km s^{-1} at the base of the fourth layer (*Hermann and Jokat*, 2013). The sedimentary cover has an average thickness of 0.2 km, but locally increases to 1–3 km in small basins (*Hermann and Jokat*, 2013).

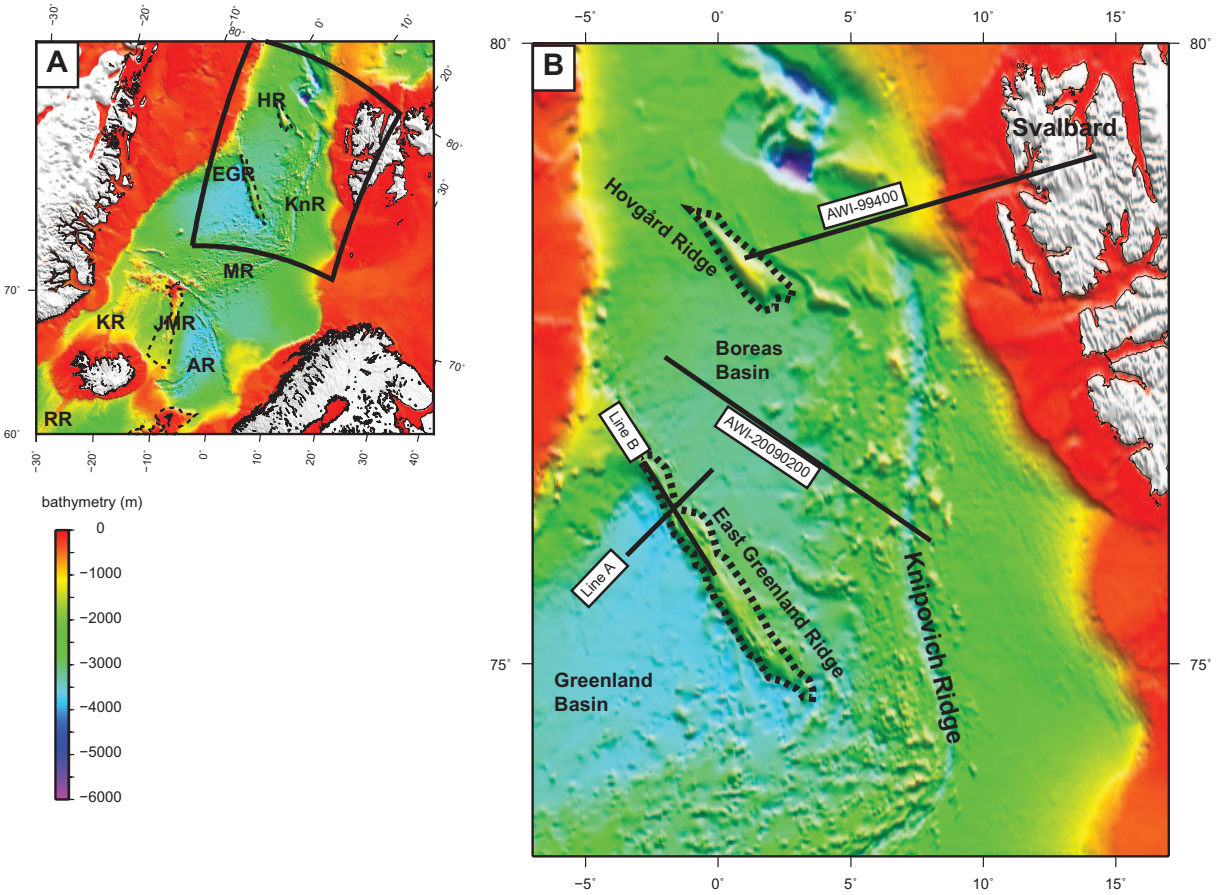

Figure 3.1: Map of the North Atlantic (A) and East Greenland Ridge (B). The approximate boundaries of the continental fragments are shown in a black dashed line. In the regional map (A), AR = Aegir Ridge, EGR = East Greenland Ridge, HR = Hovgård Ridge, JMR = Jan Mayen microcontinent, KR = Kolbeinsey Ridge, KnR = Knipovich Ridge, and MR = Mohns Ridge. The black inset shows the location of map (B): the location map with locations of refractions studies Lines A-B (*Døssing et al.*, 2008), AWI-20090200 (*Hermann and Jokat*, 2013), and AWI-99400 (*Ritzmann et al.*, 2004). Bathymetry from ETOPO-1 (*Amante and Eakins*, 2009).

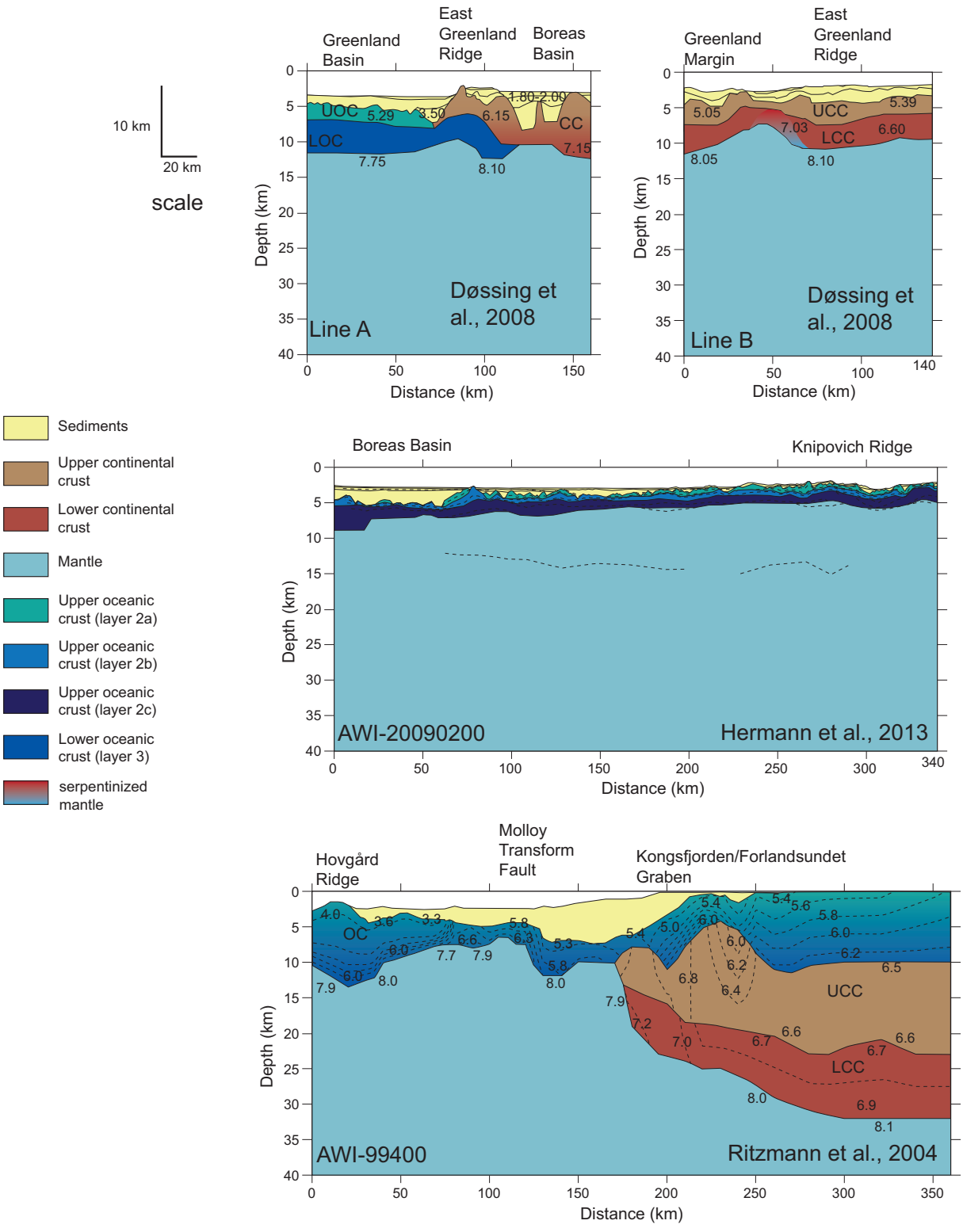

Figure 3.2: Seismic refraction lines across the East Greenland Ridge and related basins. UCC = upper continental crust, LCC= lower continental crust, UOC = upper oceanic crust, LOC = lower oceanic crust. Numbers are seismic velocities in km s^{-1}. All lines are redrawn to a 4:1 vertical exaggeration (modified from *Ritzmann et al.* (2004); *Døssing et al.* (2008), and *Hermann and Jokat* (2013)).

4 THE IRISH MARGIN

4.1 Geologic Background

A series of continental fragments rifted off the Irish Margin includes the Hatton Bank, Rockall Bank, Porcupine Bank, Faroes, and several smaller fragments (Figure 4.1). The Hatton Bank trends NE-SW and is flanked on the east by the Hatton Basin and the west by the Hatton continental margin. The Rockall Bank trends NE-SW and is flanked on the west by the Hatton Basin and the east by the Rockall Basin. Just north of the Rockall and Hatton Basins, smaller fragments include the George Bligh Bank, Lousy Bank, Bill Bailey Bank, and the Faroe Bank (Figure 4.1). These small fragments are separated by narrow channels, which are suggested to have formed from transform faulting, because the bounding fragments lie roughly in a NE-SW line (*Funck et al.*, 2008).The Faroe Islands are on a continental fragment that connects to Iceland via the magmatic Faroe-Iceland Ridge and is separated from the Irish mainland by the Faroe-Shetland Trough. The Fugloy Ridge is a small extension of the Faroes.

The basement of the Faroe shelf and Faroe-Shetland Trough most likely belongs to the Archean Lewisian complex, which is exposed in the Shetland Islands (*Dean et al.*, 1999). Detrital zircons from the Hatton Bank have ages of 1.8 and 1.75 Ga and Hf isotopic values related to Archean crust (*Morton et al.*, 2009). Structural fabric of the basement in the Rockall Bank, and most likely the Hatton Bank as well, run approximately NNE-SSW to NE-SW (*Naylor and Shannon*, 2005). *Roberts et al.* (1999) suggest that the Hatton, Rockall, and Faroe Basins follow the Caledonian trend. Jurassic structures in the Faroe-Shetland Trough are oriented NNE-SSW and truncated by late Cretaceous faults oriented NE-SW (*Dean et al.*, 1999). The orientation of major structural fabric in the Porcupine Basin is N-S, possibly Caledonian or older (*Naylor and Shannon*, 2005).

Magmatic underplating and extrusions are found throughout the Irish margin. The Hatton Bank has basaltic flows topping the basement and possible magmatic underplating on the west border towards the Hatton continental margin (*Vogt et al.*, 1998; *White et al.*, 2008). Magmatic underplating and basaltic flows become more prevalent in the basins and continental fragments to the north, such as the northern Rockall basin, Lousy Bank, Bill Bailey Bank, the Faroe-Shetland Trough, and the Faroe Bank. The Faroe Islands and nearby small continental fragments and basins are covered with basalt flows. Magmatic underplating of the crust under the Faroes is found in various regions (*White et al.*, 2008; *Richardson et al.*, 1999, 1998). To the southeast, the Rockall Bank, Rockall Basin, Porcupine Bank, and Porcupine Basin lack any magmatic intrusions at the base of the crust.

4.2 Tectonic Setting

Contemporaneous rifting and subsidence for the Rockall Basin, Hatton Basin, and Porcupine Basin is advocated by many (e.g. *Shannon*, 1991; *Doré et al.*, 1999; *Coward*, 1995). Variscan intracontinental rifting occurred in the Rockall and Hatton basins, followed by Triassic marginal and non-marine facies in both areas and the Porcupine basin (*Shannon*, 1991; *Coward*, 1995). Other authors suggest that rifting initially occurred in the Jurassic in the Rockall Basin only and then concurrently with the Hatton Basin in the Cretaceous (*Corfield et al.*, 1999). The Faroe-Shetland Trough began rifting in Permo-Triassic time, followed by rifting in the Jurassic, and three rifting events in the late Cretaceous (*Dean et al.*, 1999). The main rifting stage for the Porcupine Basin was during the late Jurassic- early Cretaceous (*Naylor and Shannon*, 2005; *Calvès et al.*, 2012). The extension direction shifted during the three rifting phases for

the Porcupine and Rockall area: from NW-SE directed Permian-Triassic extension to E-W extension in the late Jurassic to the early Cretaceous, followed by Cretaceous extension oriented NW-SE (*Shannon et al.*, 2007). Compressional events in the Jurassic and Cretaceous are proposed based on stratigraphic features in the Porcupine Basin (*Shannon et al.*, 2007; *Yang*, 2012). The three basins underwent thermal subsidence in lower Cretaceous to Tertiary time (*Shannon*, 1991).

Seafloor spreading between Porcupine Bank and North America started around 110–105 Ma (*Seton et al.*, 2012). *Seton et al.* (2012) propose in their plate reconstructions that the Porcupine Abyssal Plain was a oceanic plate that was active during Labrador-Greenland spreading (84–33 Ma) and ceased spreading at 33 Ma (chron 13). Seafloor spreading between Ireland and North America near the Rockall Bank began in the late Cretaceous (around 79 or 83 Ma) (*Seton et al.*, 2012; *Gaina et al.*, 2002) and continued northwestward to the breakup of the Labrador Sea (*Roest and Srivastava*, 1989). But breakup and spreading between the Hatton Bank and Greenland began around Chron 24 (56–53 Ma), after seafloor spreading ceased in the Labrador Sea (*Elliott and Parson*, 2008).

4.3 Continental Fragment Crustal Structure

4.3.1 Hatton Bank

We discuss the Hatton Bank crustal structure in this section based on wide angle seismic refraction lines from two studies: iSIMM-5 and RAPIDS-2 (Figure 4.2). The RAPIDS-2 and iSIMM-5 seismic lines run perpendicular to the trend of the Hatton Bank (Figure 4.1). The iSIMM-5 seismic line across Hatton Bank (*Smith et al.*, 2005; *White et al.*, 2008; *White and Smith*, 2009) was carried out in 2002 and builds upon the earlier seismic results of *Fowler et al.* (1989). RAPIDS-2 traverses just south of the Hatton Bank. The crustal thickness of the Hatton Bank is estimated to be 22–24 km (*Fowler et al.*, 1989; *White and Smith*, 2009). Two crustal layers are imaged under Hatton continental margin (*Vogt et al.*, 1998). The upper crust has velocities of 5.8–6.2 km s^{-1} and the second crustal layer has velocities of 6.5–6.7 km s^{-1} (*Vogt et al.*, 1998). Further west on the RAPIDS-2 line, a lower crustal layer is found in the Hatton Bank, suggesting that the lower crustal layer possibly pinches out seaward (Figure 4.2). The tomographic study across the iSIMM-5 line does not image layers within the continental crust (*White and Smith*, 2009).

A high velocity body under the Hatton Bank continental margin is well imaged in wide-angle seismic studies (*Fowler et al.*, 1989; *White et al.*, 2008; *White and Smith*, 2009; *Vogt et al.*, 1998). P-wave velocities for this layer are 7.2–7.5 km s^{-1} (*White and Smith*, 2009; *Vogt et al.*, 1998). SDRs are interpreted in the overlying crust and sediments of the Hatton continental margin (*White et al.*, 2008; *White and Smith*, 2009).

A thin layer (0.5–2 km thick) of sediments covers the basement of the Hatton Bank (*Vogt et al.*, 1998; *White and Smith*, 2009). Two sedimentary layers with Cenozoic-age unconformities are identified on the corresponding reflection line of iSIMM-5 (*White and Smith*, 2009). Below these sediments, a layer with velocities ranging from 4.70 to 5.90 km s^{-1} covers the basement, and could be either Mesozoic/Paleozoic sediments or basaltic flows (*White and Smith*, 2009). *Vogt et al.* (1998) identifies only two sedimentary layers in the Hatton Bank and continental margin: the upper layer is 0.5–1 km thick with an average velocity of 2.0 km s^{-1}, and the lower layer is 2 km thick with an average velocity of 4.2 km s^{-1}.

4.3.2 Rockall Bank

Since the 1990's, only one seismic refraction study (RAPIDS-2) has traversed the Rockall Bank (Figure 4.3) because refraction studies of the Irish Margin crustal structure have primarily focused on the basins (Figure 4.1). The RAPIDS-2 transverse line crosses the southern part of the Rockall Bank, whereas RAPIDS-33 extends into the southern part. The crustal thickness of the Rockall Bank is about 30 km, correlating to a stretching factor of only 1–2 (*Vogt et al.*, 1998; *Morewood et al.*, 2005). Three crustal layers are imaged in the Rockall Bank by the RAPIDS-2 and RAPIDS-33 studies. The upper crust is estimated to be around 7 km thick with velocities of 6.0–6.2 km s^{-1} (*Vogt et al.*, 1998; *Morewood et al.*, 2005). *Vogt et al.* (1998) determine velocities of 6.5–6.7 km s^{-1} for the middle crust, while *Morewood et al.* (2005) estimate slightly lower velocities of 6.3–6.4 km s^{-1}. The lower crust has velocities of 6.7–6.9 km s^{-1} (*Vogt et al.*, 1998; *Morewood et al.*, 2005). A thin layer of sediments covers the Rockall Bank (0–1 km thick) with velocities around 4.0 km s^{-1} (*Vogt et al.*, 1998). No basaltic flows or magmatic intrusions are imaged on the Rockall Bank.

4.3.3 Porcupine Bank

Only two recent published seismic refraction studies (RAPIDS-33 and RAPIDS-4) extend onto the Porcupine Bank (Figure 4.4). The crustal thickness of the Porcupine Bank is about 25–28 km (*Whitmarsh et al.*, 1974; *Morewood et al.*, 2005; *O'Reilly et al.*, 2006). The Porcupine Bank has undergone stretching of a factor 1 to 2 (*Morewood et al.*, 2005). Three crustal layers were identified on the RAPIDS-3 study, with velocities of 6.0–6.2 km s^{-1} in the upper crust, 6.2–6.4 km s^{-1} in the middle crust, and 6.6–6.8 km s^{-1} in the lower crust (*Morewood et al.*, 2005). The sedimentary thickness above the Porcupine Bank is around 1 km thick with velocities of 5.0–5.1 km s^{-1}, and is related to Permo-Triassic age deposits or weathered basement (*Morewood et al.*, 2004).

4.3.4 The Faroes

Numerous wide-angle seismic studies have covered the Faroe Shelf and its margins (Figure 4.5). The Faroe Islands have a crustal thickness of about 30–35 km (*Richardson et al.*, 1999; *White et al.*, 1999). Minus the addition of basalts, *Richardson et al.* (1999) suggest that the Faroe crustal thickness is more on the order of 20 to 30 km. Using teleseismic receiver functions from land stations, *Harland et al.* (2009) determined the Moho to be around 29–32 km. Combined seismic refraction and gravity modeling across the southwestern region of Faroe Shelf identifies a crustal thickness ranging from 17 to 25 km (*Raum et al.*, 2005). The Fugløy Ridge, which is the northern arm of the Faroe shelf, has crustal thickness of around 27 km (*Roberts et al.*, 2009).

The Faroes are covered by sediments with velocities of 2.0–4.5 km s^{-1} intermingled with Tertiary basalt flows with velocities of 5.0–6.0 km s^{-1} (*Richardson et al.*, 1999; *White et al.*, 1999, 2008; *Roberts et al.*, 2009). The thickness of basalts and sediments can get up to 5–10 km on the Faroes (*Richardson et al.*, 1999). High velocity (> 4.0 km s^{-1}) sediments are interpreted to be Cretaceous or older syn-rift deposits (*Raum et al.*, 2005).

Crustal velocities on the FAST and FLARE seismic profiles range from 5.7–6.0 km s^{-1} at the top to 6.8–7.2 km s^{-1} at the base of the crust (*Richardson et al.*, 1999). *Roberts et al.* (2009) model the crust in the Fugløy Ridge with velocities ranging from 5.5 to 6.9 km s^{-1} at the base of the crust. The two seismic lines of AMG delineate two crustal layers (Figure 4.5). The upper crust of the Faroe shelf has velocities of 5.9–6.25 km s^{-1} and the lower crust has velocities of 6.5–7.0 km s^{-1} (*Raum et al.*, 2005). Seismic velocities greater than 7.0 km s^{-1} at the base of

the lower crust on the FLARE, FAST, and iSIMM seismic lines are interpreted as magmatic underplating (*Richardson et al.*, 1999; *Roberts et al.*, 2009). However, these high velocities are not modeled in the AMC seismic lines which overlap the FLARE and FAST lines (*Raum et al.*, 2005).

4.3.5 Other small continental fragments

Several small fragments around the northern Rockall Basin include the Lousy Bank, Bill Bailey Bank, Faroe Bank, and the George Bligh Bank (Figure 4.1). The crustal thicknesses of these fragments are around 24 km for the Faroe Bank (*Funck et al.*, 2008), 25 km for the Bill Bailey Bank (*Funck et al.*, 2008), 14.5 km for the George Bligh Bank (*Funck et al.*, 2008), and 18-24 km for the Lousy Bank (*Klingelhöfer et al.*, 2005; *Funck et al.*, 2008). Basalt flows extending from the Faroe Shelf cover these small continental fragments (Figure 4.5). *Klingelhöfer et al.* (2005) model these basalt flows as directly overlying the basement, whereas more recent work on perpendicular seismic lines by *Funck et al.* (2008) model a layer of mixed sediments and magmatic extrusions between the basalt and crystalline crust.

Under the crust of the Lousy Bank, a layer occurs with velocities of 7.2–7.4 km s^{-1} (*Klingelhöfer et al.*, 2005; *Funck et al.*, 2008). The Lousy Bank has an upper crust with velocities of 5.75–6.4 km s^{-1} and a lower crust with velocities of 6.6–6.8 km s^{-1} (*Klingelhöfer et al.*, 2005). *Funck et al.* (2008) divide the upper crust into two layers, therefore interpreting the Lousy Bank crust as having an upper, middle, and lower crust. The three crustal layers in seismic lines Line A and Line B are found in the Lousy Bank, George Bligh Bank, and Faroe Bank. The upper crust has typical velocities of 5.5–5.9 km s^{-1}, the middle crust has velocities of 6.0–6.2 km s^{-1}, and the lower crust has velocities of 6.5–6.8 km s^{-1} (*Funck et al.*, 2008). To the south of the Lousy Bank, the three crustal layers continue under the George Bligh Bank, but the continental fragment is underplated by magma (*Funck et al.*, 2008). The middle crust in the George Bligh Bank has higher velocities then the underlying lower crust, and is therefore interpreted as a magmatic intrusion (*Funck et al.*, 2008). The middle crust pinches out under the Bill Bailey Bank, to the north of the Lousy Bank (Figure 4.5). Further north, close to the Faroe Shelf, the small Faroe Bank is modeled with the same three crustal layers as in the neighboring fragments and the Faroe Shelf.

4.4 Basin Crustal Structure

4.4.1 Hatton Basin

The Hatton Basin separates the Hatton Bank from the Rockall Bank. The crustal thickness of the Hatton Basin ranges from 8 to 15 km (*Vogt et al.*, 1998; *Funck et al.*, 2008; *White and Smith*, 2009). The two seismic lines traversing the central and southern parts of the Hatton Basin (iSIMM-5 and RAPIDS-2) do not image any high velocity bodies under the basin, whereas Line B (*Funck et al.*, 2008), which runs along the northern axial trend of the basin, is interpreted to have a high velocity layer (7.25 km s^{-1}) under the thin continental crust. Across the southern Hatton Basin, *Vogt et al.* (1998) interpret three crustal layers, with velocities of 5.8–6.2 km s^{-1} in the upper crust, 6.5–6.7 km s^{-1} for the middle crust, and 6.8–6.9 km s^{-1} for the lower crust. The crustal velocities determined for Line B in the northern Hatton Basin yield lower velocities, with 5.45–5.70 km s^{-1} in the upper crust, 6.15–6.20 km s^{-1} in the middle crust, and 6.45–6.60 km s^{-1} in the lower crust (*Funck et al.*, 2008).

In the Hatton Basin, two sedimentary layers are well resolved (*Vogt et al.*, 1998). The upper layer is 2 to 3.5 km thick with a velocity of 2.0 km s^{-1} and the second sedimentary layer is about 3.5 km thick with velocities of 4.2–4.6 km s^{-1} (*Vogt et al.*, 1998). In the northern part

of the basin, the sedimentary thickness is about 2 km with velocities of 1.7–3.7 km s^{-1} (*Funck et al.*, 2008). Basalt flows cover the basement in the seismic lines iSIMM-5 and Line B, but not in RAPIDS 2 in the southern part of the Hatton Basin. Basaltic layers are between the sedimentary layers and upper crust and have velocities of 4.9–5.5 km s^{-1} (*Funck et al.*, 2008; *White and Smith*, 2009).

4.4.2 Rockall Basin

The RAPIDS-2 and RAPIDS-33 wide-angle seismic lines cross the Rockall Basin (Figure 4.1, 4.3). The Rockall Basin ranges from 5 to 13 km in thickness, thinning towards the south. The northern Rockall Basin, north of the Rockall Bank, has a crustal thickness of 13 km (*Klingelhöfer et al.*, 2005). The southern part of the Rockall Basin, between the Rockall Bank and the Irish Shelf and Porcupine Bank, has thicknesses of 5–7 km (*Hauser et al.*, 1995; *O'Reilly et al.*, 1995; *Morewood et al.*, 2005). Unlike the surrounding high regions, the Rockall Bank has two crustal layers identified rather than three. The upper crust has velocities of 6.0–6.4 km s^{-1} (*Hauser et al.*, 1995; *O'Reilly et al.*, 1995; *Morewood et al.*, 2005; *Klingelhöfer et al.*, 2005). In the northern Rockall Basin, the lower crust has velocities of 6.4–6.8 km s^{-1} (*Klingelhöfer et al.*, 2005). The southern part of the Rockall Basin has lower crustal velocities that are slightly higher: 6.7–6.9 km s^{-1} (*Hauser et al.*, 1995; *O'Reilly et al.*, 1995; *Morewood et al.*, 2005).

The basin fill is up to 7 km thick, and several sedimentary layers are identified via companion reflection studies. Six sedimentary layers are interpreted to be of Paleozoic to recent age (*Mackenzie et al.*, 2002; *Morewood et al.*, 2004). The small perched basins on the margins of the Rockall Basin (the Erris, Macdara, and Conall basins: Figure 4.3) have the older sedimentary successions (*Morewood et al.*, 2004). Thick basaltic flows (around 1.5 km thick) layered within the sediments are identified in the northern Rockall Basin (*Klingelhöfer et al.*, 2005), but not in the southern main basin. Minor Tertiary dikes and sills are imaged in the reflection studies of the southern Rockall Basin (*Morewood et al.*, 2004).

A sub-Moho layer is imaged in the southern, main Rockall Basin, by strong mantle reflections (P_LP phase) 6 to 7 km below the Moho (*O'Reilly et al.*, 1995; *Morewood et al.*, 2004). Below the Moho, the mantle has velocities of 7.5–7.8 km s^{-1} (*O'Reilly et al.*, 1995; *Hauser et al.*, 1995; *Morewood et al.*, 2004), and the origin has been suggested to be serpentinized mantle (*Shannon et al.*, 1999) or strain-related anisotropy.

4.4.3 Porcupine Basin

The Porcupine Basin is covered by only one refraction line: the RAPIDS-4 wide angle seismic line (Figure 4.1, 4.4). The crustal thickness is asymmetric and possibly thins from 2–3 km to nothing (*O'Reilly et al.*, 2006). Crustal velocities are around 6.0–6.5 km s^{-1} (*O'Reilly et al.*, 2006). The sedimentary basin fill is around 10 km thick, with three layers identified through wide-angle seismic methods (*O'Reilly et al.*, 2006). The upper sedimentary layer has velocities of 2.0–2.4 km s^{-1} and is interpreted as Cenozoic and mostly Neogene (*O'Reilly et al.*, 2006). The second layer has thicknesses ranging from 3 to 7 km with velocities of 3.2–3.8 km s^{-1}, interpreted as Cenozoic (Paleogene) sediments (*O'Reilly et al.*, 2006). The third, basal sedimentary layer is 4 to less than 1 km thick with velocities of 4.5–5.0 km s^{-1} and is interpreted as Jurassic age sediments (*O'Reilly et al.*, 2006). Thin high velocity layers (5.5–6.0 km s^{-1}) within the Cenozoic sediments are interpreted as basalt flows and sills (*O'Reilly et al.*, 2006). Perched basins on the edge of Porcupine Bank contain Jurassic to Tertiary age sediments (*Morewood et al.*, 2004).

Below the extremely thinned crust at the center of the Porcupine Basin, the mantle has a layer with low velocities of 7.2–7.5 km s^{-1} that grades laterally to high values of 8.2 km s^{-1} towards the basin margins (*O'Reilly et al.*, 2006). Similar to the low velocity layer under the Rockall Basin, this sub-Moho layer is interpreted as serpentinized mantle.

4.4.4 Faroe-Shetland Trough

The Faroe-Shetland Trough is crossed by several refraction seismic lines (Figure 4.1 and 4.5). The two AMG lines cross the Corona and Judd basins, which are perched basins on the south-west margin of the Faroe-Shetland Trough. The FAST and FLARE seismic lines cross into the Faroe-Shetland Trough (Figure 4.5). The Faroe-Shetland Trough has a crustal thickness of around 15–20 km (*Richardson et al.*, 1999). *Raum et al.* (2005) estimate a crustal thickness around 8 km under the Judd Basin and 15 km under the Corona Basin/Faroe-Shetland Basin. The crust has velocities of 6.4 km s^{-1} at the top and 6.8 km s^{-1} at the base (*Richardson et al.*, 1999). Two crustal layers are identified in the AMG lines, with velocities of 5.9–6.25 km s^{-1} in the upper crust and 6.5–7.0 km s^{-1} in the lower crust (*Raum et al.*, 2005).

The basement is overlain by rift-related sediments intermingled with magmatic extrusions and intrusions. The basin fill is up to 5 km in the FLARE and FAST seismic lines (*Richardson et al.*, 1999) and up to 1 km in the perched Judd Basin (*Raum et al.*, 2005). The basaltic flows on the Faroe shelf pinch out into the basin (*Richardson et al.*, 1999; *Raum et al.*, 2005).

4.4.5 Crustal lows between small continental fragments

The Lousy Bank, George Bligh Bank, Bill Bailey Bank, and Faroe Bank are separated by narrow channels with thinned continental crust. These narrow basins are filled with the same basalt flows and sedimentary layers that cover the surrounding small continental fragments. The crustal thickness of these regions are much lower than the continental fragments with thicknesses as low as 8 km (*Funck et al.*, 2008). On seismic line AMP-A, these thinned crustal regions correspond to areas where the middle crust pinches out (Figure 4.5).

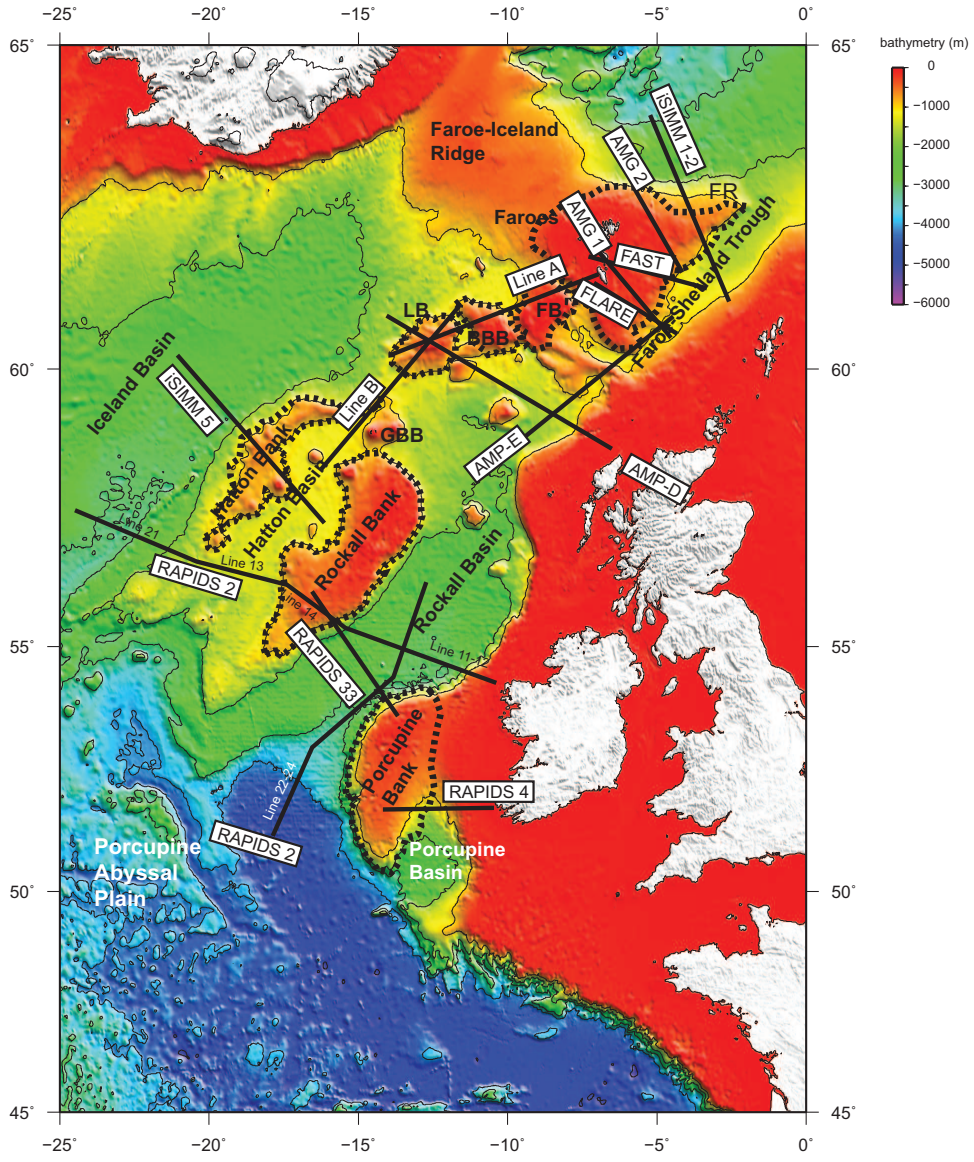

Figure 4.1: Map of the Irish Margin. The approximate boundaries of the continental fragments are shown in a black dashed line. BBB = Bill Bailey Bank, FB = Faroe Bank, FR = Fugloy Ridge, GBB = George Blight Bank, LB = Lousy Bank. The locations of refractions lines iSIMM 5 (*Smith et al.*, 2005; *White et al.*, 2008), RAPIDS 2-transverse (*O'Reilly et al.*, 1995; *Vogt et al.*, 1998), RAPIDS 2-axial (*Hauser et al.*, 1995), RAPIDS 33 (*Mackenzie et al.*, 2002; *Morewood et al.*, 2004, 2005), RAPIDS 4 (*O'Reilly et al.*, 2006), Line A and B *Funck et al.* (2008), AMP-D (*Klingelhöfer et al.*, 2005), and AMP-E (*Klingelhöfer et al.*, 2005), iSIMM 1-2 (*Roberts et al.*, 2009), FLARE (*Richardson et al.*, 1999), FAST (*Richardson et al.*, 1999), and AMG 1 and 2 (*Raum et al.*, 2005) are shown in thick black lines. Bathymetry from ETOPO-1 (*Amante and Eakins*, 2009).

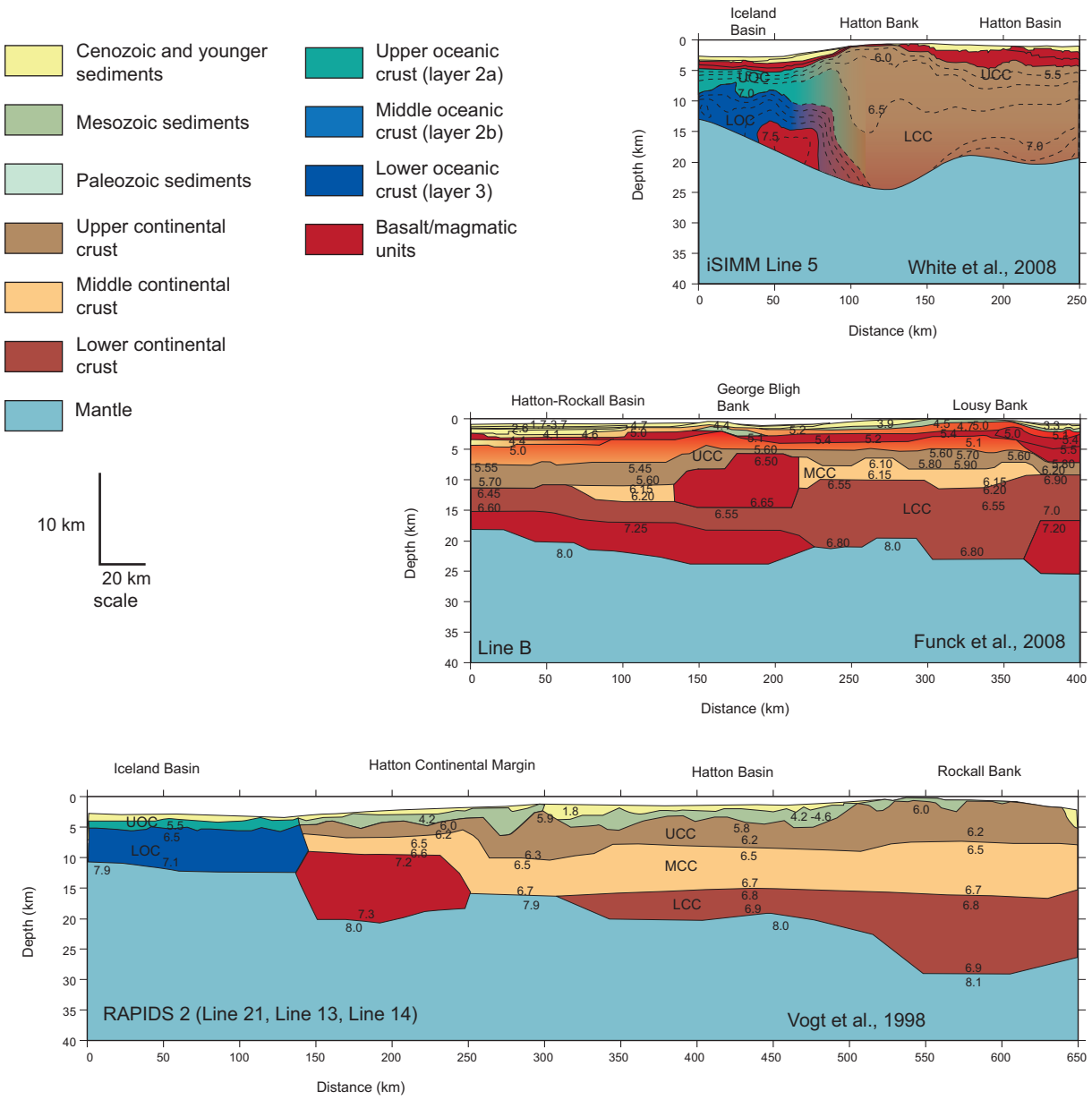

Figure 4.2: Seismic refraction lines across the Hatton Bank and Hatton Basin. UCC = upper continental crust, MCC = middle continental crust, LCC= lower continental crust, UOC = upper oceanic crust, LOC = lower oceanic crust, CC = continental crust. Numbers are seismic velocities in km s^{-1}. All lines are redrawn to a 4:1 vertical exaggeration (modified from *White et al.* (2008); *Funck et al.* (2008); *Vogt et al.* (1998)).

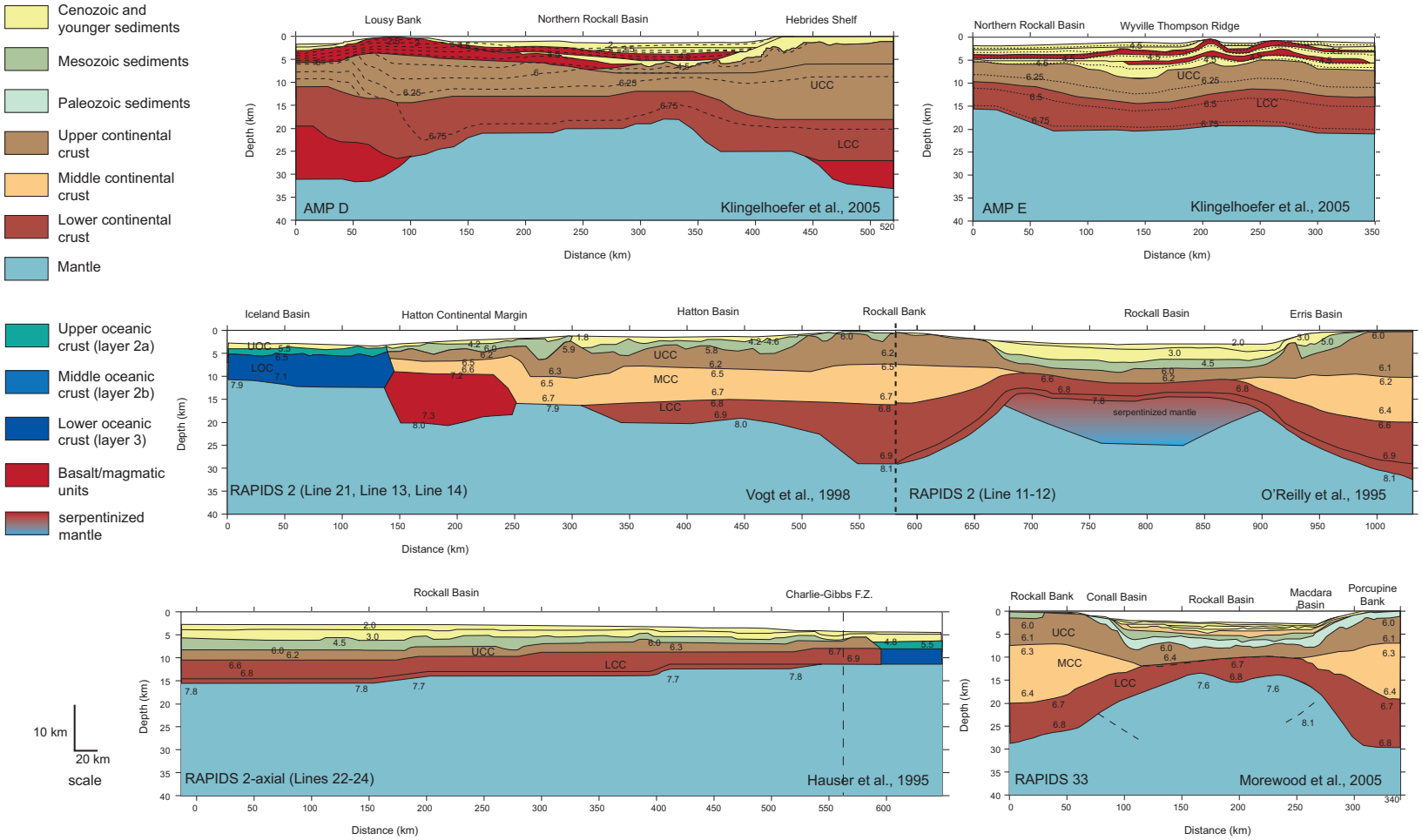

Figure 4.3: Seismic refraction lines across the Rockall Bank and Rockall Basin. UCC = upper continental crust, MCC = middle continental crust, LCC= lower continental crust, UOC = upper oceanic crust, LOC = lower oceanic crust. Numbers are seismic velocities in km s^{-1}. All lines are redrawn to a 4:1 vertical exaggeration (modified from *O'Reilly et al.* (1995); *Hauser et al.* (1995); *Vogt et al.* (1998); *Klingelhöfer et al.* (2005), and *Morewood et al.* (2005)).

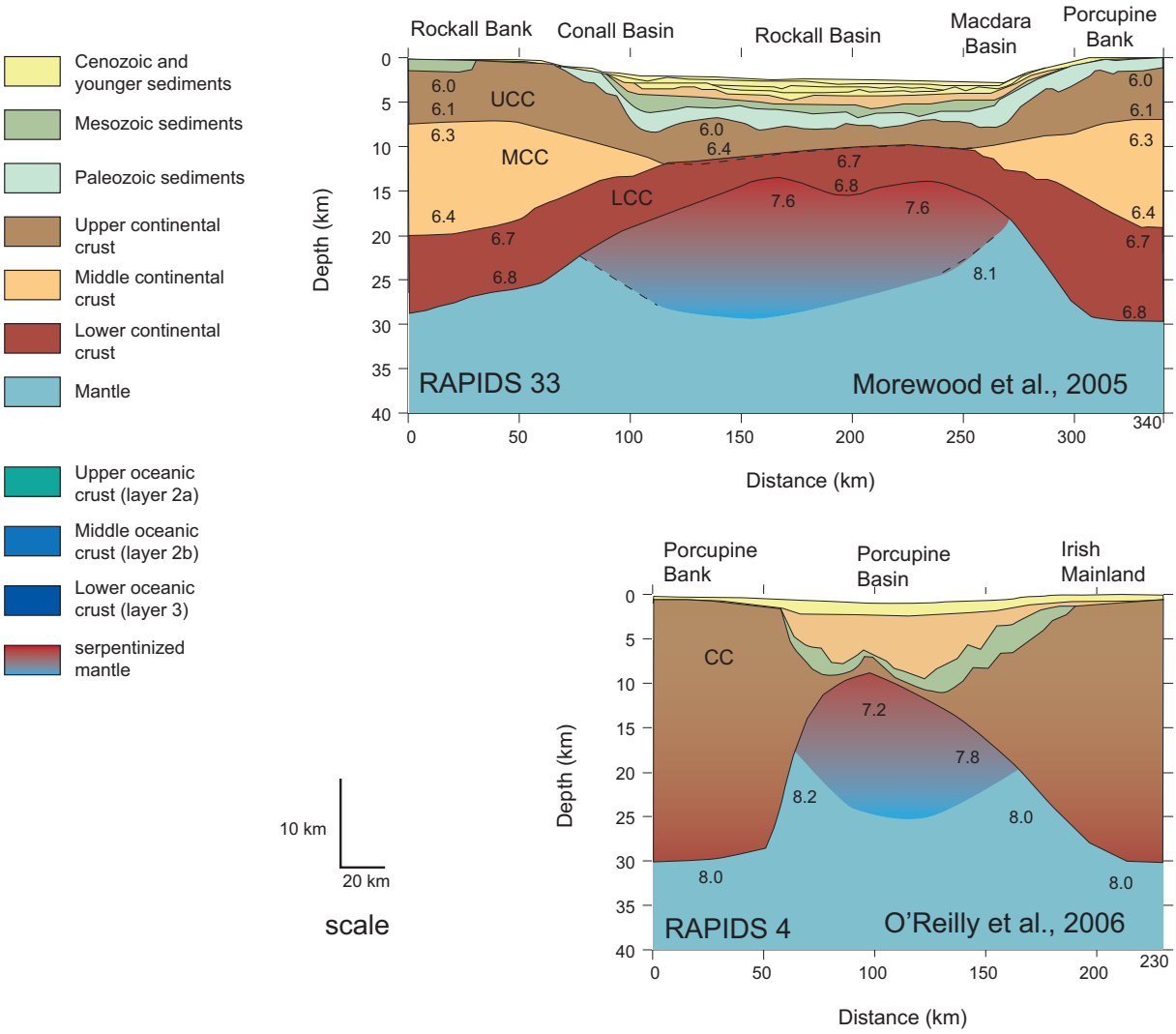

Figure 4.4: Seismic refraction lines across the Porcupine Bank and Porcupine Basin. UCC = upper continental crust, MCC = middle continental crust, LCC= lower continental crust, UOC = upper oceanic crust, LOC = lower oceanic crust. Numbers are seismic velocities in km s^{-1}. All lines are redrawn to a 4:1 vertical exaggeration (modified from *Morewood et al.* (2005) and *O'Reilly et al.* (2006)).

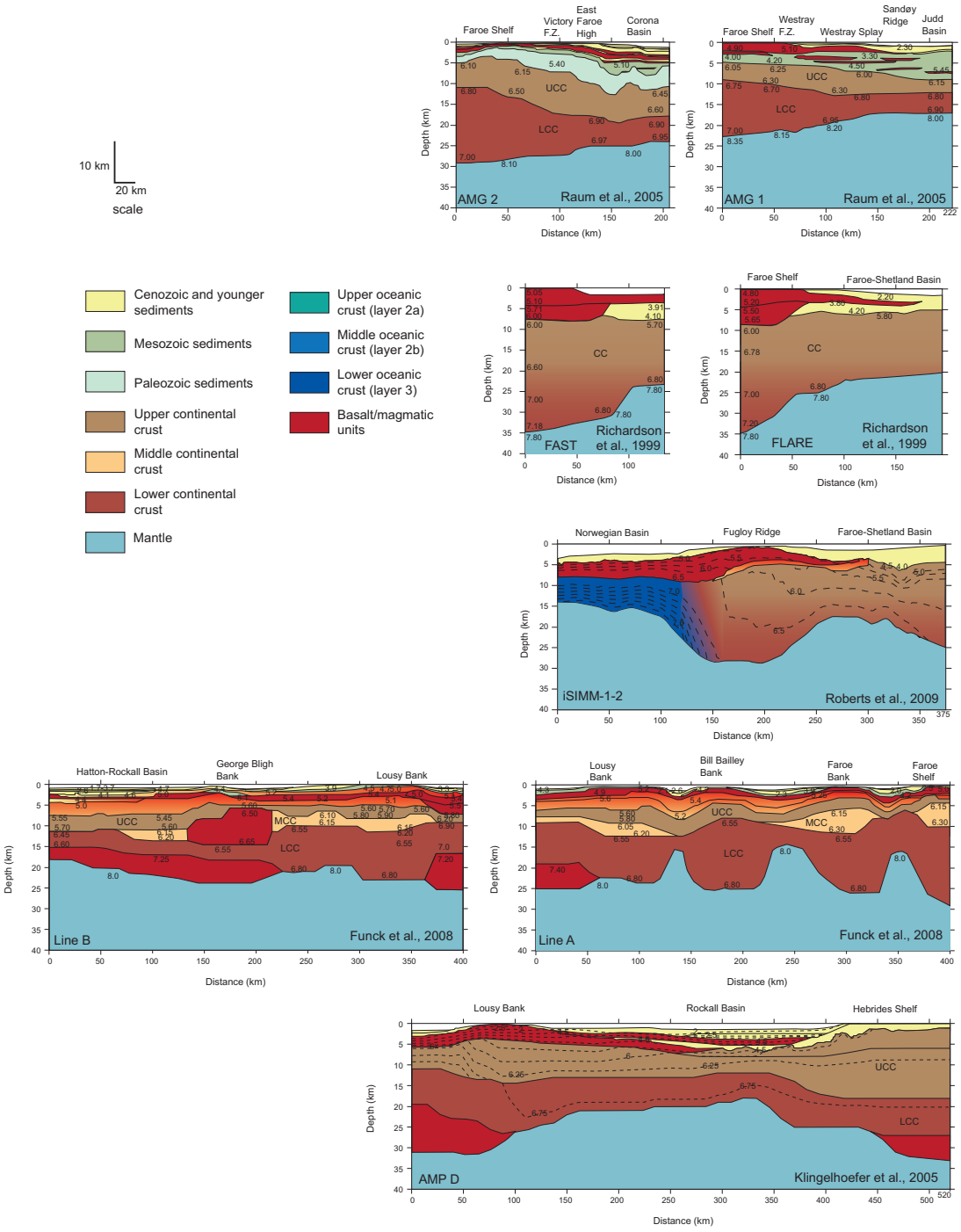

Figure 4.5: Seismic refraction lines across the Faroe Shelf, Faroe-Shetland Trough, and across the smaller continental fragments just south of the Faroe Shelf. UCC = upper continental crust, MCC = middle continental crust, LCC= lower continental crust, CC = continental crust. Numbers are seismic velocities in km s^{-1}. All lines are redrawn to a 4:1 vertical exaggeration (modified from *Richardson et al.* (1999); *Raum et al.* (2005); *Klingelhöfer et al.* (2005); *Funck et al.* (2008); *Roberts et al.* (2009)).

5 THE NEWFOUNDLAND MARGIN

5.1 Geologic Background

The Flemish Cap and Orphan Knoll are two continental fragments off the Atlantic margin of Newfoundland. The Flemish Cap is separated from the Grand Banks shelf by the narrow Flemish Pass. To the north, the Orphan Knoll is separated from Grand Banks by the Orphan Basin. The Flemish Cap and Orphan Knoll are both bordered by oceanic crust of the mid-Atlantic Ocean on the east. The basement of the Flemish Cap is composed of Hadrynian age granodiorites, and is part of the Avalon Terrane (*King et al.*, 1985). *Sibuet et al.* (2007b) suggest that the Orphan Knoll was once connected to the Flemish Cap, but was broken apart during rifting of the Orphan Basin and Flemish Pass.

5.2 Tectonic Setting

Rifting in the Orphan Basin, Flemish Pass, and Jeanne D'arc Basin occurred in the late Triassic-early Jurassic and late Jurassic-early Cretaceous (*Foster and Robinson*, 1993; *Tucholke et al.*, 2007). The Orphan Basin was formed by three rifting phases that progressed east to west: first in the late Triassic-early Jurassic in the east part of the basin, then late Jurassic to early Cretaceous in the northwest part of the Orphan Basin, and then a final stage in the late Cretaceous further to the west (*Sibuet et al.*, 2007a). Based on plate reconstructions, the Flemish Cap was effectively a microplate moving along flow lines that are oriented N20E, like the fault trends in the Orphan Basin, between M25-M0 (late Jurassic-early Aptian) (*Sibuet et al.*, 2007b).

The time and location of breakup between Newfoundland and the Iberian margin is still debated (see references in: *Seton et al.*, 2012). Breakup of Newfoundland (southeast of the Flemish Cap) with the Iberian margin is suggested to have started as early as 147 Ma (based on magnetic Anomaly M21) (*Srivastava et al.*, 2000; *Sibuet et al.*, 2007a), or at 128 Ma (chron M5) (*Russell and Whitmarsh*, 2003), or even later at 112–118 Ma (based on stratigraphic work) (*Tucholke et al.*, 2007). M21 is a low amplitude magnetic anomaly, implying an ultraslow break-up (*Srivastava et al.*, 2000; *Sibuet et al.*, 2007a; *Seton et al.*, 2012). Between Anomalies M20 and M0 (from late Jurassic to early Aptian: 156–118 Ma) the Orphan Basin and Flemish Pass were opened (*Sibuet et al.*, 2007a). Seafloor spreading between Newfoundland and Iberia after chron M0 is well established (*Sibuet et al.*, 2007a; *Seton et al.*, 2012). The ultraslow extension allowed an extensive period of mantle exhumation before seafloor spreading began in the late Aptian-early Albian (115–110 Ma) (*Tucholke et al.*, 2007).

5.3 Continental Fragment crustal structure

5.3.1 Flemish Cap

The Flemish Cap has a crustal thickness of around 30 km (*Funck*, 2003; *Gerlings et al.*, 2011) (Figure 5.1). Three crustal layers are identified on the Flemish Cap: an upper crust with velocities of 5.8–6.2 km s^{-1}, a middle crust with velocities of 6.3–6.45 km s^{-1}, and a lower crust with velocities of 6.6–6.85 km s^{-1} (*Funck*, 2003; *Gerlings et al.*, 2011). Pockets of sediments cover the Flemish Cap. A 6 km-thick layer with velocities of 5.4 km s^{-1} overlain by a less than 1 km-thick layer with velocities of 2.8 km s^{-1} are found in a perched basin at the northwest part of the Flemish Cap (*Funck*, 2003). On a perpendicular transverse, *Gerlings et al.* (2011) model two sedimentary layers in that region with velocities of 2.9–3.1 km s^{-1} and 4.7–4.9 km s^{-1}. The second sedimentary layer is poorly resolved on both seismic lines, and therefore loosely interpreted as pre-rift sediments/igneous rocks (*Funck*, 2003).

5.3.2 Orphan Knoll

The Orphan Knoll is covered by only one published wide-angle refraction line (*Chian et al.*, 2001) (although results of the recent OBWAVE project should be published soon). The crustal thickness of the Orphan Knoll is around 12–15 km (*Chian et al.*, 2001). A thick sedimentary package overlies the Orphan Knoll and Orphan Basin. *Chian et al.* (2001) correlated the velocity model from the seismic reflection study to stratigraphic data from Blue well H-28. Several thin sedimentary layers (less than 1 km thick) with velocities under 3 km s^{-1} overlie two thick layers (3–5 km thick) with velocities of 3.2–3.3 km s^{-1} and 4.1–4.7 km s^{-1}, which are correlated to Cretaceous and Triassic-Jurassic stratigraphic layers, respectively (*Chian et al.*, 2001).

The upper crust, which was originally interpreted by *Chian et al.* (2001) as metasedimentary basement cover due to the low velocities (5.3–5.9 km s^{-1}) calculated from the crustal velocity model, most likely has velocities around 6.0 km s^{-1}, similar to those on Grand Banks and Flemish Cap (*Peron-Pinvidic and Manatschal*, 2010). The middle crust has velocities of 6.1–6.5 km s^{-1} and the lower crust has velocities of 6.8–7.0 km s^{-1} (*Chian et al.*, 2001).

5.4 Basin crustal structure

5.4.1 Flemish Pass

The Flemish Pass has a crustal thickness of 12 km according to a 1-D velocity model (*Keen and Barrett*, 1981). More recent wide-angle seismic studies are not well resolved and estimate the thickness of the Flemish Pass around 15–20 km (*Van Avendonk et al.*, 2006; *Gerlings et al.*, 2011). The crust has three layers with velocities of 5.8–6.1 km s^{-1}, 6.3–6.45 km s^{-1}, and 6.65–6.85 km s^{-1} (*Gerlings et al.*, 2011).

5.4.2 Orphan Basin

The Orphan Basin has a crustal thickness of 6-20 km (*Keen and Barrett*, 1981; *Chian et al.*, 2001). A 1-D velocity profile under the Orphan Basin reveals two crustal layers with velocities of 6.11 km s^{-1} and 7.39 km s^{-1} (*Keen and Barrett*, 1981). The more recent wide-angle study of *Chian et al.* (2001) does not yield velocities of 7.35 km s^{-1} in the lower crust and therefore the authors interpret this to indicate there is no lower crustal magmatic underplating. *Chian et al.* (2001) identified two crystalline crust layers with velocities of 6.1-6.5 km s^{-1} and 6.8-7.0 km s^{-1}. Overlying these two layers, a heavily faulted layer with layers of 5.1-6.0 km s^{-1} is interpreted as acoustic basement, such as a pre-rift metasedimentary layer (*Chian et al.*, 2001). This layer is most likely an upper crustal layer. The basin fill is up to 10 km thick, and consists of layers correlated to recent (1.8-1.85 km s^{-1}), Miocene (2.0-2.2 km s^{-1}), Paleocene-Eocene (2.4-2.6 km s^{-1}), Cretaceous-Paleocene (3.1-3.3 km s^{-1}), and Paleozoic stratigraphy (4.1-4.9 km s^{-1}) (*Chian et al.*, 2001). The Paleozoic layer fills in troughs between the ridges of upper crustal layer.

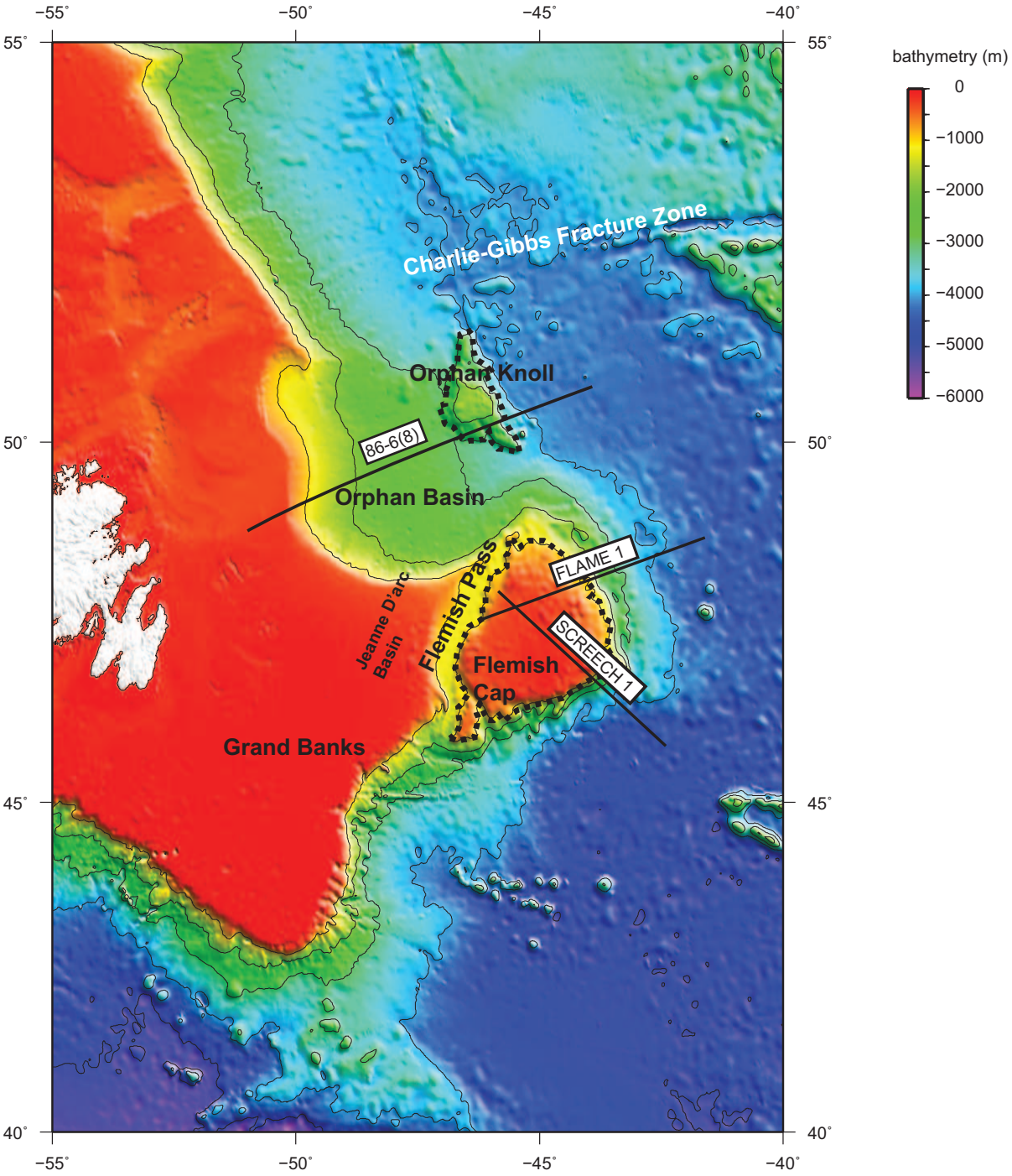

Figure 5.1: Map of the Grand Banks Margin. The approximate boundaries of the continental fragments are shown in a black dashed line. The locations of refractions lines 86-6 and 86-8 (*Chian et al.*, 2001), FLAME-1 (*Funck*, 2003), SCREECH-1 (*Gerlings et al.*, 2011). Bathymetry from ETOPO-1 (*Amante and Eakins*, 2009).

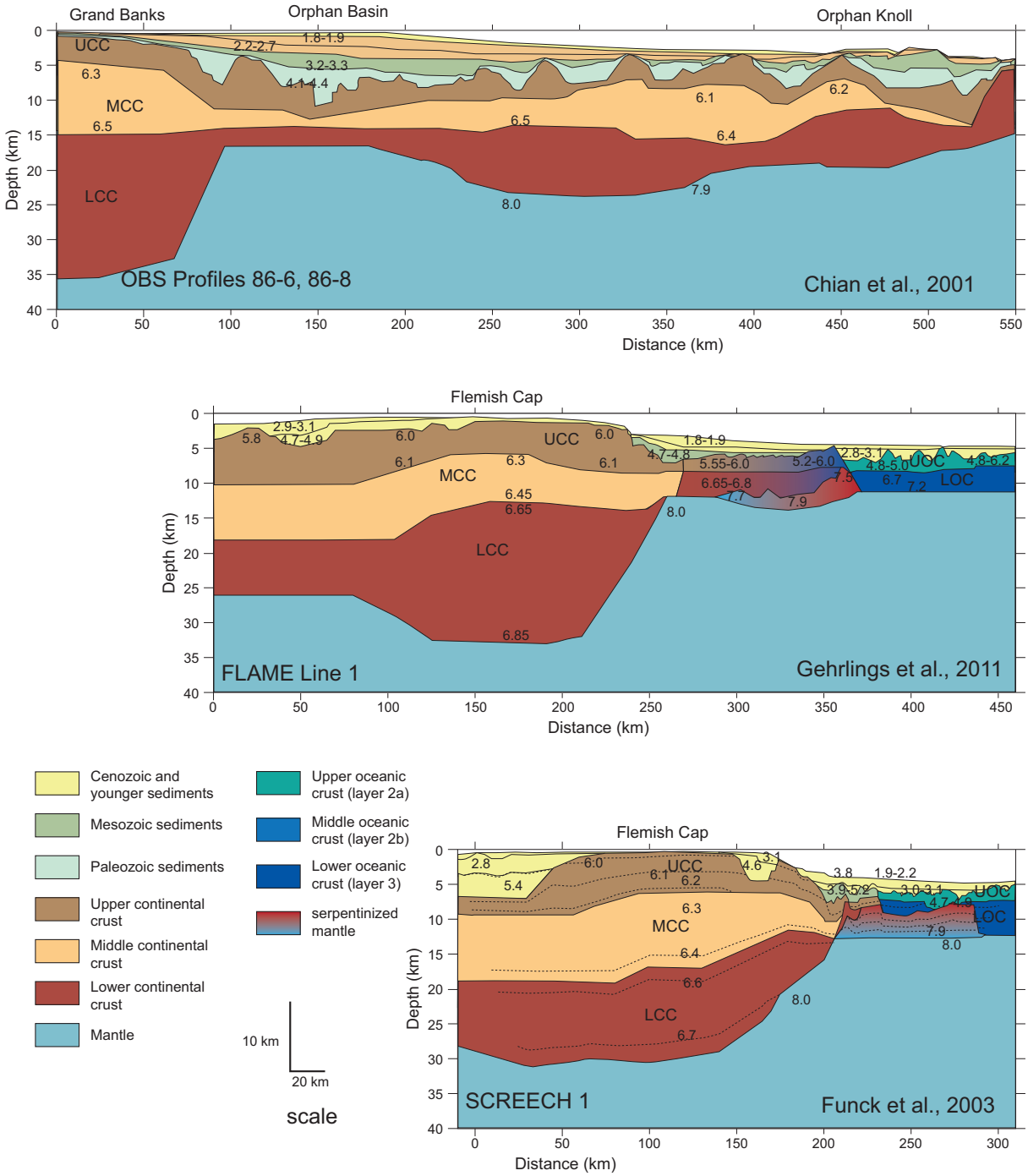

Figure 5.2: Seismic refraction lines across the Grand Banks region. UCC = upper continental crust, MCC = middle continental crust, LCC= lower continental crust, UOC = upper oceanic crust, LOC = lower oceanic crust. Numbers are seismic velocities in km s^{-1}. All lines are redrawn to a 4:1 vertical exaggeration (modified from *Chian et al.* (2001); *Funck* (2003), and *Gerlings et al.* (2011)).

6 GALICIA BANK

6.1 Geologic Background

The Galicia Bank is a small continental fragment on the Iberia margin, separated from the continental shelf on the east by the Galicia Interior Basin (Figure 6.1). To the west of the Galicia Bank lies the small Galicia Basin followed by exhumed continental mantle and then ocean floor of the North Atlantic. Pre-rifting, the Galicia Bank is believed to have been connected to the Flemish Cap and Orphan Knoll continental fragments (*Sibuet et al.*, 2007b).

6.2 Tectonic Setting

The initial phase of rifting, from late Triassic to early Jurassic, opened up rift basins on the Iberia margin and the Galicia Interior Basin, as well as along the Flemish Pass and Orphan Basin, but not between the Flemish Cap, Orphan Knoll, and Galicia Bank (*Tucholke et al.*, 2007). From basin stratigraphy, the main rifting stage in the Galicia Interior Basin is posited to have occurred during Berriasian to Valanginian (140–132 Ma) (*Tucholke et al.*, 2007). The Galicia Bank rifted away from the Flemish Cap and Newfoundland margin by the Hauterivian-Barremian (126 Ma), but seafloor spreading might not have initiated until the late Aptian-early Albian (115–110 Ma) (*Tucholke et al.*, 2007). However, other models of the Newfoundland-Iberia break-up suggest that rifting between the Galicia Bank and Flemish Cap was concurrent with rifting in the Galicia Interior Basin, Flemish Pass, and Orphan Basin, with seafloor spreading initiating much earlier around 147 Ma (*Srivastava et al.*, 2000; *Sibuet et al.*, 2007a). Still other studies suggest a different time for Newfoundland-Iberia break-up, around 120 Ma, following the main rifting event between the Flemish Cap and Galicia Bank (*Russell and Whitmarsh*, 2003; *Welford et al.*, 2010).

6.3 Continental Fragment Crustal Structure

The Galicia Bank crustal thickness ranges from 13 to 19 km thick (*González et al.*, 1999; *Pérez-Gussinyé et al.*, 2003; *Zelt et al.*, 2003; *Clark et al.*, 2007). Two crustal layers are identified by *Pérez-Gussinyé et al.* (2003): an upper crust with velocities of 5.0–6.3 km s^{-1} and a lower crust with velocities of 6.6–7.0 km s^{-1}. The seismic velocity models of *Zelt et al.* (2003) and *Clark et al.* (2007) do not include crustal reflections, so crustal layering was not addressed in these studies. In these two studies the seismic velocities for the Galicia Bank crust range from 5.5–6.7 km s^{-1} (*Zelt et al.*, 2003; *Clark et al.*, 2007). The Galicia Bank is covered by about 1 km of sediments, which have velocities of 1.8–3.3 km s^{-1} and are correlated to Late Aptian and younger ages (*Pérez-Gussinyé et al.*, 2003). On the N-S oriented refraction line of ISE-9, sediments with velocities of 2.8–3.5 km s^{-1} were imaged with thicknesses around 1 km across the bank and increasing to 3.5 km locally (in small fault-bounded basins) (*Clark et al.*, 2007). Pockets of Hauterivian to late Aptian age sediments are found on the eastern flank of the Galicia Bank (*Pérez-Gussinyé et al.*, 2003).

6.4 Basin Crustal Structure

The Galicia Bank is bound by the Galicia Interior Basin on the east and the Galicia Basin oceanward (Figure 6.1). Further west, the region of exhumed mantle called the Peridotite Ridge is exposed. The southern boundary of the Galicia Bank is marked by thinned continental crust that extends nearly 140 km long from the bank to the Southern Iberian Abyssal Plain, which is believed to be a massive crustal slump (*Clark et al.*, 2007). This mass-wasting hypothesis for the Galicia Bank-Southern Iberian Abyssal Plain boundary is supported by the lack of syn-rift

sediments above the thinned crust in this region (*Clark et al.*, 2007). The Galicia Interior Basin has a crustal thickness ranging from about 5–8 km (*Pérez-Gussinyé et al.*, 2003) to 10–13 km (*González et al.*, 1999; *Zelt et al.*, 2003). *Pérez-Gussinyé et al.* (2003) estimate that the Galicia Interior Basin has undergone a stretching of factor 1.5–2 (at the basin edges) that increases to 5.5 at the center of the basin. At the Galicia Basin, the crust is as thin as 3 km, corresponding to a stretching factor of 10 (*González et al.*, 1999).

Crustal velocities for the Galicia Interior Basin range from 6.2–6.9 km s^{-1} (*Zelt et al.*, 2003) and *Pérez-Gussinyé et al.* (2003) note that the upper crustal layer found on the bounding Galicia Bank and Iberian Shelf thins to less than 1 km in the basin. The upper crust has a high velocity gradient from 5.3–6.3 km s^{-1} and is composed of many small ridges (*Pérez-Gussinyé et al.*, 2003). The lower crust has velocities of 6.6–6.9 km s^{-1} and thins to 5 km in the center of the Galicia Interior Basin (*Pérez-Gussinyé et al.*, 2003). The crustal velocity model beneath the Iberian Shelf is best fit when including a middle crust, but this layer does not continue into the Galicia Interior Basin (*Pérez-Gussinyé et al.*, 2003). Below the Moho, the mantle has low velocities of 7.7–7.8 km s^{-1}, but these velocities are so far unexplained (*Pérez-Gussinyé et al.*, 2003).

The basin fill in the center of the Galicia Interior Basin reaches a thickness of about 5–6 km (*Pérez-Gussinyé et al.*, 2003; *Zelt et al.*, 2003). Using tomographic methods on wide-angle data, *Zelt et al.* (2003) identify three sedimentary layers with velocities ranging from 3 km s^{-1} at the top to 4.7 km s^{-1} at the base. *Pérez-Gussinyé et al.* (2003) identify five sedimentary layers with reflection and refraction methods, with velocities of 1.8–2.9 km s^{-1}, 3.1–3.3 km s^{-1}, 3.35–3.4 km s^{-1}, 3.8–4.3 km s^{-1}, and 4.7–4.9 km s^{-1}. The first three layers correspond to Late Aptian and younger sediments, based on the basal unconformity under layer 3 (*Pérez-Gussinyé et al.*, 2003). Layer 4 and 5 are interpreted as Hauterivian and Valanginian deposits, respectively (*Pérez-Gussinyé et al.*, 2003).

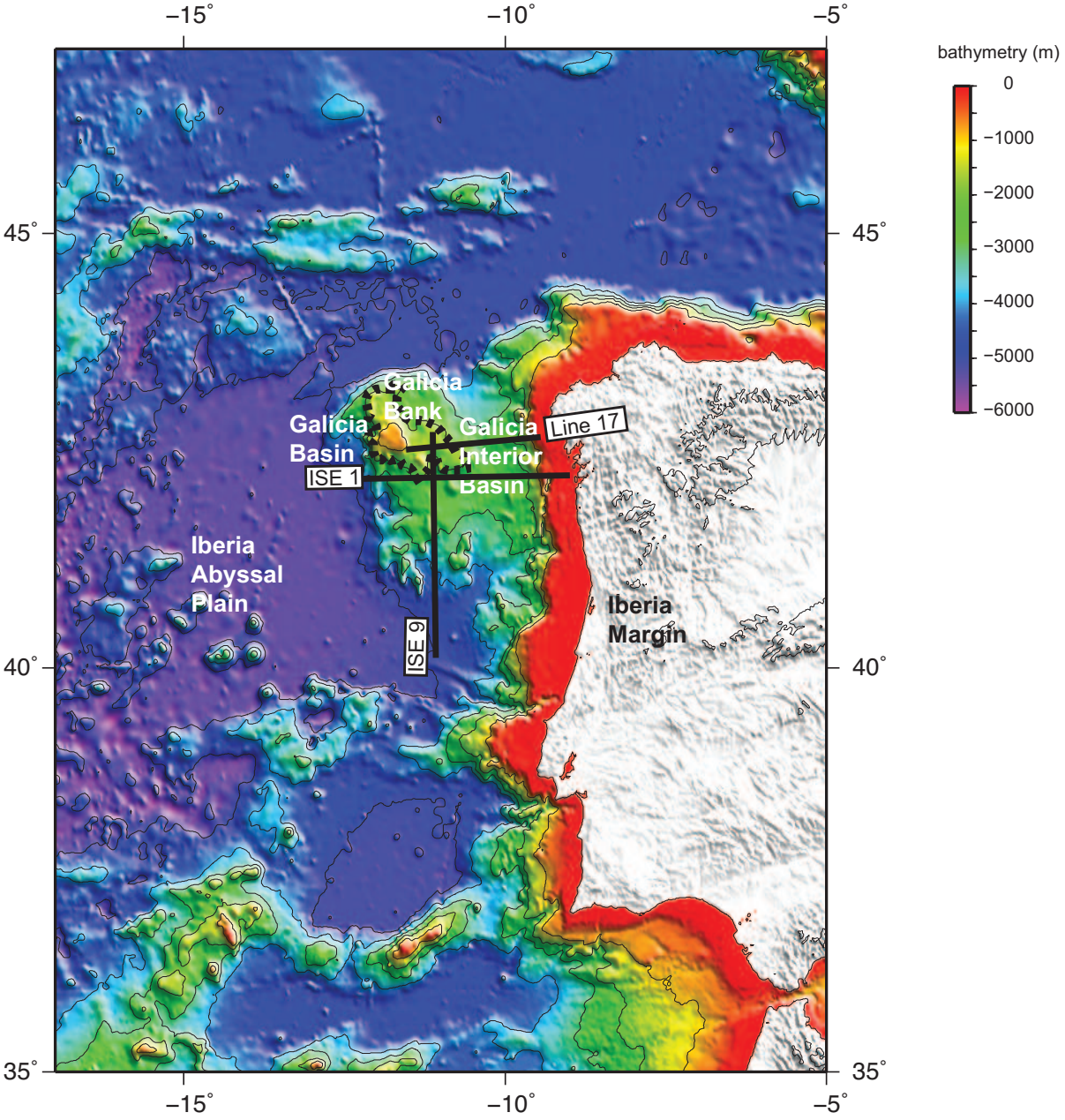

Figure 6.1: Map of the Iberian Margin. The approximate boundaries of the continental fragments are shown in a black dashed line. Seismic refraction/reflection studies from ISE -1 (*Zelt et al.*, 2003), ISE-9 (*Clark et al.*, 2007), and ISE-7 (*Pérez-Gussinyé et al.*, 2003). Bathymetry from ETOPO-1 (*Amante and Eakins*, 2009).

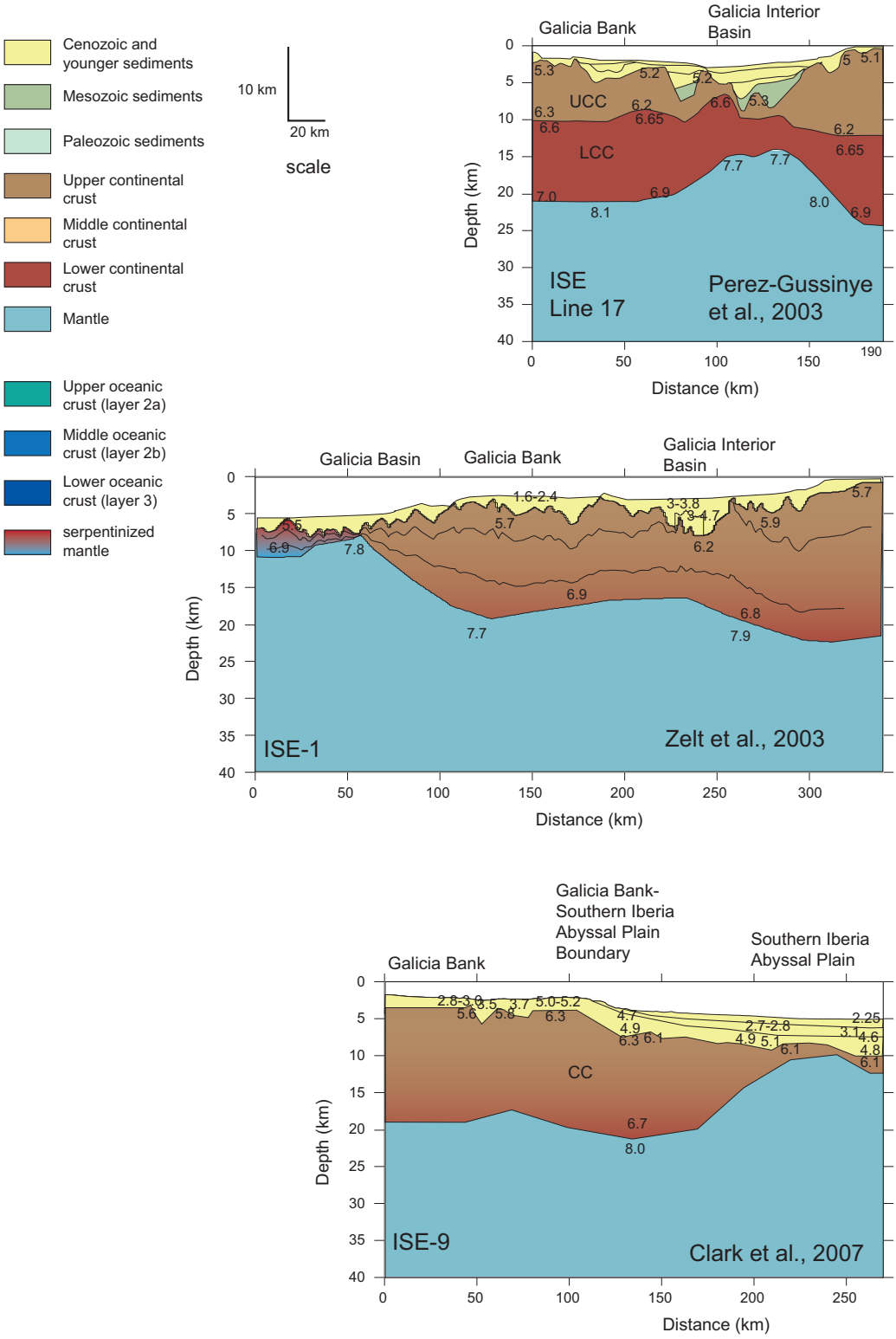

Figure 6.2: Seismic refraction lines across the Grand Banks region. UCC = upper continental crust, LCC= lower continental crust, CC = continental crust. Numbers are seismic velocities in km s^{-1}. All lines are redrawn to a 4:1 vertical exaggeration (modified from *Pérez-Gussinyé et al.* (2003); *Zelt et al.* (2003), and *Clark et al.* (2007)).

7 EAST AUSTRALIAN MARGIN (TASMAN FRONTIER)

7.1 Geologic Background

Off the eastern margin of Australia, several submarine highs of possibly continental origin exist in the Tasman Frontier (Figure 7.1). The Lord Howe Rise, Dampier Ridge, Fairway Ridge, Norfolk Ridge, and New Caledonia Ridge are long, N-S trending fragments between the Tasman Sea and the New Hebrides and Tonga subduction zones. At 1600 km long and 400-500 km wide, the Lord Howe Rise is the largest submarine high in the Tasman Frontier (*Alcock et al.*, 2006), and continues south to the Challenger Plateau and New Zealand continent. The entire region of the Lord Howe Rise-Norfolk Ridge-New Caledonia Ridge and Basin is suspected to be underlain by continental crust and called Zealandia. One hypothesis for formation of the continental fragments surrounding the Tasman Sea is rifting due to rift jumping produced by a plume or hot-spot (*Gaina et al.*, 1998, 2003; *Crawford et al.*, 2003). The ribbon-like continental fragments to the east of the Lord Howe Rise (Norfolk Ridge, New Caledonia Ridge, Fairway Ridge) are separated by thin and long basins which formed due to repetitive back arc-extension and slab rollback (*Sdrolias et al.*, 2003; *Schellart et al.*, 2006; *Sdrolias and Müller*, 2006). To the east and south of these fragments, island arcs that are parallel to the continental fragments include the Loyalty Ridge and the Three Kings Ridge. To the north of the Lord Howe Rise, various submarine highs with possibly continental yet still unconfirmed origin include the Mellish Rise, Louisade Plateau, Kenn Plateau, and Chesterfield Plateau.

The continental affinity of many of these fragments is based on rock samples from dredging, drilling, and field collection on islands. The sparsity of wide-angle seismic data in this region has made it difficult to confirm gravity-derived thicknesses and crustal structure. The crustal thickness of Zealandia ranges from 13 to 30 km, as determined from combined gravity and crustal modeling (*Segev et al.*, 2012). The Zealandia continental crust is suspected to be a continuation of the Lachlan or New England orogens from Australia into New Zealand (*Sutherland*, 1999). The basement beneath the Lord Howe Rise has been drilled and identified as Permian metasedimentary rocks from the Australian New England Orogen (*Mortimer et al.*, 2008). Dating of drill and dredge samples from the Dampier Ridge and Norfolk Ridge indicate they are underlain by continental crust (*McDougall et al.*, 1994; *Mortimer et al.*, 1998).

7.2 Tectonic Setting

Prior to rifting and extension in Zealandia, the region was in compression under the Mesozoic subduction of the Phoenix-Pacific plate. The Norfolk Ridge and its northern extension, the New Caledonia Ridge, separated from the Lord Howe Rise and Australia by the opening via back-arc spreading of the New Caledonia Basin in the early Cretaceous around 120 Ma (*Sdrolias et al.*, 2003; *Schellart et al.*, 2006). Later, the Lord Howe Rise started rifting from continental Australia after 95 Ma (*Gaina et al.*, 1998). Conversely, *Bache et al.* (2014) suggest that concurrent widespread rifting occurred in Zealandia under the New Caledonia Basin and Tasman Sea in the Jurassic to early Cretaceous (between 100 to 85 Ma). At 84 Ma, the rifting in the Lord Howe and Middleton Basins would separate the Lord Howe Rise from the Dampier Ridge (*Gaina et al.*, 1998). The movement of the Lord Howe Rise and Dampier Ridge are suggested to be produced by the hot spot that created the Tasman sea volcanic chain (*Gaina et al.*, 2003). Seafloor sea spreading was active in the Tasman Sea from about 83 to 52 Ma (*Gaina et al.*, 1998, 2003). The Fairway Basin opened in Upper Cretaceous (Cenomanian) and separated the Fairway Ridge from the Lord Howe Rise (*Collot et al.*, 2009). The Norfolk Basin was active

in the late Oligocene to Early Miocene (*Mortimer et al.*, 2014). The Fairway, New Caledonia, and Norfolk basins possibly opened as back-arc basins due to slab rollback (*Schellart et al.*, 2006).

7.3 Continental Fragment Crustal Structure

Very few wide-angle seismic studies have covered the Tasman Frontier. Wide angle seismic studies via two ships performed in the late 60s resulted in 1-D crustal velocity profiles on many of the structures. Only one modern (post 1990s) refraction study has been undertaken to examine the crustal nature of these submarine highs. Of the numerous continental fragments and basins in the Tasman Frontier, only the Lord Howe Rise, Norfolk-New Caledonia Ridge, Fairway Ridge, and their related basins are covered by wide-angle seismic lines that can confirm their crustal thickness, structure, and nature.

7.3.1 Lord Howe Rise

The 1D crustal velocity model of *Shor et al.* (1971) found a crustal thickness of around 27 km on Lord Howe Rise (Figure 7.3). *Klingelhöfer et al.* (2007) models the crustal thickness a bit thinned, at 18-25 km thickness, using wide-angle seismic refraction and gravity methods. The two Zoneco lines cross the Lord Howe Rise and are modeled with three crustal layers (Figure 7.2). The upper crust has a velocity of 4.5–5.8 km s^{-1}, the middle crust has velocities of 6.4–6.6 km s^{-1}, and the lower crust has velocities of 6.6–6.8 km s^{-1} (*Klingelhöfer et al.*, 2007). The low (< 5 km s^{-1}) velocities found in the upper crust lead *Klingelhöfer et al.* (2007) to interpret this layer as volcanic or sedimentary rocks. In comparison, the early crustal velocity profile of *Shor et al.* (1971) divides the crust into two layers with velocities of 5.95 km s^{-1} and 6.8 km s^{-1}.

The sediment thickness above the acoustic basement on Lord Howe Rise ranges from hundreds of meters to 3 km (*Klingelhöfer et al.*, 2007). On the Zoneco-N line, three sedimentary layers are modeled with velocities of 2.15 to 2.7 km s^{-1}, 2.8 to 3.15 km s^{-1}, and 3.2 to 4.6 km s^{-1} (*Klingelhöfer et al.*, 2007). The first layer is correlated to Mid Miocene and younger sediments, the second to upper Eocene to lower Miocene sediments, and the third layer to Cretaceous to Paleocene sequences (*Klingelhöfer et al.*, 2007). Two sedimentary layers are identified in the Zoneco-S line with velocities of 2.16–3.2 km s^{-1} and 3.2–4.3 km s^{-1}(*Klingelhöfer et al.*, 2007). These two layers are correlated to mid Miocene to present sequence and a Cretaceous to Miocene sequence, respectively (*Klingelhöfer et al.*, 2007).

7.3.2 Norfolk-New Caledonia Ridge

The Norfolk Ridge and its northern extension, the New Caledonia Ridge, are covered by four wide-angle seismic lines (Figure 7.2, 7.3). The Norfolk Ridge has a crustal thickness of 17 km and the New Caledonia Ridge has a crustal thickness of 24.5 km (*Klingelhöfer et al.*, 2007). Further south, *Shor et al.* (1971) finds the Moho at 22 km depth and a crustal thickness of 15 km.

The early refraction study of *Shor et al.* (1971) found crustal velocities in the range of 5.9–6.2 km s^{-1}, overlain by a layer with velocities of 4.9 km s^{-1}. The more recent Zoneco lines shed better light on the crustal structure of the Norfolk Ridge. Based on the two wide-angle seismic lines of the Zoneco 11 study, the Norfolk-New Caledonia Ridge has three crustal layers like the rest of Zealandia modeled in these lines (*Klingelhöfer et al.*, 2007). The upper crust has a velocity of 5.0–5.8 km s^{-1}, the middle crust has velocities of 6.4–6.6 km s^{-1}, and the lower crust has velocities of 6.6–6.8 km s^{-1} (*Klingelhöfer et al.*, 2007).

On the Zoneco-S profile, up to 5 km of sediments overlie the basement of the Norfolk Ridge (Figure 7.2). The two sedimentary layers have velocities of 2.16 to 3.2 km s^{-1} and 3.2 to 4.3 km s^{-1}, corresponding to Miocene to younger sediments and Cretaceous to Miocene sequences, respectively (*Klingelhöfer et al.*, 2007). To the north, the New Caledonia Ridge is only covered by a thin (less than 1 km thick) layer of sediments with velocities around 2.2 km s^{-1} (*Klingelhöfer et al.*, 2007).

7.3.3 Fairway Ridge

The Fairway Ridge is only covered by the two Zoneco seismic lines (Figure 7.2). The crust of the Fairway Ridge is about 20–22 km thick, and divided into the same three layers as found on the Lord Howe Rise and Norfolk-New Caledonia Ridge (*Klingelhöfer et al.*, 2007). The velocities for the upper crust, middle crust, and lower crust are 4.75–5.8 km s^{-1}, 6.4–6.6 km s^{-1}, and 6.6–7.25 km s^{-1}, respectively (*Klingelhöfer et al.*, 2007). The east flank of the Fairway Ridge has high lower crustal velocities (7.0–7.25 km s^{-1}), which could be from magmatic underplating in the adjacent New Caledonia Basin. The upper crust is composed of faulted ridges separating smaller basins. The total sedimentary cover thickness varies from 1 to 3 km, and has two layers with velocities of 2.1–2.15 km s^{-1} and 3.2–4.6 km s^{-1} (*Klingelhöfer et al.*, 2007).

7.4 Basin Crustal Structure

7.4.1 New Caledonia Basin

The New Caledonia Basin, to the east of the Lord Howe Rise, has a crustal thickness of 4.5 to 14.7 km according to the early two-ship refraction study of *Shor et al.* (1971) and a thickness of 8 to 10 km on the more recent wide-angle refraction studies of *Klingelhöfer et al.* (2007). The upper crust and lower crust are significantly thinner in the basin than in the surrounding continental fragments (Figure 7.2, 7.3). The upper crust has velocities of 4.0–5.5 km s^{-1}, the middle crust has velocities of 6.4–6.6 km s^{-1}, and the lower crust has velocities of 6.75–7.25 km s^{-1} (*Klingelhöfer et al.*, 2007). In the Zoneco-N seismic line, the crust is interpreted as continental but in the Zoneco-S line it is interpreted as oceanic due to the thinner crustal thickness (*Klingelhöfer et al.*, 2007). The lower crust in Zoneco-N has higher velocities (7.25 km s^{-1}) than typical oceanic crust and continental crust, which could be a result of magmatic underplating but is suggested to possibly be serpentinized mantle (*Klingelhöfer et al.*, 2007).

There is a strong mantle reflector at 35 km depth below the New Caledonia Basin in the Zoneco-N line (Figure 7.2), which is interpreted as lithospheric anisotropy due to extensional shearing rather than a partial melt reservoir because of the lack of excessive magmatism in this region (*Klingelhöfer et al.*, 2007).

The basin fill in the Caledonia Basin is up to 5 km thick. Three sedimentary layers are identified in the Zoneco-N line and two layers in the Zoneco-S line. The OBS stations over the New Caledonia Basin in the NOVA study also identify three layers in the northern part of the basin and two layers further south (*Shor et al.*, 1971). The uppermost sedimentary layer in all refraction studies has velocities around 2.0–2.2 km s^{-1} (*Shor et al.*, 1971; *Klingelhöfer et al.*, 2007). The other two sedimentary layers in the northern part of the basin have velocities around 2.8–3.2 km s^{-1} and 3.2 to 4.9 km s^{-1} (*Shor et al.*, 1971; *Klingelhöfer et al.*, 2007). In the southern part of the New Caledonia Basin, with only two sedimentary layers, the second layer has velocities of 3.2 to 4.3 km s^{-1} (*Shor et al.*, 1971; *Klingelhöfer et al.*, 2007). The three layers in the northern part of the basin, from top to bottom, are interpreted as mid Miocene to present, upper Eocene to lower Miocene, and Cretaceous to Paleocene sequences (*Klingelhöfer et al.*, 2007). In the

southern part of the basin, the two sedimentary layers are interpreted as mid Miocene to present and Cretaceous to Miocene deposits (*Klingelhöfer et al.*, 2007).

7.4.2 Fairway Basin

The Fairway Basin is covered only by the two Zoneco lines (Figure 7.2) and is modeled with a crustal thickness ranging from 10 to 15 km on the Zoneco seismic lines (*Klingelhöfer et al.*, 2007). In the Zoneco-N seismic refraction line, the lower crust and upper crust are significantly thinner in the basin than the surrounding Lord Howe Rise and Fairway Ridge (Figure 7.2). The three crustal layers found in the surrounding continental fragments continue into the Fairway Basin. The upper crust has velocities of 4.75–5.25 km s^{-1}, the middle crust has velocities of 6.4–6.6 km s^{-1}, and the lower crust has velocities of 6.6–6.8 km s^{-1} in the north and 6.6–7.2 km s^{-1} (*Klingelhöfer et al.*, 2007). The higher velocities in the lower crust in the Zoneco-S profile are attributed to possible magmatic intrusions during rifting (*Klingelhöfer et al.*, 2007).

The sedimentary thickness in the Fairway Basin is 3 km in the Zoneco-S line with two sedimentary layers and 4 km in the Zoneco-N line with three layers (*Klingelhöfer et al.*, 2007). In the north, the basin has layers with velocities of 2.10–2.15 km s^{-1}, 2.8–3.15 km s^{-1}, and 3.2–4.6 km s^{-1}, correlated to the same stratigraphic sequences in the basins and fragments of Zealandia (mid Miocene to recent, upper Eocene to lower Miocene, and Cretaceous to Paleocene, respectively) (*Klingelhöfer et al.*, 2007). In the south, the basin fill is thinner and the crust is thicker. The two sedimentary layers in the Zoneco-S line have velocities of 2.16–3.2 km s^{-1} and 3.2–3.8 km s^{-1}, and are correlated to mid Miocene and younger deposits and Cretaceous to Miocene deposits, respectively (*Klingelhöfer et al.*, 2007).

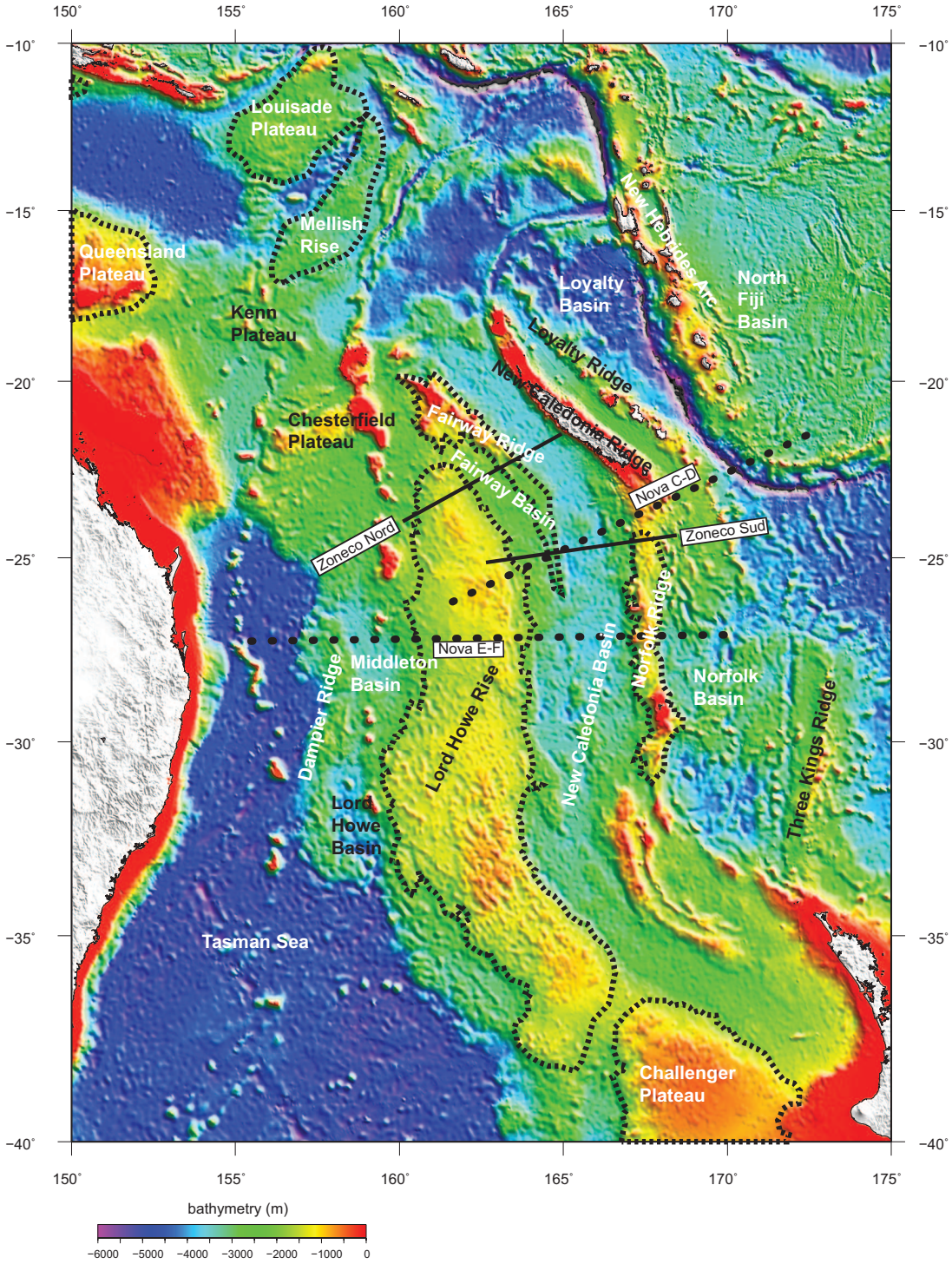

Figure 7.1: Map of the southwest Pacific Ocean. The approximate boundaries of the continental fragments are shown in a black dashed line. The locations of refraction lines from NOVA (*Shor et al.*, 1971) and Zoneco (*Klingelhöfer et al.*, 2007) studies are shown. The two lines from the NOVA study are dotted to signify that this study only resolved 1-D velocity profiles directly under OBS. Bathymetry from ETOPO-1 (*Amante and Eakins*, 2009).

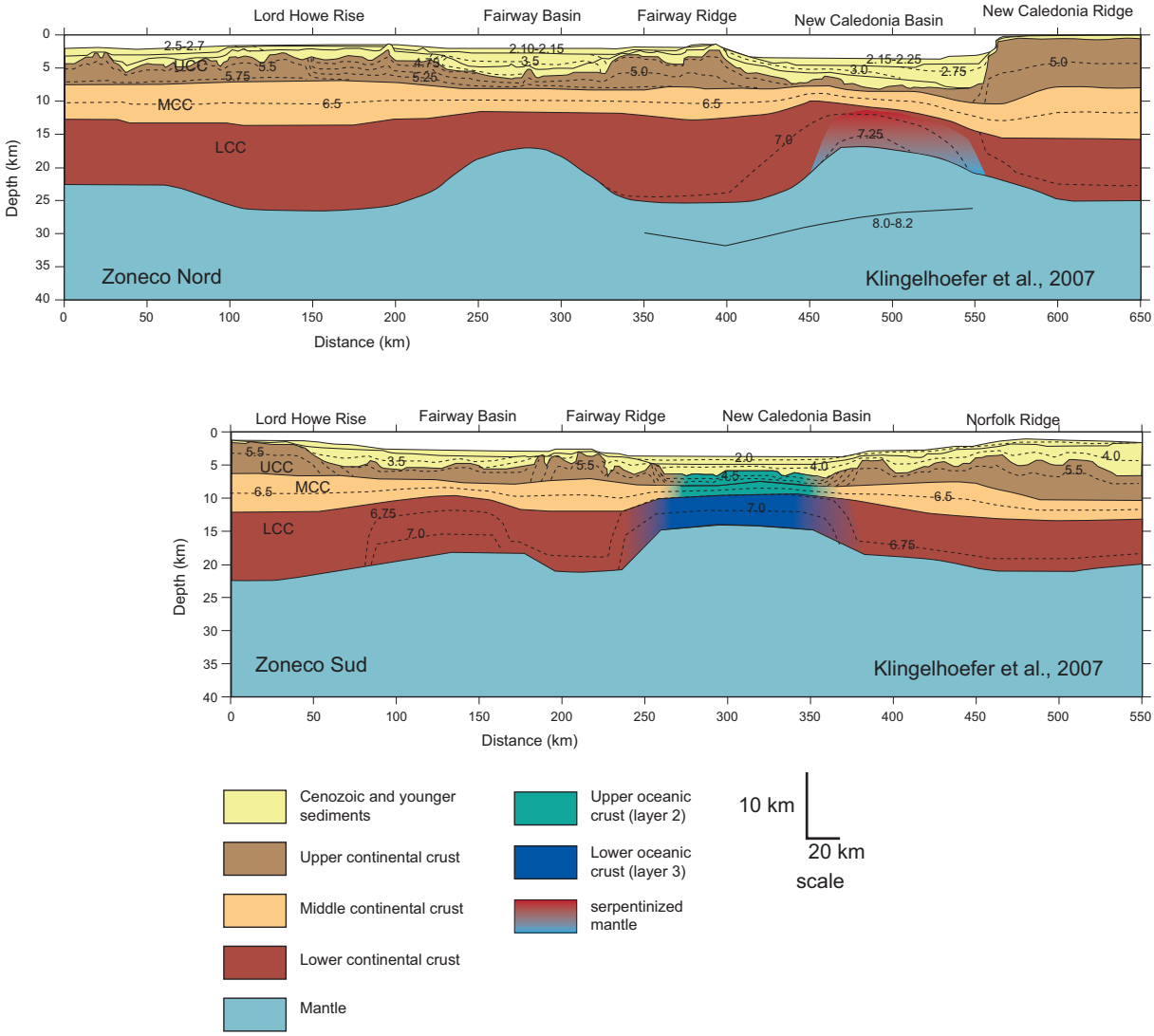

Figure 7.2: Zoneco seismic refraction lines. UCC = upper continental crust, MCC = middle continental crust, LCC= lower continental crust, UOC = upper oceanic crust, LOC = lower oceanic crust. Numbers are seismic velocities in km s^{-1}. All lines are redrawn to the same scale, modified from *Klingelhöfer et al.* (2007). Vertical exaggeration is 4:1.

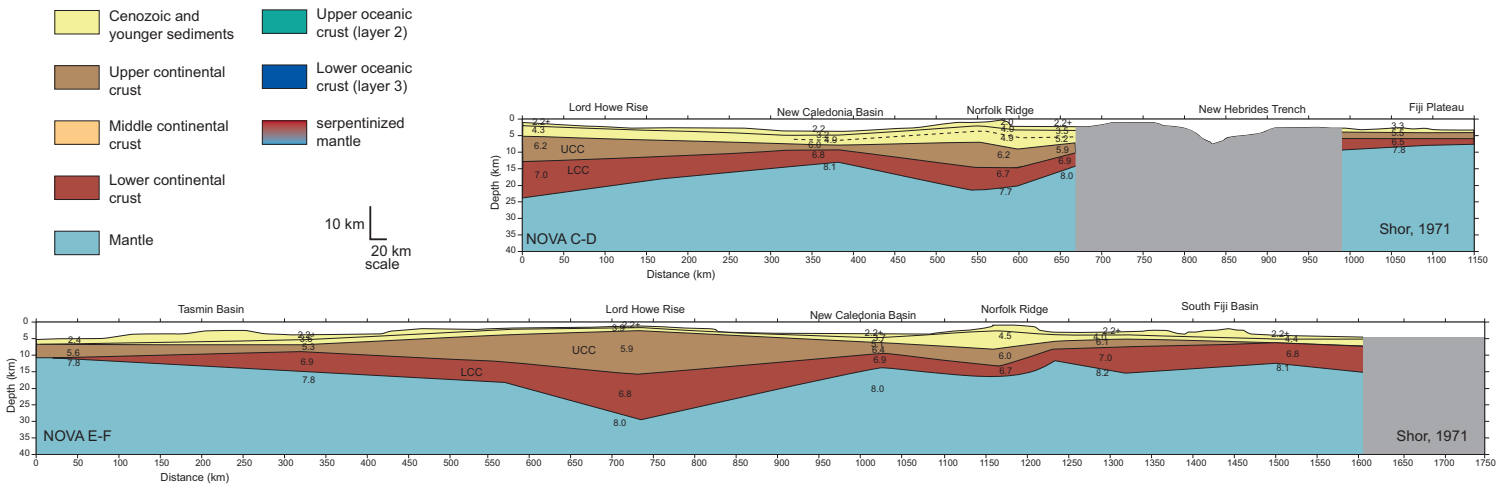

Figure 7.3: NOVA seismic lines across the region. UCC = upper continental crust, LCC= lower continental crust. All lines are redrawn to the same scale, modified from *Shor et al.* (1971). Gray areas represent regions without data coverage. Numbers are seismic velocities in km s^{-1}. Vertical exaggeration is 4:1.

8 THE NEW ZEALAND MARGIN

8.1 Geologic Background

Off the south and eastern margin of New Zealand, a few continental plateaus are perched on the continental shelf. The Campbell Plateau, Bounty Platform, Chatham Rise, Gilbert Seamount, and Bollons Seamount are separated from the North and South Islands by narrow basins (Figure 8.1). To the northeast, the Hikurangi oceanic plateau meets the Chatham Rise at a fossilized Mesozoic subduction zone dipping south. The Bounty Trough separates the Chatham Rise from the Bounty Platform and the Great South Basin separates the Campbell Plateau from the South Island. The Bollons Seamount is a small circular submarine high off the southern margin of the Bounty Platform and is identified as having continental crust based on its high gravity anomaly (*Davy*, 2006). To the west of the South Island, the Challenger Plateau (not a continental fragment) and the Gilbert Seamount are extensions of the Lord Howe Rise and Zealandia. Basement outcrops in the Chatham Islands, the only emergent part of the Chatham Rise, are correlated to the Permo-Triassic Torlesse Supergroup, which underlies the South Island of New Zealand (*Stillwell and Consoli*, 2012).

8.2 Tectonic Setting

Prior to the mid Cretaceous, the Chatham Rise was the active subduction margin of Gondwanaland. The Hikurangi Plateau briefly attempted to subduct under the Chatham Rise at around 105 Ma, before shifting to subduction under the North Island (*Davy et al.*, 2008). Rifting between the Chatham Rise and West Antarctica began around 90 Ma (*Larter et al.*, 2002). The Bounty Trough, separating the Chatham Rise from the Bounty Platform, is suggested to also have opened with the break-up of the Chatham Rise-Antartica rift (*Carter et al.*, 1994; *Larter et al.*, 2002). Extension in the Great South Basin and the Bounty Trough is estimated to have ended by 83 Ma (*Eagles et al.*, 2004). The Bollons Seamount was created by rift jumps during the opening of the Bounty Trough and was transported away from the Bounty Platform along transform faults (*Davy*, 2006). After chron 34–33 (83–76 Ma), seafloor spreading between Zealandia and Marie Byrd Land in Antarctica began, and the ancient Bellinghausen Plate was created (*Eagles et al.*, 2004). During this time (chron 33r: 83–79 Ma), the Campbell Plateau is separated from Antarctica (*Larter et al.*, 2002). Pre-breakup extension between the Campbell Plateau and Antarctica occurred at 89–82 Ma (*Veevers*, 2012).

Late Cretaceous extension in the Bounty Trough is theorized to have occurred in a pre-existing basement weakness due to earlier Cretaceous subduction related back-arc spreading (*Carter et al.*, 1994) or due to back-arc spreading from the Chatham subduction zone (*Schellart et al.*, 2006). The initial back-arc rifting in the Bounty Trough is linked to the New Caledonia back-arc spreading at about 105 Ma (*Uruski*, 2014). Afterwards, the Bounty Trough experienced inversion during the collision of the Hikurangi Plateau with the Chatham Rise in the late Cretaceous (*Grobys et al.*, 2008). Late Cretaceous extension in the Campbell Plateau and Great South Basin region is also suggested to be back-arc spreading related to the Chatham subduction zone (*Schellart et al.*, 2006).

On the other side of New Zealand, the Gilbert Seamount and Challenger Plateau were part of the Zealandia continental crust and connected to the Lord Howe Rise. The Gilbert Seamount rifted from the continental fragments off of the Tasmanian Margin and the Lord Howe Rise at 77 Ma (*Gaina et al.*, 2003). The opening of the Tasman Sea left the Gilbert Seamount separated as a microcontinent.

8.3 Continental Fragment Crustal Structure

8.3.1 Chatham Rise

The wide-angle seismic line AWI-20030002 of the CAMP study (herein referred to as CAMP-2) traverses into the Chatham Rise (Figure 8.1, 8.2). The crustal thickness of the Chatham Rise was previously estimated by gravity modeling to be around 23–26 km (*Davy and Wood*, 1994). Comparatively, the CAMP-2 study yields a crustal thickness of about 22 km (*Grobys et al.*, 2007). The crust is divided into two layers, with upper crustal velocities ranging from 5.5–6.5 km s^{-1} and lower crustal velocities of 6.2–7.0 km s^{-1} (*Grobys et al.*, 2007).

Two sedimentary layers overlie the basement on the Chatham Rise, as determined by the refraction study of CAMP-2 (*Grobys et al.*, 2007). The upper sedimentary layer is about 1 km thick with velocities of 2.0–3.5 km s^{-1} (*Grobys et al.*, 2007). The lower sedimentary layer has velocities of 3.3–6.0 km s^{-1} and is about 3 km thick (*Grobys et al.*, 2007).

8.3.2 Bounty Platform

The Bounty Platform is also partly covered by the CAMP-2 refraction line (Figure 8.1,8.2) and has a crustal thickness of about 23 km (*Grobys et al.*, 2007). The crust is divided into two layers with thicknesses of 8 km and 15 km (*Grobys et al.*, 2007). The upper crust has velocities of 6.0–6.5 km s^{-1} and the lower crust has a velocity of 6.2–7.0 km s^{-1} (*Grobys et al.*, 2007).

The basement is overlain by two sedimentary layers. The upper sedimentary layer has a thickness of 100 m and velocities of 2.0–3.5 km s^{-1} (*Grobys et al.*, 2007). The lower sedimentary layer has a thickness of 3–4 km with velocities ranging from 3.5 km s^{-1} at the top to 5.7–6.0 km s^{-1} at the base of the layer (*Grobys et al.*, 2007). These high seismic velocities are interpreted as a transition from sediments to basement (*Grobys et al.*, 2007).

8.3.3 Campbell Plateau

The large Campbell Plateau is only covered by one wide-angle refraction seismic line: the AWI-20030001 line, herein referred to as CAMP-1 of *Grobys et al.* (2009). Across the CAMP-1 seismic line, the Campbell Plateau has a crustal thickness of about 22–24 km (*Grobys et al.*, 2009). The upper crust has velocities of 5.0–7.1 km s^{-1} and the lower crust has velocities of 7.1–7.5 s^{-1} (*Grobys et al.*, 2009). The high velocities of the lower crust are interpreted as magmatic underplating and those in the upper crust are related to shallow diking (*Grobys et al.*, 2009).

The sedimentary cover on the Campbell Plateau is less than 2 km thick, and has four identifiable layers in the combined reflection/refraction study on seismic line CAMP-1 (*Grobys et al.*, 2009). The sedimentary layers have velocities of 1.7–2.5 km s^{-1}, 2.3–3.1 km s^{-1}, 2.5–4.0 km s^{-1}, and 4.4–4.9 km s^{-1} (*Grobys et al.*, 2009). The higher velocities of the basal sedimentary layer are suggested to be due to magmatic intrusions (*Grobys et al.*, 2009).

8.4 Basin Crustal Structure

8.4.1 Bounty Trough

Between the Chatham Rise and the Bounty Platform, the Bounty Trough is covered by the CAMP-2 refraction line (Figure 8.2) and is modeled with a crustal thickness of about 9 km which is interpreted as thinned continental crust (*Grobys et al.*, 2007). Close to the South Island, *Van Avendonk et al.* (2004) find a crustal thickness of 16 km for the Bounty Trough. On the CAMP-2 refraction line, *Grobys et al.* (2007) find an upper crust with thickness of 3

km and velocities ranging from 5.0–6.0 km s^{-1} at the top to 6.0–7.2 km s^{-1} at the base. The lower crust has a thickness of 6 km with velocities of 6.2–7.0 km s^{-1} (*Grobys et al.*, 2007). The highest velocities in the upper crust and lower crust are found in the southern part of the Bounty Trough. The lower crust at the southern Bounty Trough has velocities up to 7.2–7.7 km s^{-1} (*Grobys et al.*, 2007). The Bounty Trough imaged on the southeastern end of the SIGHT-2 seismic line has a 13 km-thick upper crust with velocities around 6.0 km s^{-1} underlain by a thin lower crust with velocities around 7.1 km s^{-1} (*Van Avendonk et al.*, 2004). These regions of the lower crust with high velocities are interpreted as magmatic intrusions within the lower crust.

On the CAMP-2 refraction line, the two sedimentary layers on the surrounding continental fragments continue into the Bounty Trough with combined thickness of 5–6 km (Figure 8.2). The upper sedimentary layer has velocities of 2.0–3.5 km s^{-1} and a thickness of around 2 km, and the lower sedimentary layer has velocities of 3.5–4.9 km s^{-1} (*Grobys et al.*, 2007). A complementary reflection study across CAMP-2 identified four sedimentary layers (*Uenzelmann-Neben et al.*, 2009). The authors were able to correlate the four layers to those found in the earlier stratigraphic study of *Carter et al.* (1994) which defines the layers as Cretaceous-Paleocene, Eocene-Oligocene, mid Oligocene-late Miocene, and late Miocene-Recent deposits.

8.4.2 Great South Basin

The Great South Basin is a narrow trough with thinned continental crust separating the Campbell Plateau from the mainland of South Island. The CAMP-1 refraction line is the only wide-angle seismic line that traverses the basin (Figure 8.2). The crustal thickness under the Great South Basin is about 13 km and is divided into two layers (*Grobys et al.*, 2009). The upper crust has velocities of 5.5–6.5 km s^{-1} and the lower crust has velocities of 6.5–7.1 km s^{-1} (*Grobys et al.*, 2009). Compared to the 30–45 km thick crust of the South Island, *Grobys et al.* (2009) estimated a stretching factor of 2.7 to 3.0 for the Great South Basin.

The basin fill is up to 8 km thick with four sedimentary layers (*Grobys et al.*, 2009). The sedimentary layers, from top to bottom, have thicknesses of 0.75 km, 0.9 km, 1.1 km, and about 2 km (*Grobys et al.*, 2009). The velocities of these layers are 1.7–2.5 km s^{-1}, 2.3–3.8 km s^{-1}, 2.5–4.0 km s^{-1}, and 3.8–5.8 km s^{-1}, respectively (*Grobys et al.*, 2009). The four layers are correlated with well logs and seismic datasets to Cretaceous, late Cretaceous-Paleocene, Eocene, and Miocene-recent deposits (*Grobys et al.*, 2009).

Below the Great South Basin, the mantle velocities are low (7.7 km s^{-1}), matching results from nearby surveys on the South Island, and are interpreted to be produced by thermal perturbations in the upper mantle (*Grobys et al.*, 2009).

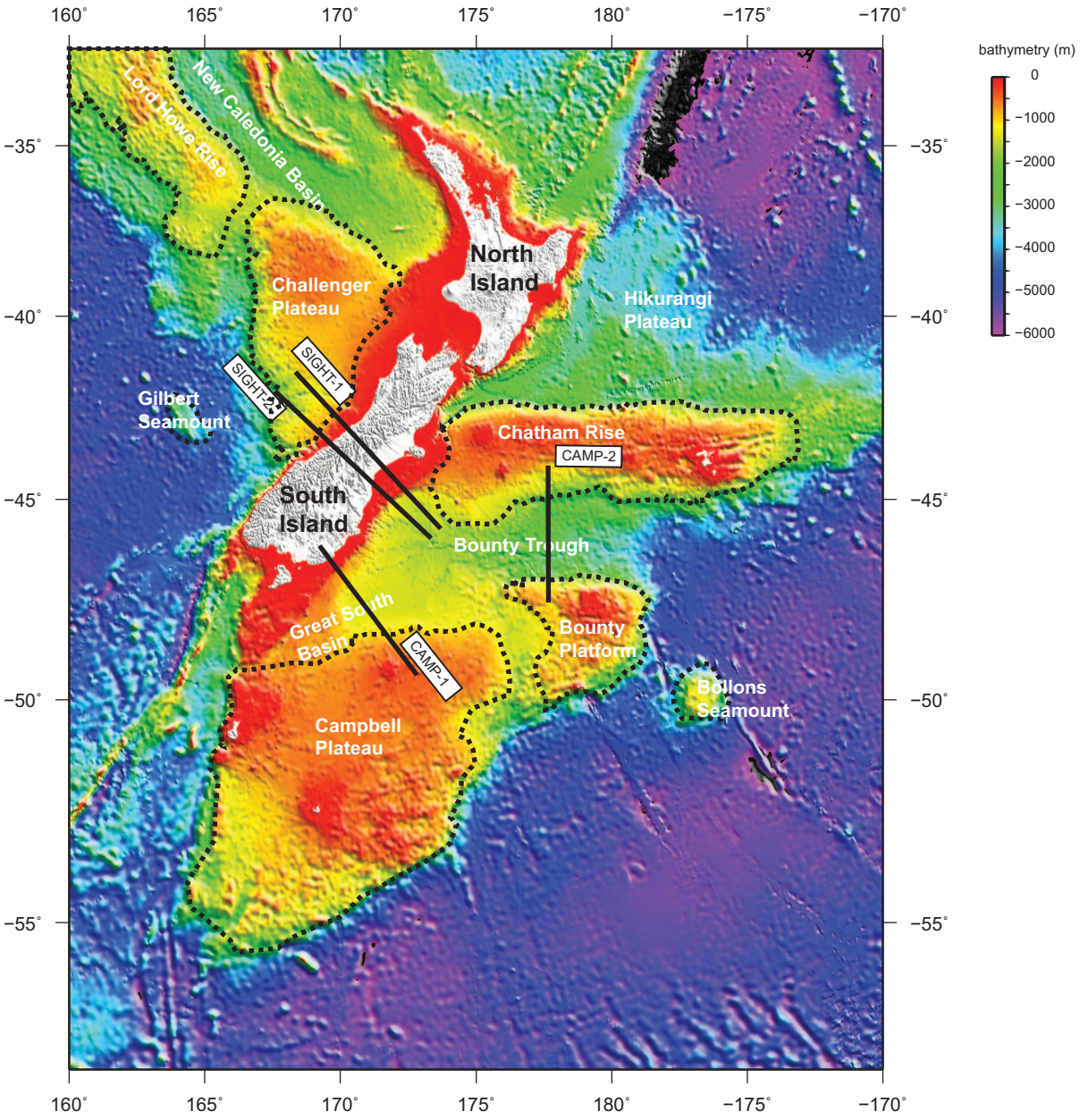

Figure 8.1: Map of the New Zealand passive margins. The approximate boundaries of the continental fragments are shown in a black dashed line. The locations of refraction lines from the CAMP-1 (*Grobys et al.*, 2009), CAMP-2 (*Grobys et al.*, 2007), SIGHT-1(*Van Avendonk et al.*, 2004), and SIGHT-2 (*Scherwath et al.*, 2003) studies are shown. Bathymetry from ETOPO-1 (*Amante and Eakins*, 2009).

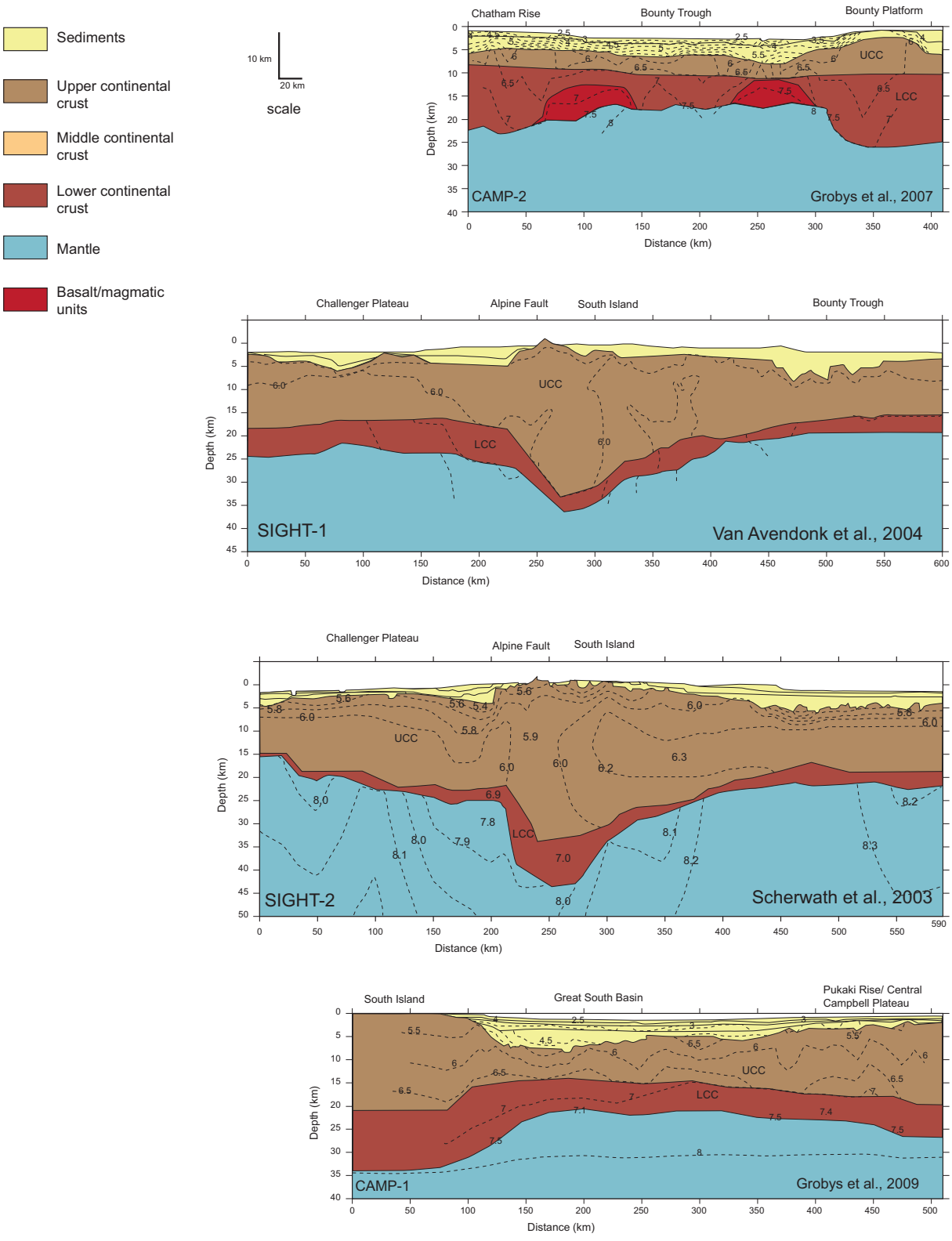

Figure 8.2: Seismic refraction lines across the region. UCC = upper continental crust, LCC= lower continental crust. All lines are redrawn to a 4:1 vertical exaggeration (modified from *Scherwath et al.* (2003); *Van Avendonk et al.* (2004); *Grobys et al.* (2007), and *Grobys et al.* (2009)). Numbers are seismic velocities in km s^{-1}.

9 THE WEST AUSTRALIAN MARGIN

9.1 Geologic Background

The passive margin of western Australia has a few small continental fragments and oceanic plateaus (Figure 9.1). The Naturaliste Plateau in the southwestern margin, is separated from Australia by the Naturaliste Trough and Mentelle Basin. In the northwestern margin, the Exmouth Plateau, Wallaby Plateau, and Zenith Plateau are all submarine highs. West of the Perth Abyssal Plain, two new small microcontinents were recently confirmed: the Batavia Knoll and the Gulden Draak Knoll (*Whittaker et al.*, 2013; *Gardner et al.*, 2015). Unfortunately, no published wide-angle seismic studies have been performed over any of the continental fragments on the western margin of Australia.

The exact crustal nature of the Wallaby Plateau is still debated. Some authors suggest that the Wallaby Plateau is thickened oceanic crust or a large igneous plateau based on seismic reflection studies and dredged basalts (*Colwell et al.*, 1994; *Mihut and Müller*, 1998; *Müller et al.*, 2002). Others believe the Wallaby Plateau to be extended continental crust that has been highly intruded by volcanics (*Brown et al.*, 2003; *Alcock et al.*, 2006). More recent paleontological and geological data from dredging and seismic reflection data strongly support the continental crust origin for the Wallaby Plateau (*Stilwell et al.*, 2012; *Goncharov and Nelson*, 2012).

The Zenith Plateau is also a submarine high of unknown crustal nature, similar to the Wallaby Plateau. Many authors believe it to be of volcanic/oceanic origin (*Mihut and Müller*, 1998; *Müller et al.*, 2002; *Alcock et al.*, 2006). Alternatively, new plate reconstructions of the India-Australia breakup position the Zenith Plateau as continental crust, related to the Wallaby Plateau (*Gibbons et al.*, 2012). Assuming the Zenith and Wallaby Plateaus have oceanic-type crustal affinities, the crustal thicknesses were isostatically modeled to be 18.2 km and 17.4 km, respectively (*Mihut and Müller*, 1998).

The Exmouth Plateau is a marginal plateau within the Carnavon Basin region that is separated from northwestern Australia by several thin basins: the Exmouth sub-basin, Dampier sub-basin, and the Barrow sub-basin (Figure 9.1). Technically the Exmouth Plateau, much like the Queensland Plateau of northeastern Australia and the Challenger Plateau of New Zealand, is not a continental fragment because it is attached to the mainland margin. Seaward dipping reflectors and intruded volcanics in the upper crust and sedimentary fill are imaged in seismic reflection lines above the Exmouth Plateau (*Mutter and Larson*, 1989; *Hopper et al.*, 1992; *Direen et al.*, 2008; *Rohrman*, 2013).

The Naturaliste Plateau is a continental fragment separated from Australia by the Naturaliste Trough and Mentelle Basin (Figure 9.1). Some authors classify the northern margin of the Naturaliste Plateau as a volcanic margin based on dredged basalts and seismically interpreted volcanics (*Borissova*, 2002; *Halpin et al.*, 2008), whereas the absence of volcanics on the southern margin of the plateau lead to the classification of that margin as a non-volcanic passive margin (*Direen et al.*, 2007). Just south of the Naturaliste Plateau is the Diamantina Fracture Zone, where exhumed and serpentinized mantle composes a wide region of the rifted passive margin. Zircon-dating of dredge samples from the Naturaliste Plateau yield Cambrian ages and are correlated to the Albany-Frasier-Wilkes orogen of Australia and Antarctica (*Halpin et al.*, 2008). Potential field modeling of the southern Naturaliste Plateau margin yields a continental crust thickness of 7 to 12 km (*Direen et al.*, 2007).

The Batavia Knoll and Gulden Draak Knoll are two small microcontinents whose continental affinity was recently confirmed by dredge samples of granites, gneisses, and schists (*Whittaker et al.*, 2013; *Gardner et al.*, 2015). Zircon-dating of the samples from the Batavia Knoll produce Paleozoic ages (540 - 530 Ma) (*Whittaker et al.*, 2013). Orthogneiss samples from the Gulden Draak Knoll have Archean (2.8 Ga) and Mesoproterozoic (1.3 - 1.2 Ga) ages and are intruded by Cambrian granites, just like the ages recovered from dredge samples from the Naturaliste Plateau; therefore the Gulden Draak Knoll is correlated to the Leeuwin Complex of western Australia (*Gardner et al.*, 2015). The inferred basement relationships of these microcontinents places them on the Indian margin of the Naturaliste Plateau, pre-breakup (*Gardner et al.*, 2015). *Gibbons et al.* (2012) suggest that these microcontinents and the Wallaby, Zenith, and Naturaliste continental fragments were created by a series of small rift jumps from 136 Ma to about 100 Ma.

9.2 Tectonic Setting

Seismic stratigraphy work by *Driscoll and Karner* (1998) indicate that early rifting in the Carnavon Basin occurred around the Permian, followed by rifting in the Exmouth and Dampier sub-basins in the Late Triassic. Continental breakup of Australia with Greater India occurred in the Argo Abyssal Plain with seafloor spreading in the Late Jurassic (*Veevers et al.*, 1991). Recent stratigraphic and magnetic studies on the Gascoyne and Argo Abyssal plains pinpoint seafloor spreading around 155.0 Ma (*Heine and Müller*, 2005; *Seton et al.*, 2012). Coinciding with the opening of the Cuvier Abyssal Plain in chron M11 (around 130 Ma), extension and magmatism occurred in the Wallaby Plateau and Wallaby Saddle (*Sayers et al.*, 2002). *Gibbons et al.* (2012) suggest that rifting in the Cuvier Abyssal Plain jumped at 128 Ma and abandoned the Wallaby Saddle.

Further south along the western margin of Australia, the Perth Abyssal Plain marked the opening between India and Australia-Antarctica. The first stage of rifting in the Perth Basin (at the continental edge of the Perth Abyssal Plain) and the Mentelle Basin was during the Early to Mid Permian, forming N-NNW oriented intracratonic grabens (*Hall et al.*, 2013). Break-up finally occurred in the Perth Abyssal Plain in the Valanginian-Late Hauterivian (136 Ma), separating Australia from India (*Gibbons et al.*, 2012; *Hall et al.*, 2013; *Williams et al.*, 2013). Extension and breakup occurred in the Mentelle Basin also around 136 Ma, finally separating the Naturaliste Plateau from Australia (*Maloney et al.*, 2011). A rift jump in the Perth Abyssal Plain around 127 Ma separated the Gulden Draak Knoll and Batavia Knoll from Australia and the Naturaliste Plateau (*Gibbons et al.*, 2012; *Whittaker et al.*, 2013). Westward ridge jumps during the formation of the Perth Abyssal Plain is posited to be caused by the Kerguelen Plume, which eventually produced the Broken Ridge-Kerguelen large igneous province (*Williams et al.*, 2013). Slow extension between Australia and Antarctica starting in the Campanian (83 Ma), which led to the exhumed mantle in the Diamantina Zone, and final break-up at 43 Ma separated the Naturaliste Plateau from Antarctica (*Borissova*, 2002).

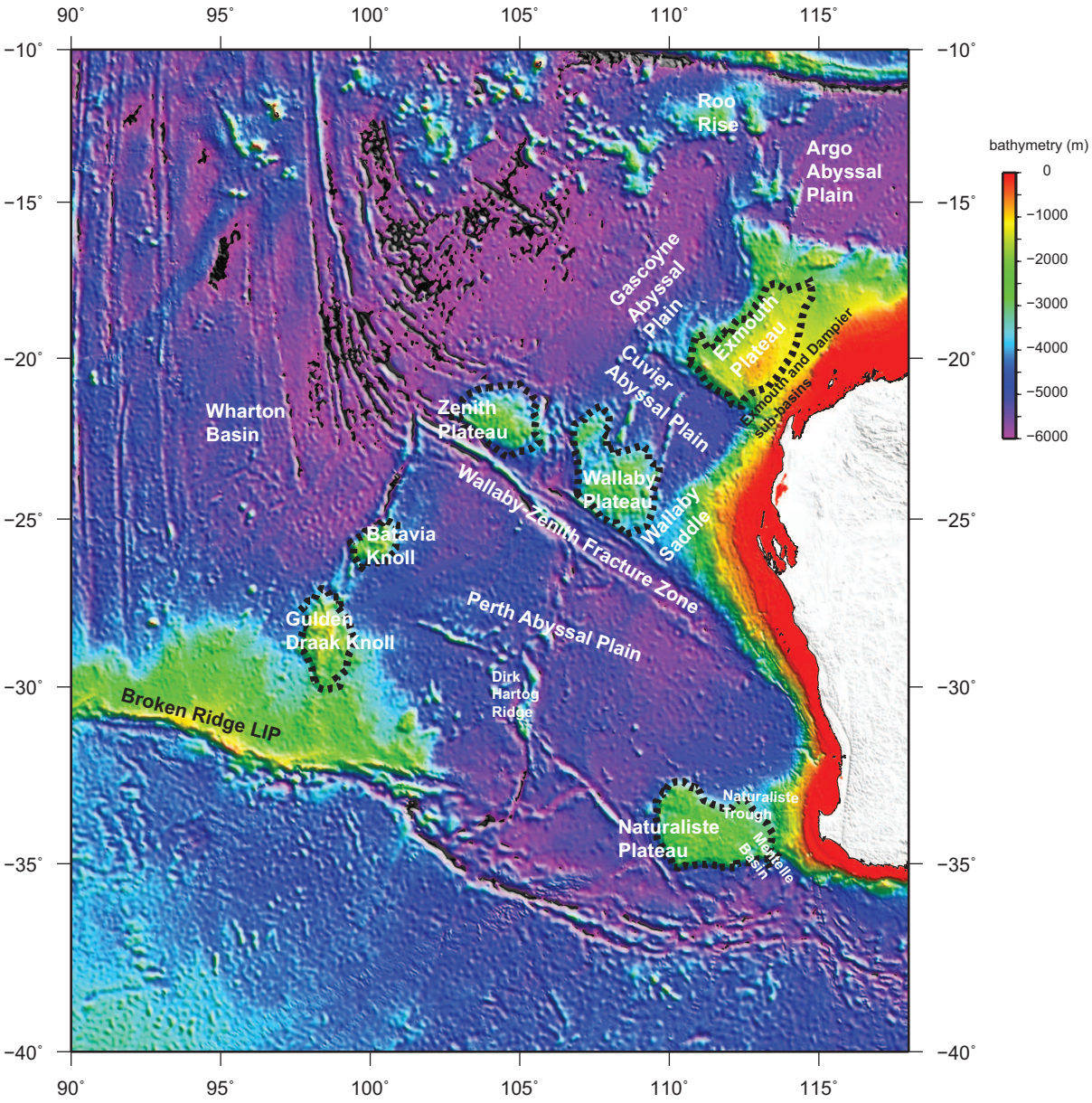

Figure 9.1: Map of the western Australia passive margin. The approximate boundaries of the continental fragments Naturaliste Plateau, Exmouth Plateau, Wallaby Plateau, Zenith Plateau, Batavia Knoll, and Gulden Draak Knoll are shown in a black dashed line. The Broken Ridge and Roo Rise oceanic plateaus are also shown. Bathymetry from ETOPO-1 (*Amante and Eakins*, 2009).

10 THE TASMANIAN MARGIN

10.1 Geologic Background

The East Tasman Plateau and South Tasman Rise are two continental fragments separated from Tasmania by narrow basins (Figure 10.1). There are no wide-angle seismic refraction lines covering this region. Numerous samples from dredging and drills as well as seismic reflection data confirm the continental origin of these plateaus (*Exon et al.*, 1997; *Hill and Moore*, 2001). However, the East Tasman Plateau is capped by the large volcanic Cascade Seamount, suggesting that high amounts of Tertiary volcanism occurred in this region (*Exon et al.*, 1997). The Cascade Seamount volcanics are dated at 36 - 40 Ma and are related to basalts in the l'Atalante Depression, both interpreted as having a hot spot signature (*Hill and Moore*, 2001). Geologically, the South Tasman Rise is composed of two terranes connect by left-lateral wrenching: the western domain was originally part of Antarctica and the eastern domain was part of Tasmania (*Royer and Rollet*, 1997).

10.2 Tectonic Setting

Rifting in the late Cretaceous occurred in the East Tasman Saddle and South Tasman Saddle with the opening of the the Tasman Sea (*Exon et al.*, 1997; *Royer and Rollet*, 1997). Seafloor spreading in the Tasman Sea began by chron 34 (83 Ma), separating the East Tasman Plateau from the Lord Howe Rise (*Royer and Rollet*, 1997; *Gaina et al.*, 2003). *Royer and Rollet* (1997) suggested that a short-lived triple junction (from chron 33 to chron 30) formed between the South Tasman Rise, East Tasman Plateau and Lord Howe Rise. *Gaina et al.* (2003) suggest that the South Tasman Rise rifted from the Gilbert Seamount at 77 Ma. The South Tasman Rise did not separate from Antarctica until the Eocene (circa 40 Ma) (*Royer and Rollet*, 1997; *Gaina et al.*, 1998). A possible hotspot under the Tasman Sea is invoked to produce the ridge jumps in the Tasman Sea which led to the the formation of the two continental fragments in the Tasman Rise region (*Gaina et al.*, 2003).

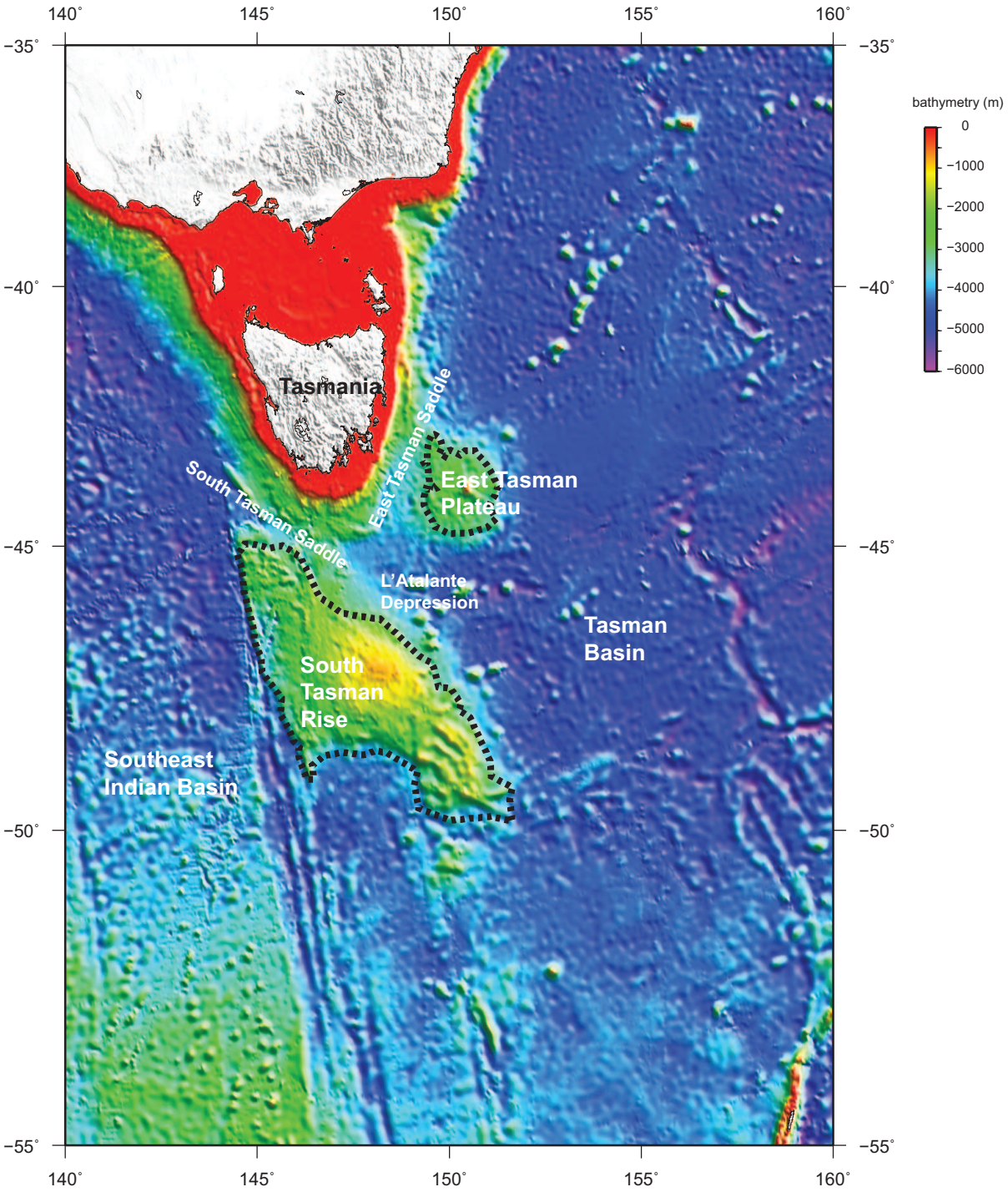

Figure 10.1: Map of the South Tasman Rise region. The approximate boundaries of the continental fragments South Tasman Rise and East Tasman Plateau are shown in a black dashed line. Bathymetry from ETOPO-1 (*Amante and Eakins*, 2009).

11 ELAN BANK MICROCONTINENT

11.1 Geologic Background

The Elan Bank is a microcontinent stranded in the large igneous province (LIP) of the Cretaceous Kerguelen Plateau in the Southern Indian Ocean (Figure 11.1). To the west of the Elan Bank lies the Enderby Basin and to the north, the Crozet Basin. The Kerguelen Plateau-Elan Bank composite terrane is on the Antarctic plate and is bordered by the Labuan Basin and Southwest Indian Ridges to the east and to the south by the Princess Elizabeth Trough.

The continental nature of the Elan Bank is supported by Proterozoic gneiss clasts found in ODP 1137 that are correlated to the Eastern Ghats Belt of India (*Nicolaysen et al.*, 2001; *Ingle et al.*, 2002). Plate reconstructions suggest that Elan Bank was once part of Greater India, but separated from India during the India-Antarctic breakup and subsequent Kerguelen-Broken Ridge emplacement (*Gaina et al.*, 2003; *Gibbons et al.*, 2013). The exact extent of continental crust under the Kerguelen Plateau is still unknown and the microcontinent may be larger based on low seismic velocities in the Raggatt Basin correlated to continental crust and a continental signature in geochemical analyses of Kerguelen magmas (*Operto and Charvis*, 1995; *Borissova et al.*, 2003; *Benard et al.*, 2010).

11.2 Tectonic Setting

The Elan Bank microcontinent formed during the break-up of Australia, India, and Antarctica. *Seton et al.* (2012) suggest that rifting in the Enderby Basin began at 160 Ma, to coincide with the initiation of rifting between India and Antarctica. Break-up and seafloor spreading in the Enderby Basin between Australia-Antarctica and Greater India followed at around 130 Ma, with Elan Bank still attached to Greater India, the same time as rifting and seafloor spreading in the Perth Abyssal Plain in southwestern Australia occurred (*Gaina et al.*, 2003). Spreading in the Princess Elizabeth Trough, as a continuation of the Enderby Basin seafloor spreading, also occurred around 130 Ma (*Gibbons et al.*, 2013). At circa 120 Ma, the rift jumped north towards the Kerguelen plume and the Elan Bank was separated from India (*Gaina et al.*, 2003, 2007). However, seafloor spreading did not cease until 115 Ma in the Enderby Basin, south of Elan Bank (*Gibbons et al.*, 2013).

The Kerguelen hotspot, which produced the Kerguelen Plateau, Broken Ridge, Ninetyeast Ridge, Australian Bunbury basalts, and Indian Rajmahal Traps, was active from about 130 Ma to present (*Coffin*, 1992; *Coffin et al.*, 2002). Initial emplacement of the Bunbury basalts in western Australia at 132 Ma coincided with the spreading in the Perth Abyssal Plain and in the Enderby Basin (*Coffin*, 1992). The Kerguelen LIP was emplaced in parts, from south to north starting around 120 Ma (*Coffin et al.*, 2002; *Duncan*, 2002), around the time that the rift jumped and separated the Elan Bank from India. The Kerguelen-Elan Bank composite terrane broke apart from the younger Broken Ridge and Ninetyeast Ridge LIPs with the opening of the Australia-Antarctic basin around 40 Ma (*Borissova et al.*, 2002; *Seton et al.*, 2012).

11.3 Crustal Structure

Only one seismic refraction line, Line 6 of *Borissova et al.* (2003), has been carried out across the Elan Bank (Figure 11.1, 11.2). The crustal thickness of the Elan Bank, not including the thin layer of sediments, is 16–17 km thick (*Borissova et al.*, 2003). The upper crust is 2–3 km thick and interpreted to be lava flows, based on a similar layer that has been drilled in the Kerguelen Plateau (*Borissova et al.*, 2003). Velocities within the upper crust range from 4.4–4.9 km s^{-1} at

the top and 5.2–5.9 km s^{-1} at the base (*Borissova et al.*, 2003). The lower crust is about 14 km thick with velocities ranging from 6.0–6.7 km s^{-1}, indicative of continental crust (*Borissova et al.*, 2003). The Moho is imaged with a strong reflection at 18 km depth, and another strong reflection (R3) within the crust is found at 12.5 km depth (*Borissova et al.*, 2003). The basement is overlain with a thin layer of sediments (up to 1 km thick) with velocities modeled at 2.1 km s^{-1} (*Borissova et al.*, 2003).

11.4 Basin Crustal Structure

The Enderby Basin bounds the Elan Bank on the west and south (Figure 11.1) and is crossed by one seismic refraction line (Line 7) near the Elan Bank margin (Figure 11.2). The Enderby Basin is oceanic with a thickness of 10–13 km under Line 7 (*Charvis and Operto*, 1999). Velocities in the upper crust (oceanic layer 2) range from 5.0 km s^{-1} to 6.3–6.5 km s^{-1} at the base (*Charvis and Operto*, 1999). The lower crust (oceanic layer 3) has velocities of 6.7–6.87 km s^{-1} at the top of the layer grading to 7.24–7.32 km s^{-1} at the base (*Charvis and Operto*, 1999). The sedimentary layers is less than 1 km thick.

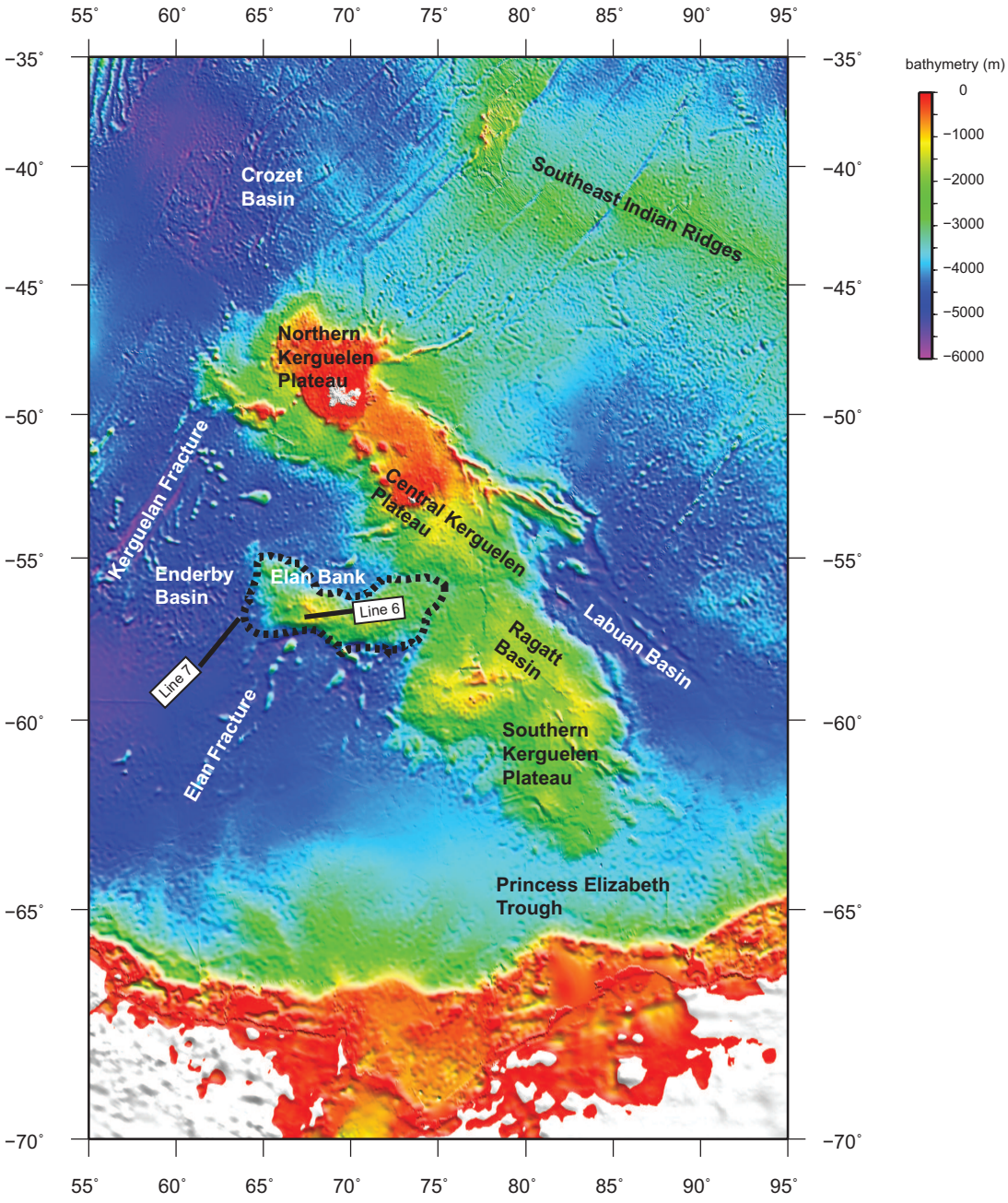

[h!]

Figure 11.1: Map of the South Indian Ocean. The approximate boundary of the continental fragment Elan Bank is shown in a black dashed line. Seismic refraction lines 6 (*Borissova et al.*, 2003) and 7 (*Charvis and Operto*, 1999) are shown in thick black lines. Bathymetry from ETOPO-1 (*Amante and Eakins*, 2009).

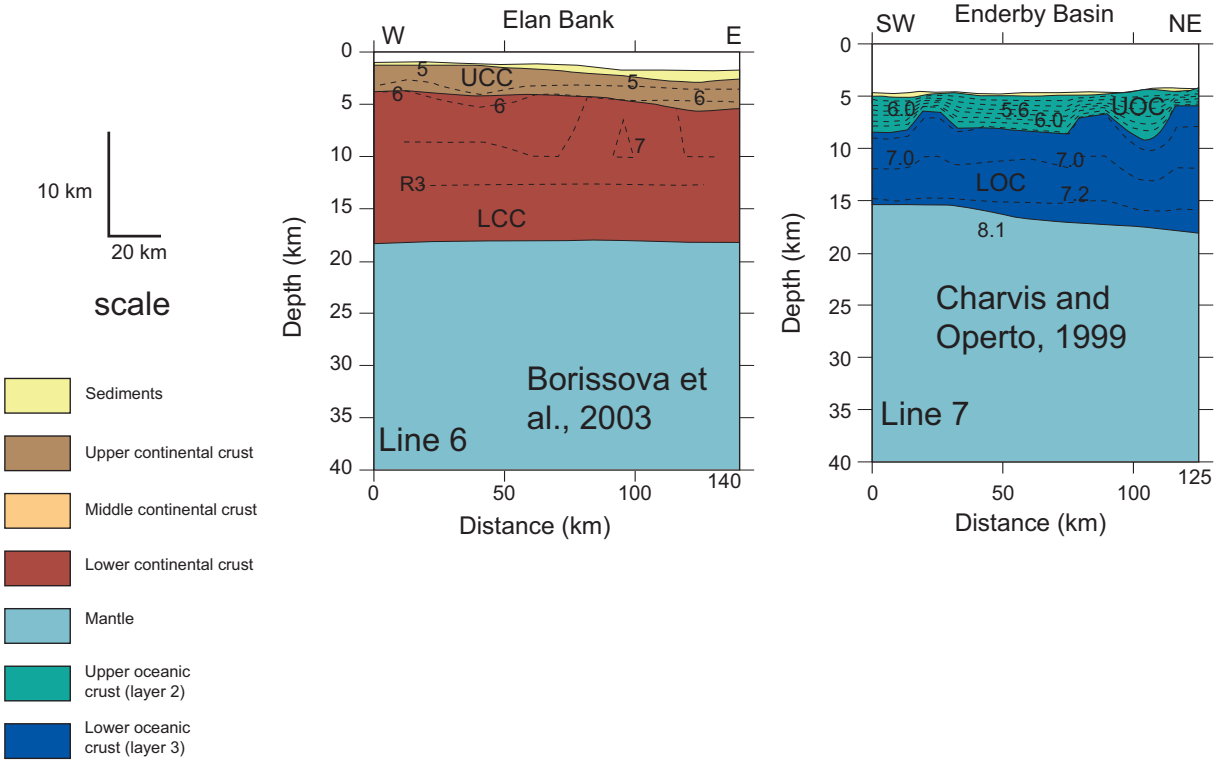

Figure 11.2: Seismic refraction lines across the Elan Bank and Enderby Basin. UCC = upper continental crust, LCC= lower continental crust, UOC = upper oceanic crust, LOC = lower oceanic crust. Numbers are seismic velocities in km s^{-1}. All lines are redrawn to a 4:1 vertical exaggeration (modified from *Borissova et al.* (2003) and *Charvis and Operto* (1999)).

12 SEYCHELLES MICROCONTINENT

12.1 Geologic Background

The Seychelles microcontinent is an arcuate continental sliver in the Indian Ocean (Figure 12.1), with 115 islands atop the submerged Seychelles plateau. The Mascarene Basin borders the Seychelles Plateau to the south. The Seychelles Plateau is separated from the Indian subcontinent by the Carlsberg Ridge in the Indian Ocean and from Africa by the West Somali Basin. To the southeast, the Seychelles continue into the Mascarene Ridge, whose crustal affinity is still debated. However, recent receiver function studies and zircon dating of xenocrysts in exposed volcanics suggest that continental crust likely continues under the islands and plateaus of the Mascarene Ridge and Mauritius (*Hammond et al.*, 2013; *Torsvik et al.*, 2013). Zircon dating of granites from several of the Seychelles Islands yields ages of 750-800 Ma, which are correlated to the Malani Igneous Suite of India and plutonic rocks in Madagascar (*Torsvik et al.*, 2001; *Tucker et al.*, 2001).

12.2 Tectonic Setting

The Seychelles Plateau was originally part of Greater India, and broke first from Madagascar and then from India. Break-up between the Seychelles and Madagascar first began in the Cretaceous marked by seafloor spreading from chron 34 (84 Ma) (*Plummer and Belle*, 1995; *Seton et al.*, 2012). Spreading in the Mascarene Basin ceased in a southward direction from around 67 until 59 Ma (*Bernard and Munschy*, 2000). Rifting between Seychelles and India first started in the Gop Rift, with possible seafloor spreading at about 71–66 Ma (*Collier et al.*, 2008). Paleomagnetic analysis and dating of dikes on Seychelles pinpoints the beginning of seafloor spreading between the Laxmi Ridge and Seychelles around 63–62 Ma (*Ganerød et al.*, 2011; *Torsvik et al.*, 2013). The Deccan Traps, a large continental LIP, was emplaced around 65 Ma in southwest India (*Courtillot and Renne*, 2003). Both the break-up between Madagascar and India and the break-up between Seychelles and India have been related to plumes and hotspots (*Buiter and Torsvik*, 2014).

12.3 Crustal Structure

Only recently has a crustal-scale wide-angle seismic study been performed over the Seychelles continental margin (*Collier et al.*, 2009). Previous seismic crustal studies were performed in the 1960s (*Francis and Shor*, 1966). The crust of the Seychelles Plateau is 32 km thick (*Collier et al.*, 2009). The crust is divided into three layers (Figure 12.2), with velocities ranging from 5.5 km s^{-1} in the upper crust to 6.5 km s^{-1} in the middle crust and 6.8–7.0 km s^{-1} in the lower crust (*Collier et al.*, 2009). Under the lower crust there is a 4 km-thick layer with velocities of 7.6–7.8 km s^{-1} that is interpreted as magmatic underplating (*Collier et al.*, 2009). Including the magmatic underplating layer, the Seychelles Plateau is about 40 km thick. A very thin sedimentary layer overlies the Seychelles Plateau in small basins 1–2 km thick (*Collier et al.*, 2009). The sedimentary deposits have velocities of 2.5–3.5 km s^{-1} (*Collier et al.*, 2009).

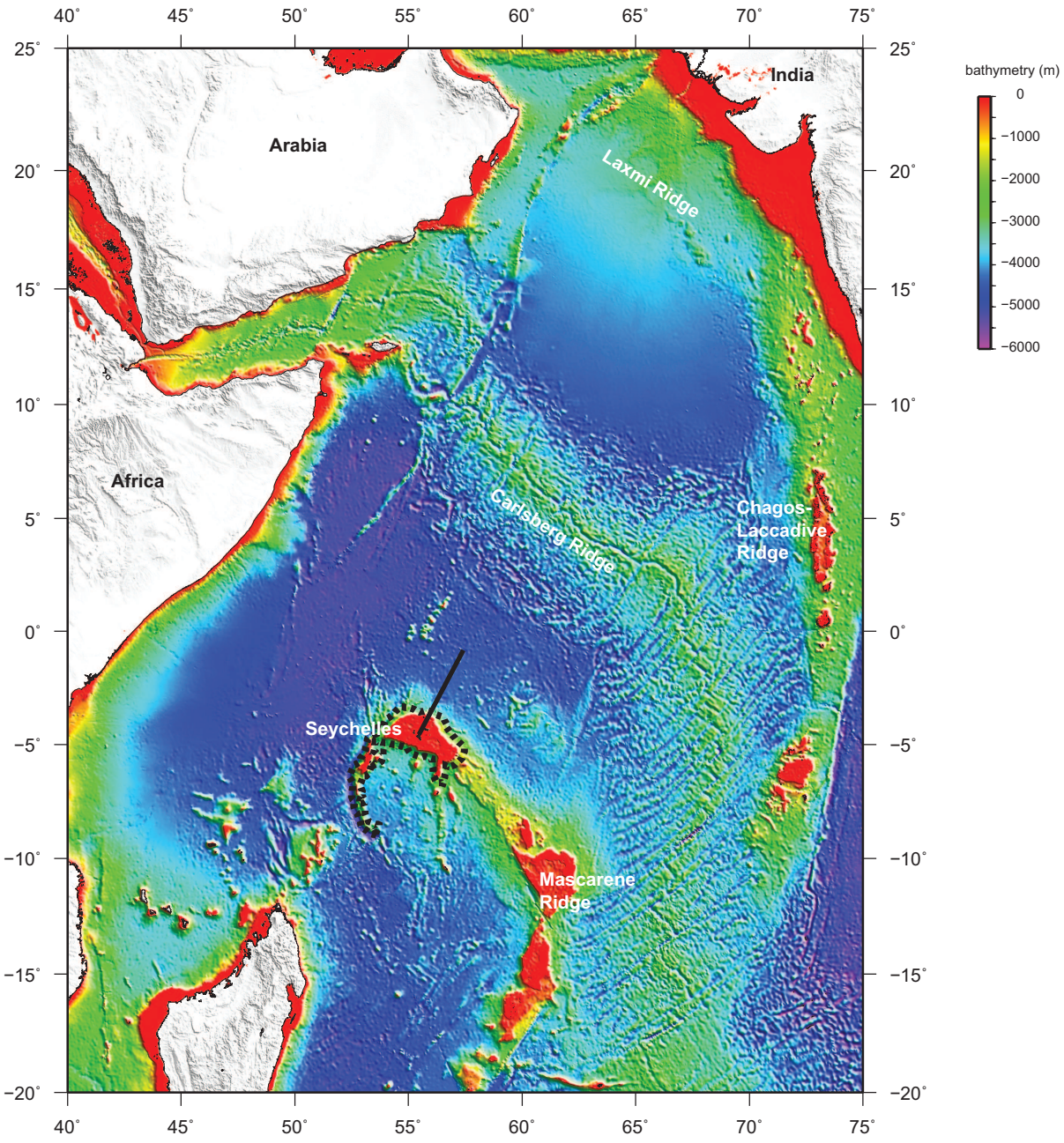

Figure 12.1: Map of the South Indian Ocean. The approximate boundary of the Seychelles microcontinent is shown in a black dashed line. The seismic refraction line of *Collier et al.* (2009) is shown in a thick black line. Bathymetry from ETOPO-1 (*Amante and Eakins*, 2009).

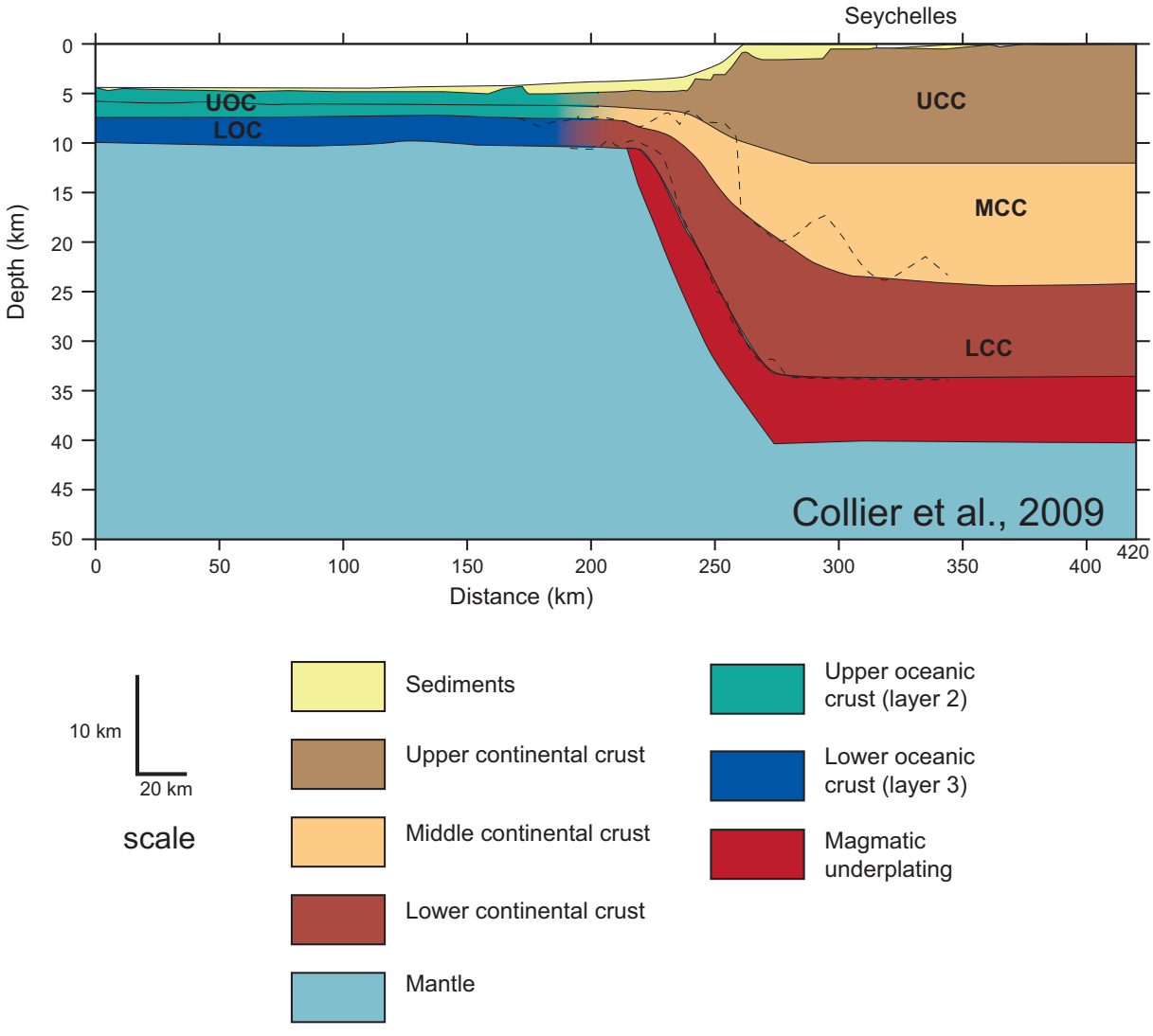

Figure 12.2: Seismic refraction lines across the Seychelles microcontinent. UCC = upper continental crust, MCC = middle continental crust, LCC= lower continental crust, UOC = upper oceanic crust, LOC = lower oceanic crust. All lines are redrawn to a 4:1 vertical exaggeration (modified from *Collier et al.* (2009)).

13 THE ARCTIC REGION

13.1 Geologic Background

Several large, ribbon-like submarine highs cross the Arctic Ocean. The Arctic Ocean is divided into the Amerasian Basin and the Eurasian Basin by the long Lomonosov Ridge. Parallel to that fragment is the Alpha-Mendeleev Ridge, a possibly composite large igneous province-continental fragment. Within the Amerasian Basin, the Lomonosov Ridge is separated from the Alpha-Mendeleev Ridge by the Makarov and Podvodnikov basins. On the opposite side of the Mendeleev Ridge lie the Mendeleev Basin, Chukchi Plateau, and Northwind Ridge. In the oceanic Eurasian Basin, the Gakkel Spreading Ridge separates the Amundsen Basin to the north from the Nansen Basin.

The exact crustal nature of these fragments is still uncertain. While there is general agreement that the Lomonosov Ridge, Chukchi Plateau, and Northwind Ridge are continental, the crustal affinity of the Alpha-Mendeleev Ridge and bordering basins is debated. The Alpha-Mendeleev Ridge is suggested to be heavily intruded with magmatism, but it is still discussed whether the core of the ridge is a continental crust or igneous (LIP) crust (*Jokat*, 2003; *Lebedeva-Ivanova et al.*, 2006; *Miller et al.*, 2006; *Funck et al.*, 2011; *Døssing et al.*, 2013). Some authors suggest that the High Arctic large igneous province (HALIP) includes part of the Alpha Ridge or possibly the entire Alpha-Mendeleev Ridge (*Funck et al.*, 2011; *Døssing et al.*, 2013; *Pease et al.*, 2014). Seismic reflection data, gravity and magnetic studies, plate reconstructions, and detrital zircon analyses provide evidence that support both theories (*Jokat*, 2003; *Lebedeva-Ivanova et al.*, 2006; *Miller et al.*, 2006; *Dove et al.*, 2010; *Funck et al.*, 2011; *Døssing et al.*, 2013; *Jokat et al.*, 2013; *Pease et al.*, 2014).

13.2 Tectonic Setting

Partly because the crustal nature of many of the Arctic continental fragments and basins is still undecided, the plate tectonic history is also debated. Here we provide a very general outline of the Arctic tectonic setting, based on what is generally agreed upon.

Rifting in the Arctic first occurred in the Jurassic Amerasian Basin and was followed by Cenozoic break-up of the Eurasian Basin. The Amerasian Basin opened in a “windshield” manner, rotating in two stages (*Grantz et al.*, 2011). First, rifting occurred in the Canada Basin, within the Amerasian Basin, starting in the Early Jurassic and leading to break-up in the Late Jurassic, separated the Northwind Ridge from Alaska (*Grantz et al.*, 1998). The Chukchi Plateau and Northwind Ridge were then separated from the Alpha-Mendeleev Ridge in the early Cretaceous (*Alvey et al.*, 2008; *Seton et al.*, 2012). The second stage, between 131 and 127 Ma, corresponds to seafloor spreading in the proto-Amerasian Basin (*Grantz et al.*, 2011). *Alvey et al.* (2008) and *Gaina et al.* (2014) suggest that the Podvodnikov and Makarov Basins opened between the Late Cretaceous and the Tertiary, based on plate reconstructions and gravity modeling. Basalts from the Alpha Ridge were given an age of about 82 Ma from Ar-Ar dating methods, suggesting that emplacement occurred in the Late Cretaceous if the ridge is part of the HALIP (*Jokat*, 2003).

Cretaceous rifting in the Eurasian Basin first separated the Lomonosov Ridge from Eurasia (*Seton et al.*, 2012). Seafloor spreading in the Eurasian Basin completed break-up between Lomonosov Ridge and the Barents Sea and is recorded in Anomaly 25 (53–55 Ma) (*Gaina et al.*, 2002; *Seton et al.*, 2012; *Pease et al.*, 2014). Alternatively, a slightly older (58 Ma) is

proposed for break-up in the Eurasian Basin (*Glebovsky et al.*, 2006).

13.3 Continental Fragment Crustal Structure

Due to the geographic constraints of the Arctic, deep crustal seismic studies were performed using sonobuoys or vertical geophones placed on the ice. Various modeling techniques enabled the researchers to develop crustal models with reflection and refraction waves, in innovative methods. The crustal velocities do not fully constrain the crustal nature of the Arctic regions, and the values can be interpreted to be from either igneous (LIP) or continental crust.

13.3.1 Alpha Ridge

The two seismic refraction lines of the ARTA study cover part of the Alpha Ridge (Figure 13.2). The crustal thickness of the Alpha Ridge is around 23–28 km thick (*Funck et al.*, 2011). The continental margin traversed by the main ARTA seismic line is the margin of the Svedrup Basin Magmatic Province in Greenland. The Alpha Ridge has three crustal layers: an upper volcanic crust, a middle crust, and a lower crust (*Funck et al.*, 2011). The upper crust has velocities of 4.7–5.4 km s^{-1}, the middle crust has velocities of 6.1–6.6 km s^{-1}, and the lower crust has velocities of 6.8–7.3 km s^{-1} (*Funck et al.*, 2011). The seismic velocities of the Alpha Ridge crust are interpreted to be too high for continental values, and therefore suggested to be igneous layers like in the LIPs of the south Pacific Ocean (*Funck et al.*, 2011). The upper crust is interpreted to be volcanics such as basalt flows (*Funck et al.*, 2011). When compared to the crustal velocities modeled for the Canadian shelf, the seismic velocities of the Alpha Ridge are noticeably higher. In the region where the Canadian shelf crust transitions to crust of the Alpha Ridge on the ARTA main line, a layer of high velocities underlies the lower crust. This lower crustal body has velocities ranging from 7.5–7.6 km s^{-1}, and is interpreted as magmatic underplating (*Funck et al.*, 2011). The cross line, ARTA-X, covers only the crust of the Alpha Ridge and returns similarly high seismic values for the crustal layers. In the ARTA-X line the upper crust has velocities of 4.7–5.4 km s^{-1}, the middle crust has velocities of 6.3–6.5 km s^{-1}, and the lower crust has velocities of 6.8–7.3 km s^{-1} (*Funck et al.*, 2011). Tomographic inversions of the travel times from both lines are in good agreement with the crustal thickness and velocities produced by forward and inverse modeling (*Funck et al.*, 2011).

The sediment thickness above the Alpha Ridge on the ARTA main line is less than 2 km, but increases locally into a basin at the Canadian continental margin (Figure 13.2). *Funck et al.* (2011) report velocities of 2.2–4.6 km s^{-1} in five sedimentary layers in the basin between the Canadian margin and the Alpha Ridge. The uppermost sedimentary layer, with velocities of 2.2 km s^{-1} continues onto the Alpha Ridge (*Funck et al.*, 2011). In the ARTA-X line, the sedimentary thickness varies from 0.4–1.5 km and has velocities of 2.0 km s^{-1} (*Funck et al.*, 2011).

13.3.2 Mendeleev Ridge

The Mendeleev Ridge segment of the Alpha-Mendeleev Ridge has been covered by three deep seismic sounding lines, the TransArctic (TRA)-1989-91, Arctic-2000, and Arctic-2005 (Figure 13.1, 13.2). On the TRA-1989-91 and Arctic-2000 lines, *Lebedeva-Ivanova et al.* (2006, 2011) model the crystalline crust with two layers, but the acoustic basement is at the top of an additional layer. Similarly, the Arctic-2005 line is modeled with two crystalline crustal layers with an overlying metasedimentary layer (*Poselov et al.*, 2012a). The crustal thickness (from the base of the acoustic basement) of the Mendeleev Ridge is 32 km in the Arctic-2000 transect (*Lebedeva-Ivanova et al.*, 2006) and 29–32 km in the Arctic-2005 transect (*Poselov et al.*, 2012a). The TRA-1989-91 line crosses the edge of the Alpha-Mendeleev Ridge in the cen-

ter of the Amerasian Basin, and the crustal thickness of the ridge is modeled to be around 22 km (*Lebedeva-Ivanova et al.*, 2011). The layer just below the acoustic basement has values of 5.0–5.4 km s^{-1}, with thicknesses pinching out at the top of the Alpha-Mendeleev Ridge on TRA-1989-91 (*Lebedeva-Ivanova et al.*, 2011). On Arctic-2000, this layer also has velocities of 5.0–5.4 km s^{-1} above the Mendeleev Ridge (*Lebedeva-Ivanova et al.*, 2006). The seismic velocities of this layer can be correlated to Mesozoic-Paleozoic basement rocks, sedimentary (carbonate) rocks, basalt flows, or a mix of sediments and volcanics (*Lebedeva-Ivanova et al.*, 2006, 2011). On the Arctic-2005 line, the layer below the acoustic basement has velocities of 4.8–5.1 km s^{-1}, and is correlated to late Paleozoic sediments in a related multichannel seismic line (*Poselov et al.*, 2012a). This sedimentary/volcanic layer has a thickness on the order of 2–4 km (*Lebedeva-Ivanova et al.*, 2006, 2011; *Poselov et al.*, 2012a). Below the layer of sediments/volcanics, the upper crystalline crust in the Mendeleev Ridge has velocities of 6.2–6.4 km s^{-1} in the TRA-1989-91 seismic line, 5.9–6.5 km s^{-1} in the Arctic-2000 transect, and 6.2–6.3 km s^{-1} in the Arctic-2005 transect (*Lebedeva-Ivanova et al.*, 2006, 2011; *Poselov et al.*, 2012a). The upper crustal thickness in the Mendeleev Ridge ranges from 4–8 km (*Lebedeva-Ivanova et al.*, 2006, 2011; *Poselov et al.*, 2012a). The lower crystalline crust has velocities of 6.7–7.3 km s^{-1} and a thickness of 19–21 km in the Arctic-2000 line and 10–15 km in the TRA-1989-91 line (*Lebedeva-Ivanova et al.*, 2006, 2011). In the Arctic-2005 line, the lower crust has velocities of 6.7–6.9 km s^{-1} and a thickness of 20–22 km (*Poselov et al.*, 2012a). *Lebedeva-Ivanova et al.* (2006, 2011) interpret the crust as continental, although they do acknowledge that these seismic velocities can also correspond to more mafic compositions. *Poselov et al.* (2012a) also interprets the Mendeleev Ridge as extended continental crust from the seismic velocities and interpreted tectonic features in the related seismic reflection lines.

On the TRA-1989-91 transect, less than 1 km of sediments overlie the acoustic basement (*Lebedeva-Ivanova et al.*, 2011). Further along the Mendeleev Ridge, the Arctic-2000 seismic line has three sedimentary layers with a total thickness around 1 km over the Mendeleev Ridge (*Lebedeva-Ivanova et al.*, 2006). The three layers have velocities of 1.7 km s^{-1}, 2.3 km s^{-1} and 2.6 km s^{-1} (*Lebedeva-Ivanova et al.*, 2006).

Below the crust, in the Arctic-2000 transect, a layer with high seismic velocities is modeled (*Lebedeva-Ivanova et al.*, 2006). This layer is about 5–7 km thick under the Mendeleev Ridge with velocities of 7.4–7.6 km s^{-1}, and is interpreted as magmatic underplating (*Lebedeva-Ivanova et al.*, 2006). A similar layer is not found in any of the TRA-1989-91 or Arctic-2005 lines (Figure 13.2). The Arctic-2000 line is also interpreted by *Poselov et al.* (2012a), but no lower crustal high seismic velocity body is produced with their forward and inverse modeling of the data.

13.3.3 Lomonosov Ridge

Several deep crustal seismic studies have crossed the Lomonosov Ridge (Figure 13.1). The LORITA (main and cross lines) (*Jackson and Dahl-Jensen*, 2010), Arctic-2007 (main and cross lines) (*Poselov et al.*, 2012b), and TRA-1992 (*Poselov et al.*, 2012b) studies cover various margins of the ridge (Figure 13.3). The TRA-1990 segment touches on the edge of Lomonosov Ridge at the center of the Makarov Basin, but will not be included because the ray coverage at the end of the lines is not so good. In all three wide-angle seismic studies, the Lomonosov Ridge is interpreted as continental. The crustal thickness of the Lomonosov Ridge ranges from 20-26 km on the five seismic lines (*Jackson and Dahl-Jensen*, 2010; *Poselov et al.*, 2012b). In all five seismic lines, the acoustic basement is measured at the top of one layer above what is deemed the crystalline crust. The layer below the acoustic basement has velocities of 5.1–5.4 km s^{-1}

on the Arctic-2007 main line and 5.3–5.5 km s^{-1} on the TRA-1992 line (*Poselov et al.*, 2012b). The Arctic-2007-X line crosses the region where the Lomonosov Ridge transitions to the De Long Plateau. In the Arctic-2007-X line, this intermediate layer has velocities of 4.5–5.0 km s^{-1} and a thickness of 10 km at the edge of the Lomonosov Ridge (*Poselov et al.*, 2012b). On the Canadian side of the Lomonosov Ridge, the layer above the crystalline upper crust has velocities of 5.4–5.9 km s^{-1} and is interpreted as metasedimentary rocks (*Jackson and Dahl-Jensen*, 2010). The crystalline crust has two layers in all five lines. The upper crust has velocities of 6.0-6.4 km s^{-1} and is 6–7 km thick in the TRA-1992, Arctic-2007 main and Arctic-2007-x lines (*Poselov et al.*, 2012b). In the LORITA main line, the upper crust of the Lomonosov Ridge has velocities of 5.95–6.7 km s^{-1}, with velocities below 6.2 km s^{-1} restricted to the upper part of a basement high where depths are as shallow as 2 km (*Jackson and Dahl-Jensen*, 2010). The upper crust in the LORITA-X line has velocities of 6.0–6.5 km s^{-1} and thickness ranging from 4–11 km (*Jackson and Dahl-Jensen*, 2010). The lower crust of the Lomonosov Ridge has velocities of 6.6–6.7 km s^{-1} and thicknesses of 8–11 km in all lines except for the LORITA-X line, where the lower crust is only 1-3 km thick (*Jackson and Dahl-Jensen*, 2010; *Poselov et al.*, 2012b).

The sedimentary thickness above the Lomonosov Ridge is on average around 1.5–3 km thick, except on the basement high of the LORITA main seismic line where the sediment thickness is much less than 1 km (Figure 13.3). Three sedimentary layers are identified on the TRA-1992 line, with velocities of 1.6–2.6 km s^{-1}, 3.6–3.9 km s^{-1}, and 4.2–4.5 km s^{-1} (*Poselov et al.*, 2012b). On the Arctic-2007 main line, two sedimentary layers with velocities of 1.9–2.5 km s^{-1} and 2.9–4.1 km s^{-1} are identified above the Lomonosov Ridge (*Poselov et al.*, 2012b). On the Arctic-X line, these two sedimentary layers have velocities of 1.8–2.3 km s^{-1} and 3.0–3.9 km s^{-1} above the ridge (*Poselov et al.*, 2012b). Three sedimentary layers are found on the LORITA lines, with velocities of 2.1–2.2 km s^{-1}, 3.1–3.2 km s^{-1}, and 4.5–5.4 km s^{-1} (*Jackson and Dahl-Jensen*, 2010).

13.4 Basin Crustal Structure

13.4.1 Podvodnikov Basin

The Podvodnikov Basin separates the Lomonosov Ridge from the Mendeleev Ridge and is covered by the TRA-1989-91 transect, the TRA-1992 line, and the Arctic-2000 line (Figure 13.1, 13.2). The crustal thickness varies from around 15–20 km in the main part of the basin and up to 24 km under the Arlis Gap, and is interpreted as extended continental crust (*Lebedeva-Ivanova et al.*, 2006, 2011; *Poselov et al.*, 2012b). Like the surrounding ridges on these seismic lines, the crust of the Podvodnikov Basin is modeled as having three layers, of which two are crystalline basement. The top layer of the crust, just below the acoustic basement, has velocities of 5.3–5.5 km s^{-1} and is 4–4.5 km thick along the TRA-1992 seismic line (*Poselov et al.*, 2012b). Across the TRA-1989-91 transect, this layer has velocities of 5.0–5.1 km s^{-1} and a thickness of 2–4 km (*Lebedeva-Ivanova et al.*, 2011). In the Arctic-2000 line, the layer below the acoustic basement has velocities of 5.0–5.7 km s^{-1} (*Lebedeva-Ivanova et al.*, 2006). The upper crystalline crust has velocities of 6.0–6.1km s^{-1} in the TRA-1992 line, 6.0–6.5 km s^{-1} in the Arctic-2000 line, and 5.9–6.4 km s^{-1} in the TRA-1989-91 transect (*Lebedeva-Ivanova et al.*, 2006, 2011; *Poselov et al.*, 2012b). The thickness of the upper crust varies considerably in the TRA-1989-91 transect: ranging from almost 0 km to 6 km under the Arlis Gap (*Lebedeva-Ivanova et al.*, 2011). The lower crust has thicknesses varying from 5–7 km in the southern part of the basin to 10–15 km under the Arlis Gap and northern part of the Podvodnikov Basin (*Lebedeva-Ivanova et al.*, 2011). The velocities of the Podvodnikov Basin lower crust in the TRA-1989-91 transect are

6.7–7.2 km s^{-1} (*Lebedeva-Ivanova et al.*, 2011). In the nearby Arctic-2000 seismic line, the lower crust ranges from 7–14 km in thickness and has velocities of 6.7–7.3 km s^{-1} (*Lebedeva-Ivanova et al.*, 2006). In the TRA-1992 line, the lower crust similarly is modeled with velocities of 6.7–6.8 km s^{-1} (*Poselov et al.*, 2012b).

The sediment fill in the Podvodnikov Basin has a thickness of 2–7 km, with the greatest thickness in the southern part of the basin (*Lebedeva-Ivanova et al.*, 2006, 2011; *Poselov et al.*, 2012b). Three sedimentary layers are modeled in all the seismic lines covering the basin. The top sedimentary layer has a thickness around 0.5 km and velocities of 1.7 km s^{-1} in the Arctic-2000 line, 1.6–2.6 km s^{-1} in the TRA-1992 line, and 1.7–1.9 km s^{-1} in the TRA-1989-91 transect (*Lebedeva-Ivanova et al.*, 2006, 2011; *Poselov et al.*, 2012b). The second sedimentary layer has velocities of 3.6–3.9 km s^{-1} in the TRA-1992 line but has lower velocities ranging from 2.2–3.0 km s^{-1} in the TRA-1989-91 and Arctic-2000 lines (*Lebedeva-Ivanova et al.*, 2006, 2011; *Poselov et al.*, 2012b). The lowermost sedimentary layer is modeled with velocities of 3.2–3.6 km s^{-1} in the Arctic-2000 line, 3.5–4.0 km s^{-1} in the TRA-1989-91 transect, and 4.2–4.5 km s^{-1} in the TRA-1992 line (*Lebedeva-Ivanova et al.*, 2006, 2011; *Poselov et al.*, 2012b). This layer also has the greatest thickness, varying from 2–5 km (*Lebedeva-Ivanova et al.*, 2006, 2011; *Poselov et al.*, 2012b).

13.4.2 Makarov Basin

The Makarov Basin separates the Lomonosov Ridge from the Alpha Ridge and is crossed by the TRA-1989-91 transect (Figure 13.1, 13.2). On the TRA-1989-91 transect, basement highs possibly corresponding to a continuation of the Marvin Spur and other possible continental fragments are within the Makarov Basin. Based on the crustal thickness (8–12 km) and variability in seismic crustal velocities, the Makarov Basin crust is interpreted to be oceanic crust with small continental fragments under the basement highs (*Lebedeva-Ivanova et al.*, 2011). On the TRA-1989-91 transect, *Lebedeva-Ivanova et al.* (2011) observe the acoustic basement to be one layer above the interpreted crystalline basement. The layer between the acoustic basement and the crystalline crust has velocities of 5.0–5.3 km s^{-1} with thicknesses varying from 0.5–4.0 km (*Lebedeva-Ivanova et al.*, 2011). The crystalline crust has an upper crust with velocities ranging from 5.9–6.3 km s^{-1} in the thinnest section of the basin to 6.0–6.2 km s^{-1} in the basement highs (*Lebedeva-Ivanova et al.*, 2011). The lower crust has thicknesses of 2 km in the interpreted oceanic part and up to 7 km in the basement highs (*Lebedeva-Ivanova et al.*, 2011). The seismic velocities of the lower crust in the Makarov Basin vary from 6.9 to 7.2 km s^{-1}, with the highest velocities in the interpreted oceanic part (*Lebedeva-Ivanova et al.*, 2011).

The basin fill is approximately 5 km thick above the interpreted oceanic trough and thins above the basement highs (Figure 13.2). The three identified sedimentary layers in the TRA-1989-91 transect have velocities of 1.7–1.9 km s^{-1}, 2.3–3.0 km s^{-1}, and 3.5–4.0 km s^{-1} (*Lebedeva-Ivanova et al.*, 2011).

13.4.3 Mendeleev Basin

The Mendeleev Basin lies between the Chukchi Plateau and the Mendeleev Ridge Figure 13.1). The northern edge of the basin is traversed by the Arctic-2000 seismic line (Figure 13.2). The Mendeleev Basin has a crustal thickness of about 13 km under the Arctic-2000 line (*Lebedeva-Ivanova et al.*, 2006). The crystalline crust is composed of two layers, and an overlying layer lies between the crust and the acoustic basement. The layer below the acoustic basement has velocities of 5.0–5.4 km s^{-1}, thicknesses around 3 km, and is interpreted to be carbonate sedimentary rocks of fractured basalts (*Lebedeva-Ivanova et al.*, 2006). The upper crust has veloci-

ties of 5.9–6.5 km s^{-1} and the lower crust has velocities of 6.7–7.3 km s^{-1} (*Lebedeva-Ivanova et al.*, 2006). The lower crust has a thickness of 7–14 km at the margin of the Mendeleev Basin (*Lebedeva-Ivanova et al.*, 2006). The Mendeleev Basin is interpreted to be extended continental crust based on the thick crust and similar velocities to the bordering continental fragments (*Lebedeva-Ivanova et al.*, 2006).

The sedimentary thickness above the Mendeleev Basin is 2.5–3.0 km thick and has three layers (*Lebedeva-Ivanova et al.*, 2006). The seismic velocities of the three layers are 1.7–1.9 km s^{-1}, 2.3–2.6 km s^{-1}, and 3.2–3.6 km s^{-1}, from top to base of the basin fill (*Lebedeva-Ivanova et al.*, 2006).

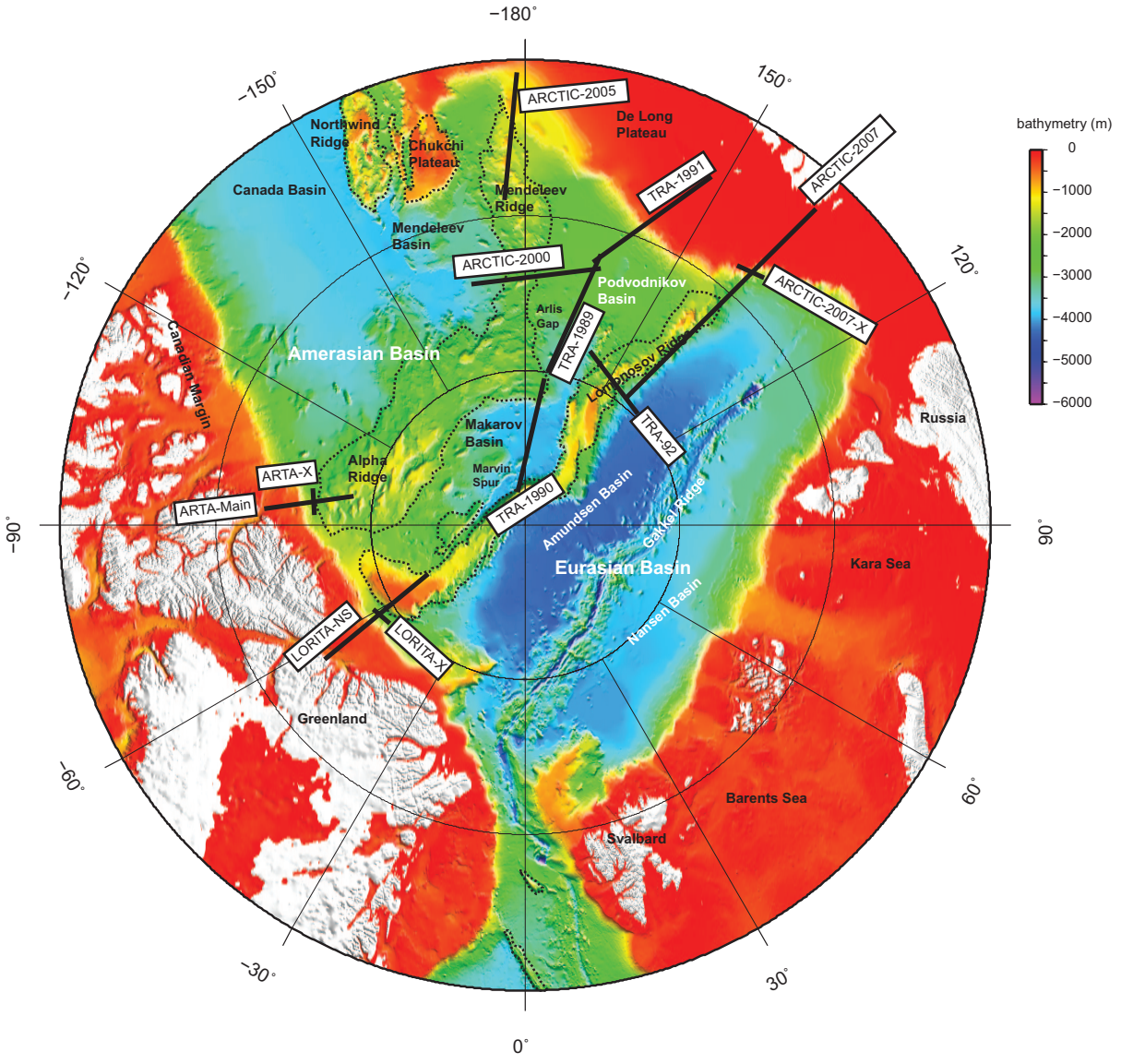

Figure 13.1: Map of the Arctic Ocean. The approximate boundary of the continental fragments are shown in a black dashed line. Seismic refraction lines Arctic-2000 (*Lebedeva-Ivanova et al.*, 2006), Arctic-2005 (*Poselov et al.*, 2012a), Arctic-2007 (*Poselov et al.*, 2012b), LORITA (*Jackson and Dahl-Jensen*, 2010), TRA-1989, 1990, 1991 (*Lebedeva-Ivanova et al.*, 2011), TRA-1992 (*Poselov et al.*, 2012b), and ARTA (*Funck et al.*, 2011) are shown in thick black lines. Cross lines are denoted with the survey name and 'X'. Bathymetry from ETOPO-1 (*Amante and Eakins*, 2009).

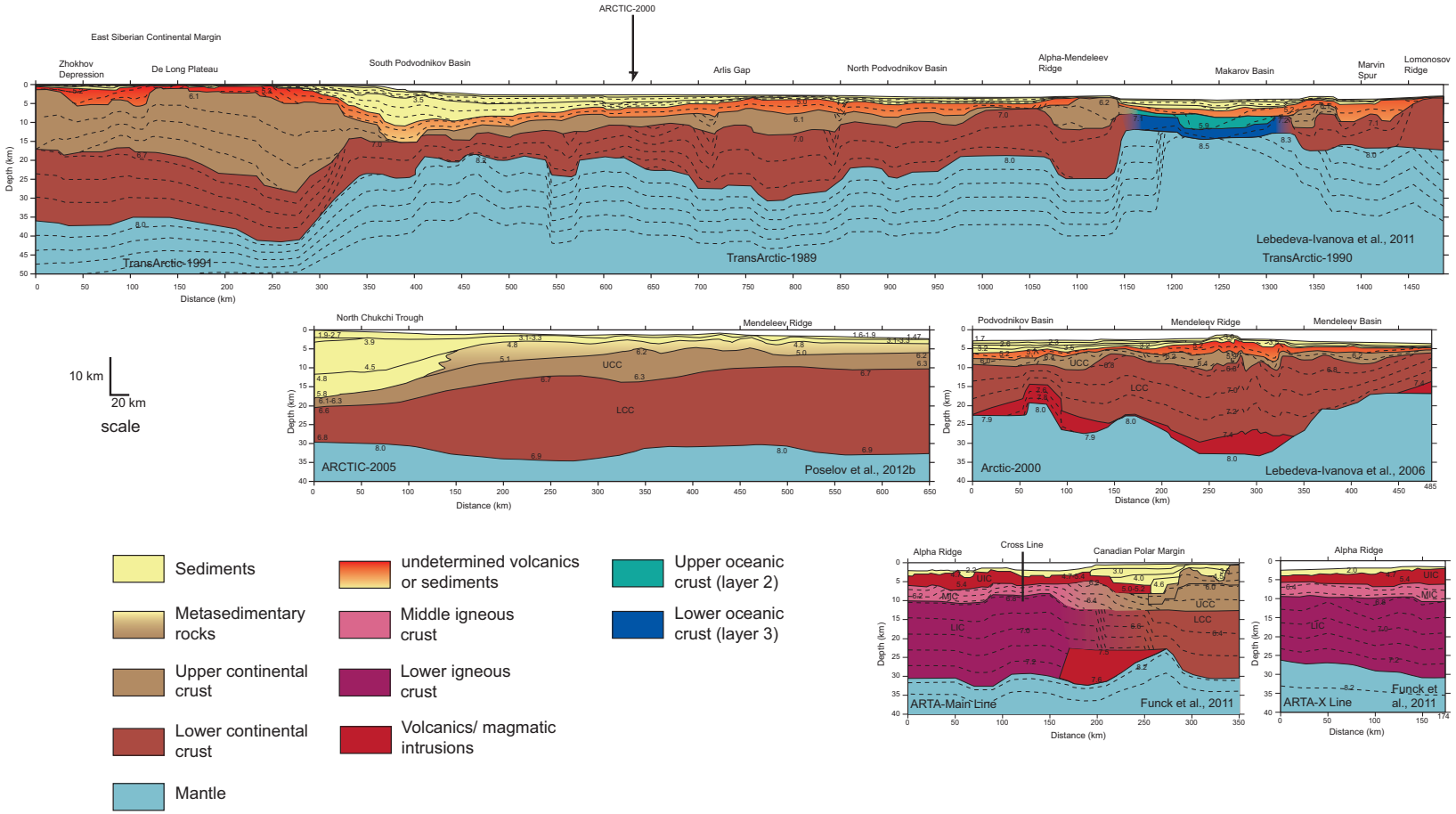

Figure 13.2: Seismic refraction lines across the Alpha-Mendeleev Ridge and related basins. UCC = upper continental crust, MCC = middle continental crust, LCC= lower continental crust, UIC = upper igneous crust, MIC = middle igneous crust, LIC = lower igneous crust. Numbers are seismic velocities in km s^{-1}. All lines are redrawn to a 4:1 vertical exaggeration (modified from *Lebedeva-Ivanova et al.* (2006); *Jackson and Dahl-Jensen* (2010); *Funck et al.* (2011); *Lebedeva-Ivanova et al.* (2011), and *Poselov et al.* (2012a)).

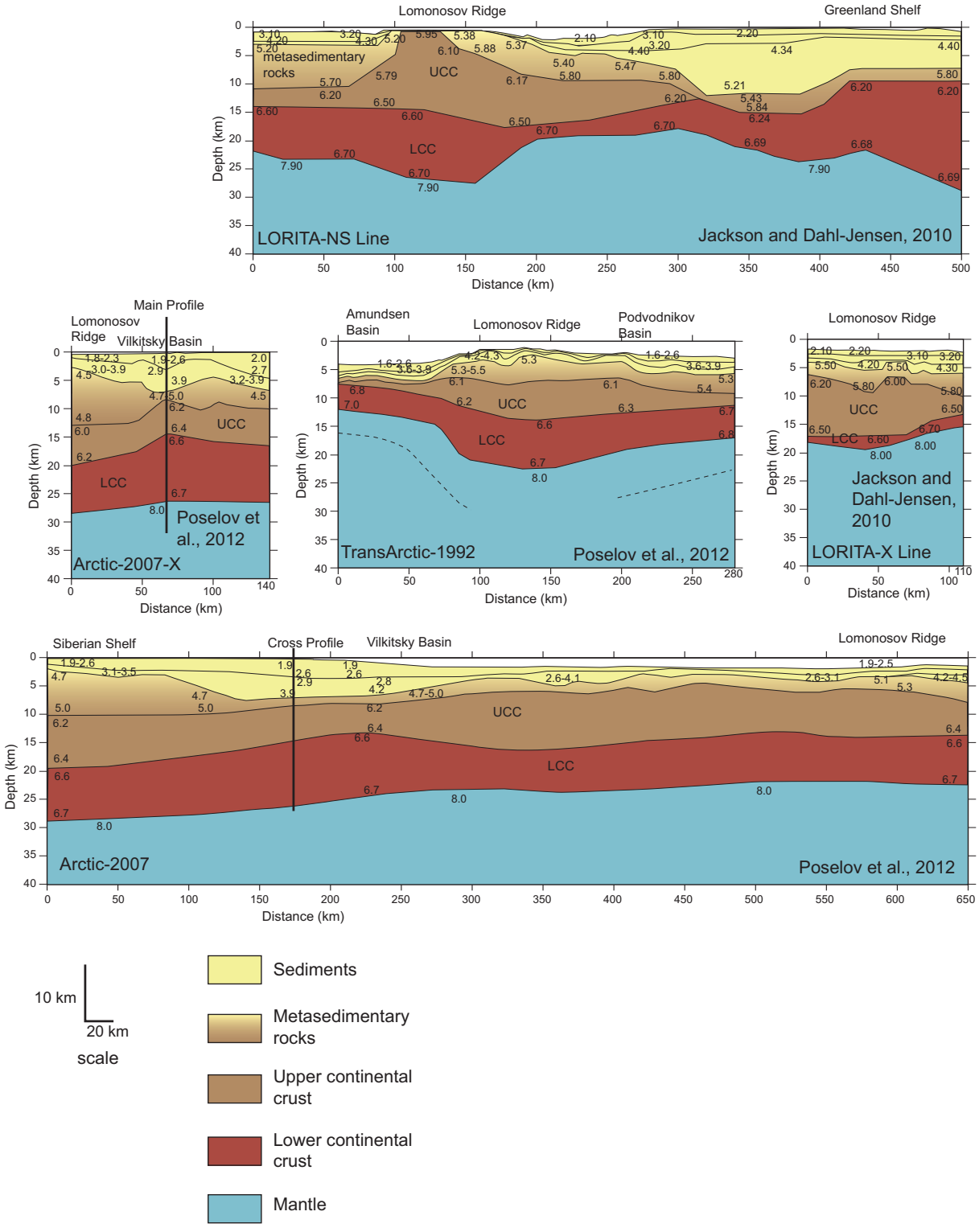

Figure 13.3: Seismic refraction lines across the Lomonosov Ridge and related basins. UCC = upper continental crust, LCC= lower continental crust. Numbers are seismic velocities in km s^{-1}. All lines are redrawn to a 4:1 vertical exaggeration (modified from *Lebedeva-Ivanova et al.* (2006); *Jackson and Dahl-Jensen* (2010); *Funck et al.* (2011); *Lebedeva-Ivanova et al.* (2011), and *Poselov et al.* (2012b)).

14 DISCUSSION

Numerous submarine highs are spread over the modern oceanic floor. Submarine crustal highs include continental fragments, microcontinents, large igneous plateaus, submarine igneous ridges, hot spot tracks, island arcs, and seamounts. For most of them, the crustal nature is known and confirmed. Yet, with more and more geological and geophysical studies, new continental fragments and microcontinents have been identified in recent years (*Torsvik et al.*, 2013; *Gardner et al.*, 2015). In the same vein, previously identified submarine igneous provinces are now being identified as continental fragments (*Corfield*, 2013; *Gibbons et al.*, 2012).

Continental fragments and microcontinents are small, isolated regions of continental crust born from rift-related tectonic processes. Our global review of the seismic crustal structure of modern continental fragments and microcontinents reveals a vast variety of crustal thicknesses in terms of the amount of stretching that the continental fragment and bordering basins have undergone (Table 14.1, 14.2, Figure 14.1, 14.2). The crustal thickness of continental fragments varies significantly across the globe, from some fragments having oceanic-type thicknesses (7–9 km) up to continental fragments and microcontinents with continental thicknesses (30–40 km). Accordingly, the bordering basins have a wide range of crustal thicknesses from less than 5 km to 20–25 km. Several continental fragments and microcontinents have thick sedimentary covers or small basins overlying the basement. These variations in crustal thickness reveal that some fragments and basins may have undergone several stages of rifting and extension before break-up and seafloor spreading, while others only experienced limited and localized rifting before break-up.

What is similar amongst all continental fragments and microcontinents? In terms of the crustal structure, we observe sharp crustal necking on the oceanic margins of many continental fragments and microcontinents. For instance, in the Flemish Cap, the crustal thickness reduces from 30 km to 10 km over a distance of about 50 km and in the Seychelles the crust thins from 40 km to 5 km in the span of around 50 km. Such geometries suggest rapid thinning due to a crustal-scale detachment during what *Peron-Pinvidic and Manatschal* (2010) call the exhumation phase.

In most continental fragments, pre-breakup rifting in the bordering regions appears to be synchronous, with a few exceptions. In the microcontinents of Jan Mayen, Seychelles, and the Elan Bank, there is little, if some stratigraphic, evidence of concurrent pre-break-up rifting on both sides of the microcontinents. But in the microcontinents and large fragments of the Arctic, there appear to be jumps in the location and timing of extension. In the Arctic, the data are sparse and still debated, but rifting in the Amerasian basin is often modelled to have jumped location from the Jurassic through the Tertiary. It is apparent that in the case of microcontinents, the transition from continental fragment to fully isolated continental crust is produced by a temporal and spatial rift jump. A jump in rift location over a distance of a few hundred kilometers can be due to shifting extension directions, as in the case of the Wallaby and Zenith plateaus. Alternatively, the rapid emplacement of hot magmatic material and raised mantle temperatures from an impinging plume could shift the location of rifting, as is probably the case for Seychelles and the Elan Bank.

It has been proposed that the magic ingredient in producing microcontinents are plumes (*Müller et al.*, 2001; *Gaina et al.*, 2003) based on the proximity of certain microcontinents (for example Jan Mayen, Seychelles, Elan Bank, and Lord Howe Rise) to plume or hotspots at the time of

rift jumping. While this is certainly likely to be the formation mechanism in some continental fragments and microcontinents, there are many continental fragments on non-volcanic margins. The Newfoundland, Iberian, Zealandia region, and parts of the Irish Margin are classified as non-magmatic margins due to the minor amount or absence of identified volcanics such as basalt flows, magmatic underplating, and SDRs. Another piece of evidence against plume-related microcontinent formation, is in the southwest Pacific, where the continental fragments of the Zealandia region were produced from active rifting by back-arc spreading in the New Hebrides-Vanuatu subduction zone.

It appears that there is not one recipe for microcontinent and continental fragment formation, but rather many different recipes that can lead to similar final products. Some possible tectonic scenarios that could lead to continental fragment formation include localization of deformation in multiple regions of inherited heterogeneity (*Peron-Pinvidic and Manatschal*, 2010), back-arc extension above a retreating subduction zone (*Sdrolias et al.*, 2003; *Schellart et al.*, 2006), misalignment of rift axes and their subsequent linkage (*Eagles et al.*, 2002), multiphase rifting, or a rift jump caused by an impinging mantle plume (*Müller et al.*, 2001; *Gaina et al.*, 2009). These hypotheses predict different amounts of stretching in the surrounding basins, timing of rifting in the basins, and amount of magmatic activity.

Evidence for plume interaction is often taken from lower crustal layers with high seismic velocities (7.2–7.5 km s^{-1}) that are typically interpreted as magmatic intrusions. Such lower crustal bodies are most often found under the thinned crust of the bordering basins, but in some cases underlie the relatively unthinned crust of continental fragments. High-velocity lower crustal bodies interpreted as magmatic underplating are identified under the Faroe-Shetland Trough, Faroe margin, Hatton continental margin, Hatton Basin, Lousy Bank margin, Bounty Trough, Alpha-Mendeleev Ridge, Seychelles microcontinent, the Faroe Islands, and Lousy Bank (Figure 14.3). Alternatively, in non-magmatic margins, some basins are underlain by high velocity bodies (7.5–7.9 s^{-1}) below the lower crust or below the Moho reflection, which are interpreted as serpentinized mantle. Often serpentinized mantle is found in the exhumed mantle on the oceanic margins of continental fragments, such as the Galicia Bank and Flemish Cap. However, under the extremely thinned crust of the Porcupine Basin and Rockall Basin, these values are found below the Moho. In the New Caledonia Basin, *Klingelhöfer et al.* (2007) interpret high velocities in the lower crust as serpentinized mantle, but because of the active tectonic setting with back-arc spreading, it is highly likely these values are due to arc magmas. More-often, continental fragments and their bordering basins do not have high-velocity lower crustal bodies. Thus, it would seem that magmatic underplating serves to localize deformation at the final break-up location but not in the surrounding basins.

In most, if not all, continental fragments, rifting in the surrounding basins occurred in the earliest stages of rifting. Between the Newfoundland-Iberia margins, the Flemish Pass, Orphan Basin, and Galicia Interior Basin all began rifting concurrently in the early Cretaceous (*Sibuet et al.*, 2007b; *Tucholke et al.*, 2007). Although still disputed, the Rockall, Hatton, Faroe-Shetland, and Porcupine basins are proposed to have opened up concurrently in the Permo-Triassic (*Shannon*, 1991). Even in the special cases of the continental fragments of Zealandia that formed due to back-arc spreading, the basins have been proposed to have initiated concurrently during a stage of intra-continental extension (*Bache et al.*, 2014).

If these basins are active in early intra-continental rifting stages, do the rifts in the surrounding basins initiate on ancient sutures? This hypothesis is generally supported in our global review of continental fragments. Off the Irish margin, the failed basins between continental fragments, in-

cluding the Rockall, Hatton, and Faroe-Shetland basins, run along old sutures (*Shannon*, 1991). In a review examining where passive margin rifting initiates, *Buiter and Torsvik* (2014) find that all modern margins, except for the Seychelles, have initiated along ancient sutures. In the cases of the Seychelles and the Elan Bank microcontinents, break-up and rift jumping are clearly related to active upwelling from a plume or hotspot. The timing of LIP eruptions around Seychelles and Elan Bank correlate well with modeled timing of break-up from plate reconstructions (*Coffin et al.*, 2002; *Gaina et al.*, 2007; *Collier et al.*, 2008; *Gibbons et al.*, 2013). The active upwelling due to hotspots or plumes can be the driving force to shift the rift location over 100 km *Gaina et al.* (2003).

In general, it is difficult to discern one special factor that contributes to continental fragment formation for all fragments because their tectonic histories are so varied. Plumes may not be the special factor that always produces microcontinents, but in several cases it is clearly the driving force. In passive margins driven by passive extension, without the influence of active upwelling due to plumes or back-arc spreading, it appears that continental fragments form following the scenario proposed by *Peron-Pinvidic and Manatschal* (2010), where rifting localizes in regions of pre-existing weaknesses.

14.1 Acknowledgements

This work was supported by Det norske oljeselskap ASA. We thank Ebbe Hartz, Hans Konrad Johnson, and Arild Saasen for support and critique. All figures were made with GMT (*Wessel and Smith*, 1991).

Table 14.1: Crustal thicknesses of continental fragments

Continental fragments	Thickness of crust (km)	Reference
Alpha Ridge	23–28	*Funck et al.* (2011)
Alpha-Mendeleev Ridge	25	*Lebedeva-Ivanova et al.* (2011)
Bill Bailey Bank	25	*Funck et al.* (2008)
Bounty Platform	23	*Grobys et al.* (2007)
Campbell plateau	24	*Grobys et al.* (2009)
Chatham Rise	22	*Grobys et al.* (2007)
Chatham Rise	20	gravity modelling: *Davy et al.* (2008)
East Greenland Ridge	6-7	*Døssing et al.* (2008)
Elan Bank	16	*Borissova et al.* (2003)
Exmouth Plateau	15	magnetotellurics: *Heinson* (2005)
Fairway Ridge	22	*Klingelhöfer et al.* (2007)
Falkland plateau	25–30	gravity modeling: *Kimbell and Richards* (2008)
Faroe Bank	24	*Funck et al.* (2008)
Faroe Islands	35–40	*Richardson et al.* (1999)
Flemish Cap	17–25	*Gerlings et al.* (2011)
Flemish Cap	30	*Funck* (2003)
Galicia Bank	19	*González et al.* (1999)
Galicia Bank	17	*Pérez-Gussinyé et al.* (2003)
Galicia Bank	15	*Zelt et al.* (2003)
Galicia Bank	16	*Clark et al.* (2007)
Hatton Bank	24	*Fowler et al.* (1989)

Table 14.1: continued.

Hatton Bank	22.50	*White and Smith* (2009)
Jan Mayen	7-9	*Breivik et al.* (2012)
Jan Mayen	24	*Kandilarov et al.* (2012)
Jan Mayen	11–15	*Kodaira et al.* (1998)
Lomonosov Ridge	26	*Jackson and Dahl-Jensen* (2010)
Lomonosov Ridge	20–25	*Poselov et al.* (2012b)
Lord Howe Rise	23	*Klingelhöfer et al.* (2007)
Lord Howe Rise	26.6	*Shor et al.* (1971)
Lousy Bank	18	*Funck et al.* (2008)
Lousy Bank	24	*Klingelhöfer et al.* (2005)
Mendeleev Ridge	32	*Lebedeva-Ivanova et al.* (2006)
Mendeleev Ridge	28–30	*Poselov et al.* (2012b)
New Caledonia Ridge	24.5	*Klingelhöfer et al.* (2007)
Norfolk Ridge	17	*Klingelhöfer et al.* (2007)
Norfolk Ridge	15.1	*Shor et al.* (1971)
Orphan Knoll	12–15	*Chian et al.* (2001)
Porcupine Bank	28	*Whitmarsh et al.* (1974)
Porcupine Bank	25	*O'Reilly et al.* (2006)
Rockall Bank	30	*Vogt et al.* (1998)
Sao Paolo Plateau	12–16	gravity modelling: *Scotchman et al.* (2010)
Seychelles	40	*Collier et al.* (2009)
Average	23± 7	

Table 14.2: Crustal thicknesses of failed basins

Failed basins	Thickness of crust (km)	Reference
Bounty Trough	15	*Grobys et al.* (2007)
Fairway Basin	10-15	*Klingelhöfer et al.* (2007)
Faroe-Shetland Basin	15	*Richardson et al.* (1999)
Faroe-Shetland Basin	9	*Roberts et al.* (2009)
Flemish Pass	15-17	*Keen and Barrett* (1981)
Galicia Interior Basin	13	*González et al.* (1999)
Galicia Interior Basin	6-8	*Pérez-Gussinyé et al.* (2003)
Great South Basin	13	*Grobys et al.* (2009)
Hatton Basin	15	*Vogt et al.* (1998)
Hatton Basin	12.5	*White and Smith* (2009)
Hatton Basin	7.5	*Funck et al.* (2008)
Hatton Continental Margin	12	*Fowler et al.* (1989)
Hatton Continental Margin	18	*White and Smith* (2009)
Jan Mayen Basin	3	*Kodaira et al.* (1998)
Makarov Basin	5-7	*Lebedeva-Ivanova et al.* (2011)
Makarov Basin	20-23	*Artyushkov* (2010)
Makarov Basin III	9-10	*Artyushkov* (2010)

Table 14.2: continued.

Mendeleev Basin	13	*Lebedeva-Ivanova et al.* (2006)
New Caledonia Basin	8-10	*Klingelhöfer et al.* (2007)
New Caledonia Basin	4.5-14.7	*Shor et al.* (1971)
Orphan Basin	14	*Chian et al.* (2001)
Orphan Basin	15-17	*Keen and Barrett* (1981)
Podvodnikov Basin	20	*Lebedeva-Ivanova et al.* (2006)
Podvodnikov Basin	10-24	*Lebedeva-Ivanova et al.* (2011)
Podvodnikov Basin	16-20	*Artyushkov* (2010)
Porcupine Basin	2	*O'Reilly et al.* (2006)
Rockall Trough	5-7	*Hauser et al.* (1995)
Rockall Trough	5-6	*O'Reilly et al.* (1996)
Rockall Trough (N Rockall Basin)	13	*Klingelhöfer et al.* (2005)
Rockall Trough (S Rockall Basin)	6	*Morewood et al.* (2005)
Shetland Trough	13-15	*England et al.* (2005)
Tasman Basin	3.3	*Shor et al.* (1971)
Average	11 ± 5	

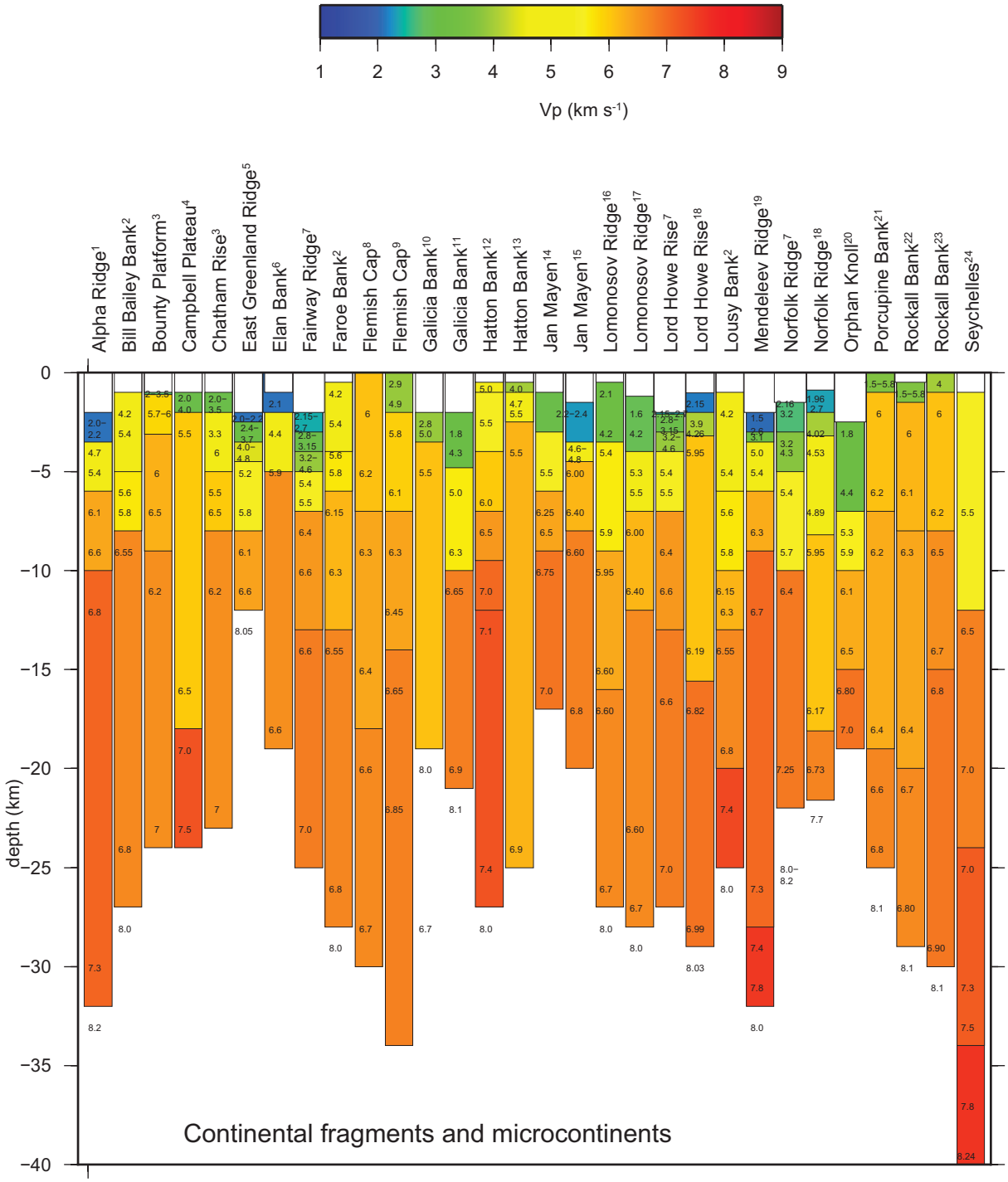

Figure 14.1: Crustal velocity profiles with depth below sea level for microcontinents and continental fragments. Velocity profiles are from (1) *Funck et al.* (2011), (2) *Funck et al.* (2008), (3) *Grobys et al.* (2007), (4) *Grobys et al.* (2009), (5) *Døssing et al.* (2008), (6) *Borissova et al.* (2003), (7) *Klingelhöfer et al.* (2007), (8) *Funck* (2003), (9) *Gerlings et al.* (2011), (10) *Clark et al.* (2007), (11) *Pérez-Gussinyé et al.* (2003), (12) *Fowler et al.* (1989), (13) *White and Smith* (2009), (14) *Breivik et al.* (2012), (15) *Kodaira et al.* (1998), (16) *Jackson and Dahl-Jensen* (2010), (17) *Poselov et al.* (2012b), (18) *Shor et al.* (1971), (19) *Lebedeva-Ivanova et al.* (2006), (20) *Chian et al.* (2001), (21) *O'Reilly et al.* (2006), (22) *Morewood et al.* (2005), (23) *Vogt et al.* (1998), and (24) *Collier et al.* (2009).

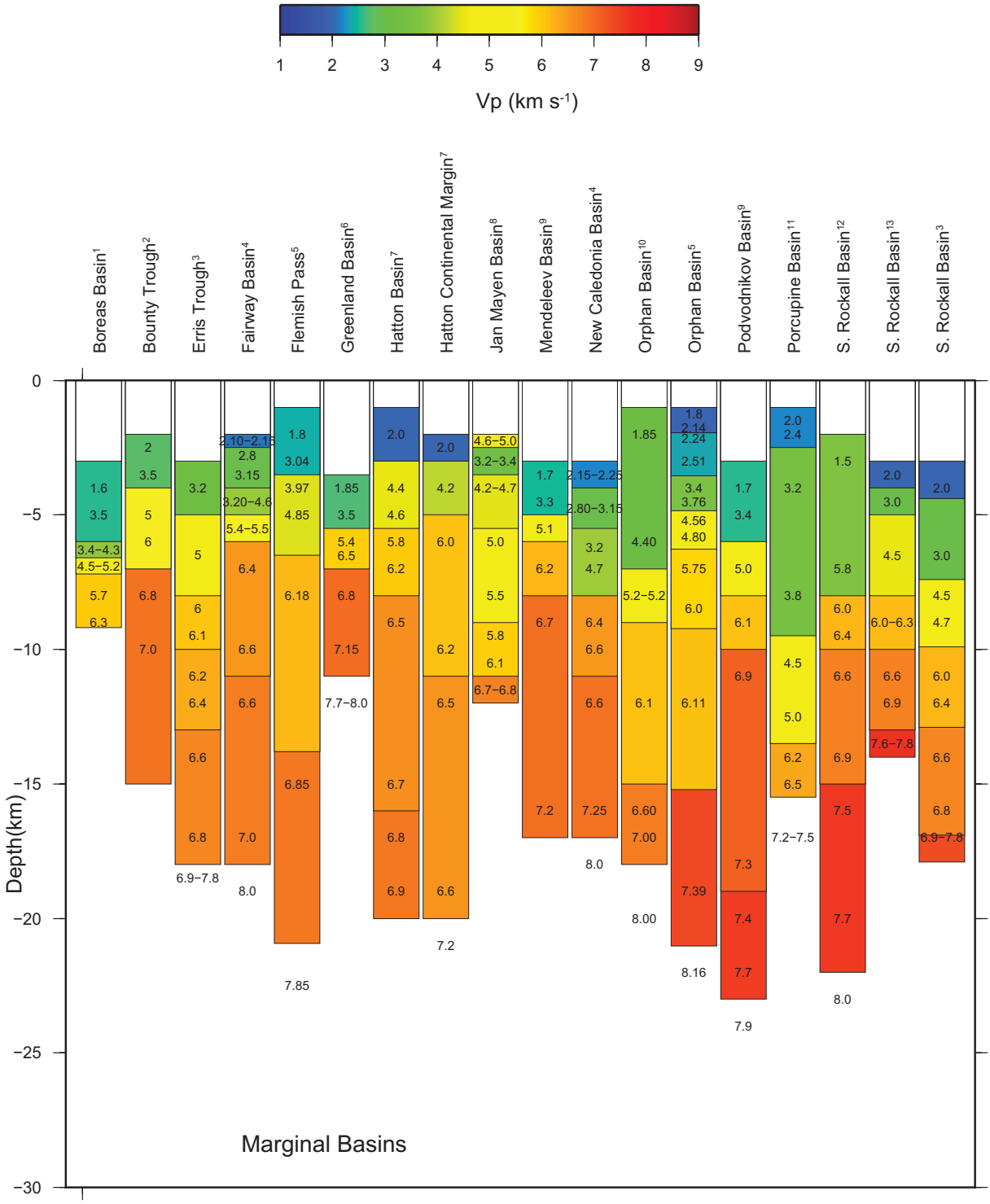

Figure 14.2: Crustal velocity profiles with depth below sea level for failed rift basins. Velocity profile are from (1) *Hermann and Jokat* (2013), (2) *Grobys et al.* (2007), (3) *O'Reilly et al.* (1995), (4) *Klingelhöfer et al.* (2007), (5) *Keen and Barrett* (1981), (6) *Døssing et al.* (2008), (7) *Vogt et al.* (1998), (8) *Kodaira et al.* (1998), (9) *Lebedeva-Ivanova et al.* (2006), (10) *Chian et al.* (2001), (11) *O'Reilly et al.* (2006), (12) *Morewood et al.* (2005), and (13) *Hauser et al.* (1995).

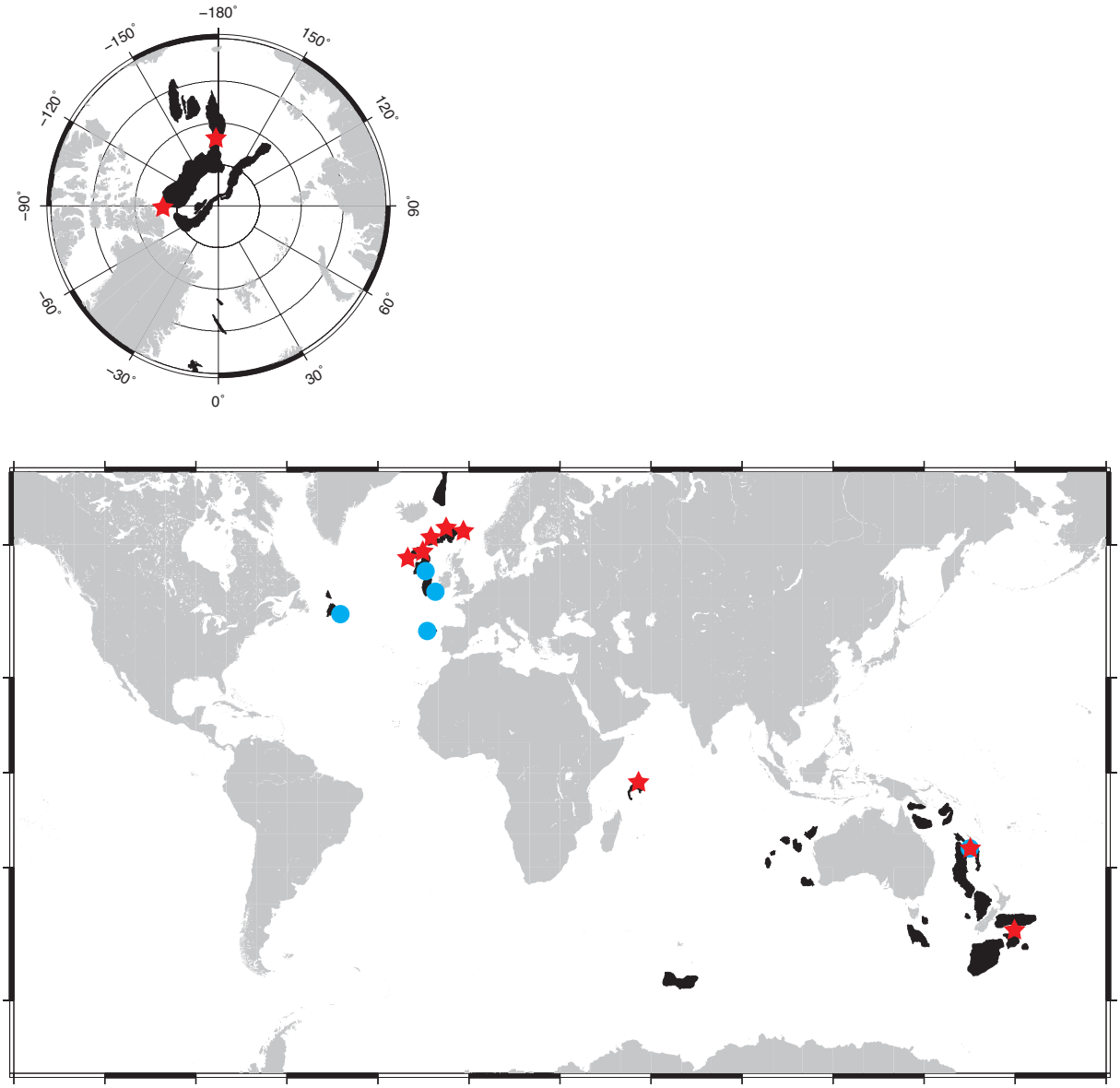

Figure 14.3: Global Map showing the locations of continental fragments (black) and the locations where magmatic underplating (red stars) and serpentinized mantle (blue circles) have been identified through deep crustal seismic studies. In the New Caledonia Basin, a red star overlies a blue circle because the interpreted serpentinized mantle region is more likely to be magmatic underplating.

15 REFERENCES

Alcock, M., H. Stagg, J. Colwell, I. Borissova, P. Symonds, and G. Bernardel (2006), Seismic transects of Australia's frontier continental margins, *Record 2006/004*, Geoscience Australia.

Alvey, A., C. Gaina, N. Kusznir, and T. Torsvik (2008), Integrated crustal thickness mapping and plate reconstructions for the high Arctic, *Earth Planet. Sci. Lett.*, *274*, 310–321, doi: 10.1016/j.epsl.2008.07.036.

Amante, C., and B. Eakins (2009), ETOPO1 1 Arc-Minute Global Relief Model: Procedures, Data Sources and Analysis, *NOAA Technical Memorandum NESDIS NGDC-24*, National Geophysical Data Center, NOAA.

Artyushkov, E. (2010), Continental crust in the Lomonosov Ridge, Mendeleev Ridge, and the Makarov basin. The formation of deep-water basins in the Neogene, *Russian Geology and Geophysics*, *51*, 1179–1191, doi:10.1016/j.rgg.2010.10.003.

Bache, F., N. Mortimer, R. Sutherland, J. Collot, P. Rouillard, V. Stagpoole, and A. Nicol (2014), Seismic stratigraphic record of transition from Mesozoic subduction to continental breakup in the Zealandia sector of eastern Gondwana, *Gondwana Res.*, *26*(3–4), 1060–1078, doi:http://dx.doi.org/10.1016/j.gr.2013.08.012.

Benard, F., J.-P. Callot, R. Vially, J. Schmitz, W. Roest, M. Patriat, B. Loubrieu, and T. E. Team (2010), The Kerguelen plateau: Records from a long-living/composite microcontinent, *Mar. Petrol. Geol.*, *27*, 633–649.

Bernard, A., and M. Munschy (2000), Le bassin des Mascareignes et le bassin de Laxmi (océan Indien occidental) se sont-ils formés àl'axe d'un même centre d'expansion ?, *Comptes Rendus de l'Académie des Sciences*, *330*(11), 777–783, doi:http://dx.doi.org/10.1016/S1251-8050(00)00221-4.

Borissova, I. (2002), Geological framework of the Naturaliste Plateau, *Geoscience Australia Record*, *Record 2002.20*, 44.

Borissova, I., A. Moore, J. Sayers, R. Parums, M. F. Coffin, and P. A. Symonds (2002), Geological framework of the Kerguelen Plateau and adjacent ocean basins, *Geoscience Australia Record*, *Record 2002/05*, 120.

Borissova, I., M. F. Coffin, P. Charvis, and S. Operto (2003), Structure and development of a microcontinent: Elan Bank in the southern Indian Ocean, *Geochem. Geophys. Geosyst.*, *4*(9), 1071, doi:10.1029/2003GC000535.

Breivik, A. J., R. Mjelde, J. I. Faleide, and Y. Murai (2012), The eastern Jan Mayen microcontinent volcanic margin, *Geophys. J. Int.*, *188*(3), 798–818, doi:10.1111/j.1365-246X.2011.05307.x.

Brown, B. J., R. D. Müller, C. Gaina, H. I. M. Struckmeyer, H. Stagg, and P. A. Symonds (2003), Formation and evolution of Australian passive margins: implications for locating the boundary between continental and oceanic crust, *Geol. Soc. Amer. Spec. Pap.*, *372*, 223–243.

Buiter, S. J. H., and T. H. Torsvik (2014), A review of Wilson Cycle plate margins: A role for mantle plumes in continental break-up along sutures?, *Gondwana Res.*, *26*(2), 627–653, doi:http://dx.doi.org/10.1016/j.gr.2014.02.007.

Calvès, G., T. Torvela, M. Huuse, and M. G. Dinkleman (2012), New evidence for the origin of the Porcupine Median Volcanic Ridge: Early Cretaceous volcanism in the Porcupine Basin, Atlantic margin of Ireland, *Geochem. Geophys. Geosyst.*, *13*(6), Q06,001, doi: 10.1029/2011GC003852.

Carter, R. M., L. Carter, and B. Davy (1994), Seismic stratigraphy of the Bounty Trough, south-west Pacific Ocean, *Mar. Petrol. Geol.*, *11*(1), 79–93, doi:http://dx.doi.org/10.1016/0264-8172(94)90011-6.

Charvis, P., and S. Operto (1999), Structure of the Cretaceous Kerguelen Volcanic Province (southern Indian Ocean) from wide-angle seismic data., *Geodynamics*, *28*, 51–71.

Chian, D., I. D. Reid, and H. R. Jackson (2001), Crustal structure beneath Orphan Basin and implications for nonvolcanic continental rifting, *J. Geophys. Res.: Solid Earth*, *106*(B6), 10,923–10,940, doi:10.1029/2000JB900422.

Clark, S. A., D. S. Sawyer, J. A. Austin, G. L. Christeson, and Y. Nakamura (2007), Characterizing the Galicia Bank-Southern Iberia Abyssal Plain rifted margin segment boundary using multichannel seismic and ocean bottom seismometer data, *J. Geophys. Res.*, *112*(B3), B03,408, doi:10.1029/2006JB004581.

Coffin, M. F. (1992), Emplacement and subsidence of Indian Ocean plateaus and submarine ridges, *Geophys. Monograph*, *70*, 115–125.

Coffin, M. F., M. S. Pringle, R. A. Duncan, T. Gladczenko, M. Storey, R. D. Müller, and L. A. Gahagan (2002), Kerguelen Hotspot Magma Output since 130 Ma, *J. Petrol.*, *43*(7), 1121–1137.

Collier, J. S., V. Sansom, O. Ishizuka, R. N. Taylor, T. A. Minshull, and R. B. Whitmarsh (2008), Age of Seychelles–India break-up, *Earth Planet. Sci. Lett.*, *272*(1–2), 264–277, doi: http://dx.doi.org/10.1016/j.epsl.2008.04.045.

Collier, J. S., T. A. Minshull, J. O. S. Hammond, R. B. Whitmarsh, J. Kendall, V. Sansom, C. I. Lane, and G. Rumpker (2009), Factors influencing magmatism during continental breakup: New insights from a wide-angle seismic experiment across the conjugate Seychelles-Indian margins, *J. Geophys. Res.*, *114*, B03,101, doi:10.1029/2008JB005898.

Collot, J., R. Herzer, Y. Lafoy, and L. Géli (2009), Mesozoic history of the Fairway-Aotea Basin: Implications for the early stages of Gondwana fragmentation, *Geochem. Geophys. Geosyst.*, *10*(12), Q12,019, doi:10.1029/2009GC002612.

Colwell, J., P. Symonds, and A. Crawford (1994), The nature of the Wallaby (Cuvier) Plateau and other igneous provines of the west Australian margin, *J. Austr. Geol. Geophys.*, *15*, 137–156.

Corfield, R. (2013), Reaching for the real Atlantis, *Chemistry and Industry*, *77*(8), 36–39.

Corfield, S., N. Murphy, and S. Parker (1999), The structural and stratigraphic framework of the Irish Rockall Trough, *Geol. Soc. London, Petrol. Geol. Conf. series*, *5*, 407–420.

Courtillot, V. E., and P. R. Renne (2003), On the ages of flood basalt events, *Comptes Rendus Geoscience*, *335*(1), 113–140, doi:http://dx.doi.org/10.1016/S1631-0713(03)00006-3.

Coward, M. P. (1995), Structural and tectonic setting of the Permo-Triassic basins of northwest Europe, *Geol. Soc. Spec. Pub.*, *91*(1), 7–39.

Crawford, A. J., S. Meffre, and P. A. Symonds (2003), 120 to 0 Ma tectonic evolution of the southwest Pacific and analogous geological evolution of the 600 to 220 Ma Tasman Fold Belt System, *Geol. Soc. Amer. Spec. Pap.*, *372*, 383–403.

Davy, B. (2006), Bollons Seamount and early New Zealand–Antarctic seafloor spreading, *Geochem. Geophys. Geosyst.*, *7*(6), Q06,021, doi:10.1029/2005GC001191.

Davy, B., and R. Wood (1994), Gravity and magnetic modelling of the Hikurangi Plateau, *Marine Geology*, *118*, 139–151.

Davy, B., K. Hoernle, and R. Werner (2008), Hikurangi Plateau: Crustal structure, rifted formation, and Gondwana subduction history, *Geochem. Geophys. Geosyst.*, *9*(7), doi:10.1029/2007GC001,855.

Dean, K., K. McLachlan, and A. Chambers (1999), Rifting and the development of the Faeroe-Shetland Basin, *Geol. Soc. London, Petrol. Geol. Conf. series*, *5*, 533–544.

Direen, N. G., I. Borissova, H. M. J. Stagg, J. B. Colwell, and P. A. Symonds (2007), Nature of the continent ocean transition zone along the southern Australian continental margin: a comparison of the Naturaliste Plateau, SW Australia, and the central Great Australian Bight sectors, *Geol. Soc. Spec. Pub.*, *282*, 239–263, doi:10.1144/SP282.12.

Direen, N. G., H. M. J. Stagg, P. A. Symonds, and J. B. Colwell (2008), Architecture of volcanic rifted margins: new insights from the Exmouth-Gascoyne margin, Western Australia, *Austr. J. Earth Sci.*, *55*(3), 341–363, doi:10.1080/08120090701769472.

Doré, A. G., E. R. Lundin, L. N. Jensen, Ø. Birkeland, P. E. Eliassen, and C. Fichler (1999), Principal tectonic events in the evolution of the northwest European Atlantic margin, *Geol. Soc. London, Petrol. Geol. Conf. series*, *5*, 41–61, doi:10.1144/0050041.

Døssing, A., and T. Funck (2012), Greenland Fracture Zone–East Greenland Ridge(s) revisited: Indications of a C22-change in plate motion?, *J. Geophys. Res.: Solid Earth*, *117*, B01,103, doi:10.1029/2011JB008393.

Døssing, A., T. Dahl-Jensen, H. Thybo, R. Mjelde, and Y. Nishimura (2008), East Greenland Ridge in the North Atlantic Ocean: An integrated geophysical study of a continental sliver in a boundary transform fault setting, *J. Geophys. Res.: Solid Earth*, *113*, B10,107, doi: 10.1029/2007JB005536.

Døssing, A., H. Jackson, J. Matzka, I. Einarsson, T. Rasmussen, A. Olesen, and J. Brozena (2013), On the origin of the Amerasia Basin and the High Arctic Large Igneous Province-Results of new aeromagnetic data, *Earth Planet. Sci. Lett.*, *363*, 219 – 230, doi:http://dx.doi.org/10.1016/j.epsl.2012.12.013.

Dove, D., B. Coakley, J. Hopper, Y. Kristoffersen, and H. G. Team (2010), Bathymetry, controlled source seismic and gravity observations of the Mendeleev ridge; implications for ridge structure, origin, and regional tectonics, *Geophys. J. Int.*, *183*(2), 481–502, doi: 10.1111/j.1365-246X.2010.04746.x.

Driscoll, N. W., and G. D. Karner (1998), Lower crustal extension across the Northern Carnarvon basin, Australia: Evidence for an eastward dipping detachment, *J. Geophys. Res.*, *103*(B3), 4975–4991, doi:10.1029/97JB03295.

Duncan, R. A. (2002), Origin and evolution of the Kerguelen Plateau, Broken Ridge and Kerguelen Archipelago: Editorial Origin and evolution of the Kerguelen Plateau, Broken Ridge

and Kerguelen Archipelago: Editorial A Time Frame for Construction of the Kerguelen Plateau and Broken Ridge A Time Frame for Construction of the Kerguelen Plateau and Broken Ridge A time frame for construction of the Kerguelen Plateau and Broken Ridge, *J. Petrol.*, *43*(7), 1109–1119.

Eagles, G., R. Gloaguen, and C. Ebinger (2002), Kinematics of the Danakil microplate, *Earth Planet. Sci. Lett.*, *203*, 607–620.

Eagles, G., K. Gohl, and R. D. Larter (2004), High-resolution animated tectonic reconstruction of the south pacific and west antarctic margin, *Geochem. Geophys. Geosyst.*, *5*(7), Q07,002, doi:10.1029/2003GC000657.

Elliott, G. M., and L. M. Parson (2008), Influence of margin segmentation upon the break-up of the Hatton Bank rifted margin, NE Atlantic, *Tectonophysics*, *457*, 161–176, doi:10.1016/j.tecto.2008.06.008.

Engen, Ø., J. I. Faleide, and T. K. Dyreng (2008), Opening of the fram strait gateway: A review of plate tectonic constraints, *Tectonophysics*, *450*(1–4), 51–69, doi:http://dx.doi.org/10.1016/j.tecto.2008.01.002.

England, R., J. McBride, and R. Hobbs (2005), The role of Mesozoic rifting in the opening of the NE Atlantic: evidence from deep seismic profiling across the Faroe-Shetland Trough, *J. Geol. Soc.*, *162*, 661–673, doi:10.1144/0016-764904-076.

Exon, N. F., A. M. G. Moore, and P. J. Hill (1997), Geological framework of the South Tasman Rise, south of Tasmania, and its sedimentary basins, *Austr. J. Earth Sci.*, *44*(5), 561–577, doi:10.1080/08120099708728337.

Foster, D. G., and A. G. Robinson (1993), Geological History of the Flemish Pass Basin, Offshore Newfoundland, *AAPG Bulletin*, *77*(4), 588–609.

Fowler, S. R., R. S. White, G. D. Spence, and G. K. Westbrook (1989), The Hatton Bank continental margin-II. Deep structure from two-ship expanding spread seismic profiles, *Geophys. J. Int.*, *96*, 295–309, doi:10.1111/j.1365-246X.1989.tb04452.x.

Francis, T. J., and G. G. Shor (1966), Seismic refraction measurements in the northwest Indian Ocean, *J. Geophys. Res.*, *71*(2), 427–449.

Funck, T. (2003), Crustal structure of the ocean-continent transition at Flemish Cap: Seismic refraction results, *J. Geophys. Res.*, *108*(B11), 2531, doi:10.1029/2003JB002434.

Funck, T., M. S. Andersen, J. K. Neish, and T. Dahl-Jensen (2008), A refraction seismic transect from the Faroe Islands to the Hatton-Rockall Basin, *J. Geophys. Res.*, *113*, B12,405, doi:10.1029/2008JB005675.

Funck, T., H. R. Jackson, and J. Shimeld (2011), The crustal structure of the Alpha Ridge at the transition to the Canadian Polar Margin: Results from a seismic refraction experiment, *J. Geophys. Res.*, *116*(B12), B12,101, doi:10.1029/2011JB008411.

Gaina, C., R. D. Müller, J. Royer, J. Stock, J. Hardebeck, and P. Symonds (1998), The tectonic history of the Tasman Sea: A puzzle with 13 pieces, *J. Geophys. Res.*, *103*(B6), 12,413–12,433, doi:10.1029/98JB00386.

Gaina, C., W. R. Roest, and R. D. Müller (2002), Late Cretaceous–Cenozoic deformation of

northeast Asia, *Earth Planet. Sci. Lett.*, *197*(3–4), 273–286, doi:http://dx.doi.org/10.1016/S0012-821X(02)00499-5.

Gaina, C., R. Müller, B. Brown, and T. Ishihara (2003), Microcontinent formation around Australia, in *Evolution and Dynamics of the Australian Plate*, *GSA Special Paper*, vol. 372, edited by R. Hillis and R. Muller, pp. 405–416, Geological Society of America.

Gaina, C., R. D. Müller, B. Brown, T. Ishihara, and S. Ivanov (2007), Breakup and early seafloor spreading between India and Antarctica, *Geophys. J. Int.*, *170*(1), 151–169.

Gaina, C., L. Gernigon, and P. Ball (2009), Palaeocene-Recent plate boundaries in the NE Atlantic and the formation of the Jan Mayen microcontinent, *J. Geol. Soc.*, *166*, 601–616, doi:10.1144/0016-76492008-112.

Gaina, C., S. Medvedev, T. Torsvik, I. Koulakov, and S. Werner (2014), 4D Arctic: A Glimpse into the Structure and Evolution of the Arctic in the Light of New Geophysical Maps, Plate Tectonics and Tomographic Models, *Surveys in Geophysics*, *35*(5), 1095–1122, doi:10.1007/s10712-013-9254-y.

Ganerød, M., T. H. Torsvik, D. J. J. van Hinsbergen, C. Gaina, F. Corfu, S. Werner, T. M. Owen-Smith, L. D. Ashwal, S. J. Webb, and B. W. H. Hendriks (2011), Palaeoposition of the Seychelles microcontinent in relation to the Deccan Traps and the Plume Generation Zone in Late Cretaceous-Early Palaeogene time, *Geol. Soc. Spec. Pub.*, *357*(1), 229–252.

Gardner, R. L., N. R. Daczko, J. A. Halpin, and J. M. Whittaker (2015), Discovery of a microcontinent (Gulden Draak Knoll) offshore Western Australia: Implications for East Gondwana reconstructions, *Gondwana Res., In Press*, xxx–xxx, doi:http://dx.doi.org/10.1016/j.gr.2014.08.013.

Gerlings, J., K. E. Louden, and H. R. Jackson (2011), Crustal structure of the Flemish Cap Continental Margin (eastern Canada): an analysis of a seismic refraction profile, *Geophys. J. Int.*, *185*, 30–48, doi:10.1111/j.1365-246X.2011.04931.x.

Gernigon, L., C. Gaina, O. Olesen, P. J. Ball, G. Péron-Pinvidic, and T. Yamasaki (2012), The Norway Basin revisited: From continental breakup to spreading ridge extinction, *Mar. Petrol. Geol.*, *35*(1), 1–19, doi:http://dx.doi.org/10.1016/j.marpetgeo.2012.02.015.

Gibbons, A. D., U. Barckhausen, P. van den Bogaard, K. Hoernle, R. Werner, J. M. Whittaker, and R. D. Müller (2012), Constraining the Jurassic extent of Greater India: Tectonic evolution of the West Australian margin, *Geochem. Geophys. Geosyst.*, *13*(5), Q05W13, doi:10.1029/2011GC003919.

Gibbons, A. D., J. M. Whittaker, and R. D. Müller (2013), The breakup of East Gondwana: Assimilating constraints from Cretaceous ocean basins around India into a best-fit tectonic model, *J. Geophys. Res.*, *118*, 808–822, doi:10.1002/jgrb.50079.

Glebovsky, V. Y., V. D. Kaminsky, A. N. Minakov, S. A. Merkurev, V. A. Childers, and J. M. Brozena (2006), Formation of the Eurasia Basin in the Arctic Ocean as inferred from geohistorical analysis of the anomalous magnetic field, *Geotectonics*, *40*(4), 263–281, doi:10.1134/S0016852106040029.

Goncharov, A., and G. Nelson (2012), From two way time to depth and pressure for interpretation of seismic velocities offshore: Methodology and examples from the Wallaby Plateau on

the West Australian margin, *Tectonophysics*, *572–573*, 26–37, doi:http://dx.doi.org/10.1016/j.tecto.2012.06.037.

González, A., D. Córdoba, and D. Vales (1999), Seismic crustal structure of Galicia Continental Margin, NW Iberian Peninsula, *Geophys. Res. Lett.*, *26*(8), 1061–1064, doi:10.1029/1999GL900193.

Grantz, A., D. L. Clark, R. L. Phillips, S. P. Srivastava, C. D. Blome, L. B. Gray, H. Haga, B. L. Mamet, D. J. McIntyre, D. H. McNeil, M. B. Mickey, M. W. Mullen, B. I. Murchey, C. A. Ross, C. H. Stevens, N. J. Silberling, J. H. Wall, and D. A. Willard (1998), Phanerozoic stratigraphy of Northwind Ridge, magnetic anomalies in the Canada basin, and the geometry and timing of rifting in the Amerasia basin, Arctic Ocean, *Geol. Soc. Am. Bull.*, *110*, 6801–6820, doi:10.1130/0016-7606(1998)110⟨0801:PSONRM⟩2.3.CO;2.

Grantz, A., P. E. Hart, and V. A. Childers (2011), Geology and tectonic development of the Amerasia and Canada Basins, Arctic Ocean, *Geol. Soc. Mem.*, *35*(1), 771–799.

Grobys, J., K. Gohl, G. Uenzelmann-Neben, B. Davy, and D. Barker (2009), Extensional and magmatic nature of the Campbell Plateau and Great South Basin from deep crustal studies, *Tectonophysics*, *472*, 213–225, doi:10.1016/j.tecto.2008.05.003.

Grobys, J. W. G., K. Gohl, B. Davy, G. Uenzelmann-Neben, T. Deen, and D. Barker (2007), Is the Bounty Trough off eastern New Zealand an aborted rift?, *J. Geophys. Res.: Solid Earth*, *112*, B03,103, doi:10.1029/2005JB004229.

Grobys, J. W. G., K. Gohl, and G. Eagles (2008), Quantitative tectonic reconstructions of Zealandia based on crustal thickness estimates, *Geochem. Geophys. Geosyst.*, *9*(1), Q01,005, doi:10.1029/2007GC001691.

Hackney, R., J. Goodwin, L. Hall, K. Higgins, N. Holzrichter, S. Johnston, M. Morse, G. K. Nayak, and P. Petkovic (2015), Potential-field data in integrated frontier basin geophysics: Successes and challenges on australia's continental margin, *Mar. Petrol. Geol.*, *59*, 611–637, doi:http://dx.doi.org/10.1016/j.marpetgeo.2014.01.014.

Hall, L., A. Gibbons, G. Bernardel, J. Whittaker, C. Nicholson, N. Rollet, and R. Müller (2013), Structural architecture of Australia's southwest continental margin and implications for Early Cretaceous basin evolution, *The Sedimentary Basins of Western Australia IV: Proceedings of the Petroleum Exploration Society of Australia Symposium*, *18-21*, 2–20.

Halpin, J. A., A. J. Crawford, N. G. Direen, M. F. Coffin, C. J. Forbes, and I. Borissova (2008), Naturaliste Plateau, offshore Western Australia: A submarine window into Gondwana assembly and breakup, *Geology*, *36*, 807–810, doi:10.1130/G25059A.1.

Hammond, J. O. S., J. M. Kendall, J. S. Collier, and G. Rumpker (2013), The extent of continental crust beneath the Seychelles, *Earth Planet. Sci. Lett.*, *381*, 166–176, doi:http://dx.doi.org/10.1016/j.epsl.2013.08.023.

Harland, K. E., R. S. White, and H. Soosalu (2009), Crustal structure beneath the Faroe Islands from teleseismic receiver functions, *Geophys. J. Int.*, *177*(1), 115–124.

Hauser, F., B. M. O'Reilly, A. W. B. Jacob, P. M. Shannon, J. Makris, and U. Vogt (1995), The crustal structure of the Rockall Trough: Differential stretching without underplating, *J. Geophys. Res.*, *100*(B3), 4097–4116, doi:10.1029/94JB02879.

Heine, C., and R. D. Müller (2005), Late Jurassic rifting along the Australian North West Shelf: margin geometry and spreading ridge configuration, *Austr. J. Earth Sci.*, *52*, 27–39, doi: 10.1080/08120090500100077.

Heinson, G. (2005), Rifting of a passive margin and development of a lower-crustal detachment zone: Evidence from marine magnetotellurics, *Geophys. Res. Lett.*, *32*, doi: 10.1029/2005GL022934.

Hermann, T., and W. Jokat (2013), Crustal structures of the Boreas Basin and the Knipovich Ridge, North Atlantic, *Geophys. J. Int.*, *193*, 1399–1414, doi:10.1093/gji/ggt048.

Hill, P., and A. Moore (2001), Geological Framework of the South Tasman Rise and East Tasman Plateau, *Geoscience Australia Record, 2001/040*, 62.

Hopper, J. R., J. C. Mutter, R. L. Larson, and C. Z. Mutter (1992), Magmatism and rift margin evolution: Evidence from northwest Australia, *Geology*, *20*, 853–857, doi:10.1130/0091-7613(1992)020⟨0853:MARMEE⟩2.3.CO;2.

Ingle, S., D. Weis, and F. A. Frey (2002), Indian Continental Crust Recovered from Elan Bank, Kerguelen Plateau (ODP Leg 183, Site 1137), *J. Petrol.*, *43*(7), 1241–1257.

Jackson, H. R., and T. Dahl-Jensen (2010), Sedimentary and crustal structure from the Ellesmere Island and Greenland continental shelves onto the Lomonosov Ridge, Arctic Ocean, *Geophys. J. Int.*, *182*, 11–35, doi:10.1111/j.1365-246X.2010.04604.x.

Jokat, W. (2003), Seismic investigations along the western sector of Alpha Ridge, Central Arctic Ocean, *Geophys. J. Int.*, *152*, 185–201, doi:10.1046/j.1365-246X.2003.01839.x.

Jokat, W., M. Ickrath, and J. O'Connor (2013), Seismic transect across the Lomonosov and Mendeleev Ridges: Constraints on the geological evolution of the Amerasia Basin, Arctic Ocean, *Geophys. Res. Lett.*, *40*(19), 2013GL057,275, doi:10.1002/grl.50975.

Jung, W.-Y., and P. R. Vogt (1997), A gravity and magnetic anomaly study of the extinct Aegir Ridge, Norwegian Sea, *J. Geophys. Res.*, *102*(B3), 5065–5089, doi:10.1029/96JB03915.

Kandilarov, A., R. Mjelde, R.-B. Pedersen, B. Hellevang, C. Papenberg, C.-J. Petersen, L. Planert, and E. Flueh (2012), The northern boundary of the Jan Mayen microcontinent, North Atlantic determined from ocean bottom seismic, multichannel seismic, and gravity data, *Marine Geophysical Research*, *33*(1), 55–76, doi:10.1007/s11001-012-9146-4.

Keen, C. E., and D. L. Barrett (1981), Thinned and subsided continental crust on the rifted margin of eastern canada: crustal structure, thermal evolution and subsidence history, *Geophys. J. R. astr. Soc.*, *65*(2), 443–465, doi:10.1111/j.1365-246X.1981.tb02721.x.

Kimbell, G. S., and P. C. Richards (2008), The three-dimensional lithospheric structure of the Falkland Plateau region based on gravity modelling, *J. Geol. Soc.*, *165*(4), 795–806.

King, L. H., G. B. Fader, W. H. Poole, and R. K. Wanless (1985), Geological setting and age of the Flemish Cap granodiorite, east of the Grand Banks of Newfoundland, *Canadian Journal of Earth Sciences*, *22*(9), 1286–1298.

Klingelhöfer, F., R. A. Edwards, R. W. Hobbs, and R. W. England (2005), Crustal structure of the NE Rockall Trough from wide-angle seismic data modeling, *J. Geophys. Res.: Solid Earth*, *110*, B11,105, doi:10.1029/2005JB003763.

Klingelhöfer, F., Y. Lafoy, J. Collot, E. Cosquer, L. Géli, H. Nouzé, and R. Vially (2007), Crustal structure of the basin and ridge system west of New Caledonia (southwest Pacific) from wide-angle and reflection seismic data, *J. Geophys. Res.*, *112*, B11,102, doi:10.1029/2007JB005093.

Kodaira, S., R. Mjelde, K. Gunnarsson, H. Shiobara, and H. Shimamura (1998), Structure of the Jan Mayen microcontinent and implications for its evolution, *Geophys. J. Int.*, *132*, 383–400, doi:10.1046/j.1365-246x.1998.00444.x.

Larter, R. D., A. P. Cunningham, P. F. Barker, K. Gohl, and F. O. Nitsche (2002), Tectonic evolution of the Pacific margin of Antarctica 1. Late Cretaceous tectonic reconstructions, *J. Geophys. Res.*, *107*(B12), 2345, doi:10.1029/2000JB000052.

Lebedeva-Ivanova, N. N., Y. Y. Zamansky, A. E. Langinen, and M. Y. Sorokin (2006), Seismic profiling across the Mendeleev Ridge at 82 N: evidence of continental crust, *Geophys. J. Int.*, *165*, 527–544, doi:10.1111/j.1365-246X.2006.02859.x.

Lebedeva-Ivanova, N. N., D. G. Gee, and M. B. Sergeyev (2011), Crustal structure of the East Siberian continental margin, Podvodnikov and Makarov basins, based on refraction seismic data (TransArctic 1989-1991), *Geol. Soc. Mem.*, *35*, 395–411, doi:10.1144/M35.26.

Mackenzie, G., P. Shannon, A. Jacob, N. Morewood, J. Makris, M. Gaye, and F. Egloff (2002), The velocity structure of the sediments in the southern Rockall Basin: results from new wide-angle seismic modelling, *Mar. Petrol. Geol.*, *19*, 989–1003, doi:10.1016/S0264-8172(02)00133-2.

Maloney, D., C. Sargent, N. G. Direen, R. W. Hobbs, and D. R. Grocke (2011), Re-evaluation of Mentelle Basin, a polyphase rifted margin basin, offshore southwest Australia: new insights from integrated regional seismic datasets, *Solid Earth*, *2*(2), 107–123.

McDougall, I., M. A. H. Maboko, P. A. Symonds, M. T. McCulloch, I. S. Williams, and H. R. Kudrass (1994), Dampier Ridge, Tasman Sea, as a stranded continental fragment, *Austr. J. Earth Sci.*, *41*(5), 395–406, doi:10.1080/08120099408728150.

Mihut, D., and R. Müller (1998), Volcanic margin formation and Mesozoic rift propagators in the Cuvier Abyssal Plain off Western Australia, *J. Geophys. Res.*, *103*(11), 27,135–27,149.

Miller, E. L., J. Toro, G. Gehrels, J. M. Amato, A. Prokopiev, M. I. Tuchkova, V. V. Akinin, T. A. Dumitru, T. E. Moore, and M. P. Cecile (2006), New insights into arctic paleogeography and tectonics from u-pb detrital zircon geochronology, *Tectonics*, *25*(3), TC3013, doi:10.1029/2005TC001830.

Mjelde, R., I. Eckhoff, S. Solbakken, S. Kodaira, H. Shimamura, K. Gunnarsson, A. Nakanishi, and H. Shiobara (2007), Gravity and S-wave modelling across the Jan Mayen Ridge, North Atlantic; implications for crustal lithology, *Marine Geophysical Research*, *28*(1), 27–41, doi:10.1007/s11001-006-9012-3.

Morewood, N. C., P. M. Shannon, and G. D. Mackenzie (2004), Seismic stratigraphy of the southern Rockall Basin: a comparison between wide-angle seismic and normal incidence reflection data, *Mar. Petrol. Geol.*, *21*(9), 1149–1163, doi:http://dx.doi.org/10.1016/j.marpetgeo.2004.07.006.

Morewood, N. C., G. D. Mackenzie, P. M. Shannon, B. M. O'Reilly, P. W. Readman, and

J. Makris (2005), The crustal structure and regional development of the Irish Atlantic margin region, *Geol. Soc. London, Petrol. Geol. Conf. series*, *6*, 1023–1033, doi:10.1144/0061023.

Mortimer, N., R. H. Herzer, P. B. Gans, D. L. Parkinson, and D. Seward (1998), Basement geology from Three Kings Ridge to West Norfolk Ridge, southwest Pacific Ocean: evidence from petrology, geochemistry and isotopic dating of dredge samples, *Marine Geology*, *148*(3–4), 135–162, doi:http://dx.doi.org/10.1016/S0025-3227(98)00007-3.

Mortimer, N., F. Hauff, and A. T. Calvert (2008), Continuation of the New England Orogen, Australia, beneath the Queensland Plateau and Lord Howe Rise, *Austr. J. Earth Sci.*, *55*(2), 195–209, doi:10.1080/08120090701689365.

Mortimer, N., P. B. Gans, J. M. Palin, R. H. Herzer, B. Pelletier, and M. Monzier (2014), Eocene and Oligocene basins and ridges of the Coral Sea-New Caledonia region: Tectonic link between Melanesia, Fiji, and Zealandia, *Tectonics*, *33*(7), 2014TC003,598, doi:10.1002/2014TC003598.

Morton, A. C., K. Hitchen, C. M. Fanning, G. Yaxley, H. Johnson, and J. Ritchie (2009), Detrital zircon age constraints on the provenance of sandstones on Hatton Bank and Edoras Bank, NE Atlantic, *J. Geol. Soc.*, *166*, 137–146, doi:10.1144/0016-76492007-179.

Müller, R., D. Mihut, C. Heine, C. O'Neill, and I. Russell (2002), Tectonic and volcanic history of the carnarvon terrace: Constraints from seismic interpretation and geodynamic modelling, in *The Sedimentary Basins of Western Australia*, vol. 3, edited by J. Gorter, pp. 719–740, Petroleum Exploration Society of Australia.

Müller, R. D., C. Gaina, W. R. Roest, and D. L. Hansen (2001), A recipe for microcontinent formation, *Geology*, *29*(3), 203–206.

Mutter, J. C., and R. L. Larson (1989), Extension of the Exmouth Plateau, offshore northwestern Australia: Deep seismic reflection/refraction evidence for simple and pure shear mechanisms, *Geology*, *17*, 15–18, doi:10.1130/0091-7613(1989)017⟨0015:EOTEPO⟩2.3.CO;2.

Naylor, D., and P. Shannon (2005), The structural framework of the Irish Atlantic Margin, *Geol. Soc. London, Petrol. Geol. Conf. series*, *6*, 1009–1021, doi:10.1144/0061009.

Nicolaysen, K., S. Bowring, F. Frey, D. Weis, S. Ingle, M. S. Pringle, and M. F. Coffin (2001), Provenance of Proterozoic garnet-biotite gneiss recovered from Elan Bank, Kerguelen Plateau, southern Indian Ocean, *Geology*, *29*(3), 235–238.

Operto, S., and P. Charvis (1995), Kerguelen plateau: A volcanic passive margin fragment?, *Geology*, *23*(2), 137–140.

O'Reilly, B. M., F. Hauser, A. B. Jacob, P. M. Shannon, J. Makris, and U. Vogt (1995), The transition between the Erris and the Rockall basins: new evidence from wide-angle seismic data, *Tectonophysics*, *241*(1-2), 143–163, doi:http://dx.doi.org/10.1016/0040-1951(94)00166-7.

O'Reilly, B. M., F. Hauser, A. W. B. Jacob, and P. M. Shannon (1996), The lithosphere below the Rockall Trough: wide-angle seismic evidence for extensive serpentinisation, *Tectonophysics*, *255*(1–2), 1–23, doi:http://dx.doi.org/10.1016/0040-1951(95)00149-2.

O'Reilly, B. M., F. Hauser, C. Ravaut, P. M. Shannon, and P. W. Readman (2006), Crustal thinning, mantle exhumation and serpentinization in the Porcupine Basin, offshore Ireland: evidence from wide-angle seismic data, *J. Geol. Soc.*, *163*(5), 775–787.

Pease, V., S. Drachev, R. Stephenson, and X. Zhang (2014), Arctic lithosphere —a review, *Tectonophysics, 628*, 1–25, doi:http://dx.doi.org/10.1016/j.tecto.2014.05.033.

Pérez-Gussinyé, M., C. R. Ranero, T. J. Reston, and D. Sawyer (2003), Mechanisms of extension at nonvolcanic margins: Evidence from the Galicia interior basin, west of Iberia, *J. Geophys. Res.*, *108*(B5), 2245, doi:10.1029/2001JB000901.

Peron-Pinvidic, G., and G. Manatschal (2010), From microcontinents to extensional allochthons: witnesses of how continents rift and break apart?, *Petroleum Geoscience*, *16*, 1–10, doi:10.1144/1354-079309-903.

Peron-Pinvidic, G., L. Gernigon, C. Gaina, and P. Ball (2012a), Insights from the Jan Mayen system in the Norwegian-Greenland sea-I. Mapping of a microcontinent, *Geophys. J. Int.*, *191*(2), 385–412, doi:10.1111/j.1365-246X.2012.05639.x.

Peron-Pinvidic, G., L. Gernigon, C. Gaina, and P. Ball (2012b), Insights from the Jan Mayen system in the Norwegian-Greenland Sea-II. Architecture of a microcontinent, *Geophys. J. Int.*, *191*(2), 413–435, doi:10.1111/j.1365-246X.2012.05623.x.

Plummer, P. S., and E. R. Belle (1995), Mesozoic tectono-stratigraphic evolution of the Seychelles microcontinent, *Sedimentary Geology*, *96*(1–2), 73–91, doi:http://dx.doi.org/10.1016/0037-0738(94)00127-G.

Poselov, V. A., V. V. Butsenko, V. D. Kaminsky, and T. S. Sakulina (2012a), Mendeleev rise (Arctic Ocean) as a geological continuation of the continental margin of Eastern Siberia, *Dokl. Earth Sc.*, *443*(1), 388–391, doi:10.1134/S1028334X12030191.

Poselov, V. A., G. P. Avetisov, V. V. Butsenko, S. M. Zholondz, V. D. Kaminsky, and S. P. Pavlov (2012b), The Lomonosov Ridge as a natural extension of the Eurasian continental margin into the Arctic Basin, *Russian Geology and Geophysics*, *53*(12), 1276–1290, doi:http://dx.doi.org/10.1016/j.rgg.2012.10.002.

Prodehl, C., and W. D. Mooney (2012), *Exploring the Earth's Crust—History and Results of Controlled-Source Seismology*, *GSA Memoirs*, vol. 208, 7–46 pp., Geological Society of America.

Raum, T., R. Mjelde, A. M. Berge, J. T. Paulsen, P. Digranes, H. Shimamura, H. Shiobara, S. Kodaira, V. B. Larsen, R. Fredsted, D. J. Harrison, and M. Johnson (2005), Sub-basalt structures east of the Faroe Islands revealed from wide-angle seismic and gravity data, *Petroleum Geoscience*, *11*, 291–308, doi:10.1144/1354-079304-627.

Richardson, K. R., J. R. Smallwood, R. S. White, D. B. Snyder, and P. K. H. Maguire (1998), Crustal structure beneath the Faroe Islands and the Faroe-Iceland Ridge, *Tectonophysics*, *300*(1-4), 159–180.

Richardson, K. R., R. S. White, R. W. England, and J. Fruehn (1999), Crustal structure east of the Faroe Islands; mapping sub-basalt sediments using wide-angle seismic data, *Petroleum Geoscience*, *5*, 161–172, doi:10.1144/petgeo.5.2.161.

Ritzmann, O., W. Jokat, W. Czuba, A. Guterch, R. Mjelde, and Y. Nishimura (2004), A deep seismic transect from Hovgard Ridge to northwestern Svalbard across the continental-ocean transition: A sheared margin study, *Geophys. J. Int.*, *157*(2), 683–702.

Roberts, A. W., R. S. White, and P. A. F. Christie (2009), Imaging igneous rocks on the North Atlantic rifted continental margin, *Geophys. J. Int.*, *179*(2), 1024–1038.

Roberts, D., M. Thompson, B. Mitchener, H. Hossack, S. Carmichael, and H. M. Bjørnseth (1999), Palaeozoic to Tertiary rift and basin dynamics: mid-Norway to the Bay of Biscay–a new context for hydrocarbon prospectivity in the deep water frontier, *Geol. Soc. London, Petrol. Geol. Conf. series*, *5*, 7–40.

Roest, W. R., and S. P. Srivastava (1989), Sea-floor spreading in the Labrador Sea: A new reconstruction, *Geology*, *17*, 1000–1003, doi:10.1130/0091-7613(1989)017⟨1000:SFSITL⟩2.3.CO;2.

Rohrman, M. (2013), Intrusive large igneous provinces below sedimentary basins: An example from the Exmouth Plateau (NW Australia), *J. Geophys. Res.: Solid Earth*, *118*(8), 4477–4487, doi:10.1002/jgrb.50298.

Royer, J.-Y., and N. Rollet (1997), Plate-tectonic setting of the Tasmanian region, *Austr. J. Earth Sci.*, *44*(5), 543–560, doi:10.1080/08120099708728336.

Russell, S. M., and R. B. Whitmarsh (2003), Magmatism at the west Iberia non-volcanic rifted continental margin: evidence from analyses of magnetic anomalies, *Geophys. J. Int.*, *154*(3), 706–730.

Sayers, J., I. Borissova, D. Ramsay, and P. A. Symonds (2002), Geological framework of the wallaby plateau and adjacent areas, *Geoscience Australia Record*, *Record 2002/21*, 133.

Schellart, W. P., G. S. Lister, and V. G. Toy (2006), A Late Cretaceous and Cenozoic reconstruction of the Southwest Pacific region: Tectonics controlled by subduction and slab rollback processes, *Earth Sci. Rev.*, *76*(3–4), 191–233, doi:10.1016/j.earscirev.2006.01.002.

Scherwath, M., T. Stern, F. Davey, D. Okaya, W. S. Holbrook, R. Davies, and S. Kleffmann (2003), Lithospheric structure across oblique continental collision in New Zealand from wide-angle P wave modeling, *J. Geophys. Res.*, *108*(B12), 2566, doi:10.1029/2002JB002286.

Scotchman, I., G. Gilchrist, N. Kusznir, A. Roberts, and R. Fletcher (2010), The breakup of the South Atlantic Ocean: formation of failed spreading axes and blocks of thinned continental crust in the Santos Basin, Brazil and its consequences for petroleum system development, *Geol. Soc. London, Petrol. Geol. Conf. series*, *7*, 855–866, doi:10.1144/0070855.

Sdrolias, M., and R. D. Müller (2006), Controls on back-arc basin formation, *Geochem. Geophys. Geosyst.*, *7*(4), Q04,016, doi:10.1029/2005GC001090.

Sdrolias, M., R. Müller, and C. Gaina (2003), Tectonic evolution of the southwest pacific using constraints from backarc basins, in *Evolution and dynamics of the Australian plate*, *GSA Special Paper*, vol. 372, edited by R. Hillis and R. Muller, pp. 343–359, Geological Society of America.

Segev, A., M. Rybakov, and N. Mortimer (2012), A crustal model for Zealandia and Fiji, *Geophys. J. Int.*, *189*(3), 1277–1292.

Seton, M., R. Müller, S. Zahirovic, C. Gaina, T. Torsvik, G. Shephard, A. Talsma, M. Gurnis, M. Turner, S. Maus, and M. Chandler (2012), Global continental and ocean basin reconstructions since 200Ma, *Earth-Science Reviews*, *113*, 212–270, doi:10.1016/j.earscirev.2012.03.002.

Shannon, P., A. W. B. Jacob, and B. M. O'Reilly (1999), Structural setting, geological development and basin modelling in the Rockall Trough, *Geol. Soc. London, Petrol. Geol. Conf. series*, *5*, 421–431.

Shannon, P. M. (1991), The development of Irish offshore sedimentary basins, *J. Geol. Soc.*, *148*(1), 181–189, doi:10.1144/gsjgs.148.1.0181.

Shannon, P. M., A. McDonnell, and W. R. Bailey (2007), The evolution of the Porcupine and Rockall basins, offshore Ireland: the geological template for carbonate mound development, *International Journal of Earth Sciences*, *96*, 21–35, doi:10.1007/s00531-006-0081-y.

Shor, G., H. Kirk, and H. Menard (1971), Crustal structure of Melanesian area, *J. Geophys. Res.*, *76*(11), 2562–2586.

Sibuet, J., S. Srivastava, and G. Manatschal (2007a), Exhumed mantle-forming transitional crust in the Newfoundland-Iberia rift and associated magnetic anomalies, *J. Geophys. Res.*, *112*(B6), B06,105, doi:10.1029/2005JB003856.

Sibuet, J.-C., S. P. Srivastava, M. Enachescu, and G. D. Karner (2007b), Early Cretaceous motion of Flemish Cap with respect to North America: implications on the formation of Orphan Basin and SE Flemish Cap–Galicia Bank conjugate margins, *Geol. Soc. Spec. Pub.*, *282*(1), 63–76, doi:10.1144/SP282.4.

Smith, L. K., R. S. White, N. J. Kusznir, and iSIMM Team (2005), Structure of the Hatton Basin and adjacent continental margin, *Geol. Soc. London, Petrol. Geol. Conf. series*, *6*, 947–956.

Srivastava, S., J.-C. Sibuet, S. Cande, W. Roest, and I. Reid (2000), Magnetic evidence for slow seafloor spreading during the formation of the Newfoundland and Iberian margins, *Earth Planet. Sci. Lett.*, *182*(1), 61 – 76, doi:http://dx.doi.org/10.1016/S0012-821X(00)00231-4.

Stillwell, J. D., and C. P. Consoli (2012), Tectono-stratigraphic history of the Chatham Islands, SW Pacific—The emergence, flooding and reappearance of eastern 'Zealandia', *Proceedings of the Geologists' Association*, *123*(1), 170–181.

Stilwell, J. D., P. G. Quilty, and D. J. Mantle (2012), Paleontology of Early Cretaceous deep-water samples dredged from the Wallaby Plateau: new perspectives of Gondwana break-up along the Western Australian margin, *Austr. J. Earth Sci.*, *59*(1), 29–49, doi:10.1080/08120099.2011.615864.

Sutherland, R. (1999), Basement geology and tectonic development of the greater New Zealand region: an interpretation from regional magnetic data, *Tectonophysics*, *308*(3), 341–362, doi:http://dx.doi.org/10.1016/S0040-1951(99)00108-0.

Talwani, M., and O. Eldholm (1977), Evolution of the Norwegian-Greenland Sea, *Geol. Soc. Am. Bull.*, *88*(7), 969–999.

Torsvik, T. H., L. D. Ashwal, R. D. Tucker, and E. A. Eide (2001), Neoproterozoic geochronology and palaeogeography of the Seychelles microcontinent: the India link, *Precambrian Research*, *110*(1–4), 47–59, doi:http://dx.doi.org/10.1016/S0301-9268(01)00180-2.

Torsvik, T. H., H. Amundsen, E. H. Hartz, F. Corfu, N. Kusznir, C. Gaina, P. V. Doubrovine, B. Steinberger, L. D. Ashwal, and B. Jamtveit (2013), A Precambrian microcontinent in the Indian Ocean, *Nature Geosci.*, *6*(3), 223–227.

Tsikalas, F., O. Eldholm, and J. Faleide (2002), Early Eocene sea floor spreading and continent-ocean boundary between Jan Mayen and Senja fracture zones in the Norwegian-Greenland Sea, *Mar. Geophys. Res.*, *23*(3), 247–270, doi:10.1023/A:1023621228605.

Tucholke, B. E., D. S. Sawyer, and J.-C. Sibuet (2007), Breakup of the Newfoundland–Iberia rift, *Geol. Soc. Spec. Pub.*, *282*(1), 9–46, doi:10.1144/SP282.2.

Tucker, R. D., L. D. Ashwal, and T. H. Torsvik (2001), U–Pb geochronology of Seychelles granitoids: a Neoproterozoic continental arc fragment, *Earth Planet. Sci. Lett.*, *187*(1–2), 27–38, doi:http://dx.doi.org/10.1016/S0012-821X(01)00282-5.

Uenzelmann-Neben, G., J. Grobys, K. Gohl, and D. Barker (2009), Neogene sediment structures in Bounty Trough, eastern New Zealand: Influence of magmatic and oceanic current activity, *Geol. Soc. Am. Bull.*, *121*(1-2), 134–149.

Uruski, C. (2014), The contribution of offshore seismic data to understanding the evolution of the New Zealand continent, *Geol. Soc. Spec. Pub.*, *413*, 1–17.

Van Avendonk, H. J. A., W. S. Holbrook, D. Okaya, J. K. Austin, F. Davey, and T. Stern (2004), Continental crust under compression: A seismic refraction study of South Island Geophysical Transect I, South Island, New Zealand, *J. Geophys. Res.: Solid Earth*, *109*(B6), B06,302, doi:10.1029/2003JB002790.

Van Avendonk, H. J. A., W. S. Holbrook, G. T. Nunes, D. J. Shillington, B. E. Tucholke, K. E. Louden, H. C. Larsen, and J. R. Hopper (2006), Seismic velocity structure of the rifted margin of the eastern Grand Banks of Newfoundland, Canada, *J. Geophys. Res.: Solid Earth*, *111*(B11), B11,404, doi:10.1029/2005JB004156.

Veevers, J., C. Powell, and S. Roots (1991), Review of seafloor spreading around Australia. I. synthesis of the patterns of spreading, *Austr. J. Earth Sci.*, *38*(4), 373–389, doi:10.1080/08120099108727979.

Veevers, J. J. (2012), Reconstructions before rifting and drifting reveal the geological connections between Antarctica and its conjugates in Gondwanaland, *Earth-Science Reviews*, *111*(3–4), 249–318, doi:http://dx.doi.org/10.1016/j.earscirev.2011.11.009.

Vogt, U., J. Makris, B. M. O'Reilly, F. Hauser, P. W. Readman, A. W. B. Jacob, and P. M. Shannon (1998), The hatton basin and continental margin: Crustal structure from wide-angle seismic and gravity data, *J. Geophys. Res.: Solid Earth*, *103*(B6), 12,545–12,566, doi:10.1029/98JB00604.

Welford, J. K., J. Hall, J. Sibuet, and S. P. Srivastava (2010), Structure across the northeastern margin of Flemish Cap, offshore Newfoundland from Erable multichannel seismic reflection profiles: evidence for a transtensional rifting environment, *Geophys. J. Int.*, *183*, 572–586, doi:10.1111/j.1365-246X.2010.04779.x.

Wessel, P., and W. H. F. Smith (1991), Free software helps map and display data, *Eos Trans. AGU*, *72*(41), 441–446.

White, R., L. Smith, A. Roberts, P. Christie, N. Kusznir, i. Team, A. Roberts, D. Healy, R. Spitzer, A. Chappell, J. Eccles, R. Fletcher, N. Hurst, Z. Lunnon, C. Parkin, and V. Tymms (2008), Lower-crustal intrusion on the North Atlantic continental margin, *Nature*, *452*(7186), 460–464, doi:10.1038/nature06687.

White, R. S., and L. K. Smith (2009), Crustal structure of the Hatton and the conjugate east Greenland rifted volcanic continental margins, NE Atlantic, *J. Geophys. Res.*, *114*, B02,305, doi:10.1029/2008JB005856.

White, R. S., J. Fruehn, K. R. Richardson, E. Cullen, W. Kirk, J. R. Smallwood, and C. Latkiewicz (1999), Faeroes Large Aperture Research Experiment (FLARE): imaging through basalt, *Geol. Soc. London, Petrol. Geol. Conf. series*, *5*, 1243–1252.

Whitmarsh, R., J. Langford, J. Buckley, R. Bailey, and D. Blundell (1974), The crustal structure beneath Porcupine Ridge as determined by explosion seismology, *Earth Planet. Sci. Lett.*, *22*, 197–204, doi:10.1016/0012-821X(74)90082-X.

Whittaker, J., J. Halpin, S. Williams, L. Hall, R. Gardner, M. Kobler, N. Daczko, and R. Müller (2013), Tectonic Evolution and Continental Fragmentation of the Southern West Australian Margin, *The Sedimentary Basins of Western Australia IV: Proceedings of the Petroleum Exploration Society of Australia Symposium*, pp. 1–18.

Williams, S. E., J. M. Whittaker, R. Granot, and D. R. Müller (2013), Early India-Australia spreading history revealed by newly detected Mesozoic magnetic anomalies in the Perth Abyssal Plain, *J. Geophys. Res.*, *118*(7), 3275–3284, doi:10.1002/jgrb.50239.

Yang, Y. (2012), Tectonostratigraphic evolution of the northern Porcupine Basin, Irish Atlantic margin, during the Late Jurassic–Early Cretaceous, implication for a regional compressional event, *Mar. Petrol. Geol.*, *36*, 140–153, doi:10.1016/j.marpetgeo.2012.05.003.

Zelt, C. A., K. Sain, J. V. Naumenko, and D. S. Sawyer (2003), Assessment of crustal velocity models using seismic refraction and reflection tomography, *Geophys. J. Int.*, *153*(3), 609–626.

GEOLOGICAL
SURVEY OF
NORWAY

· NGU ·

Geological Survey of Norway
PO Box 6315, Sluppen
N-7491 Trondheim, Norway

Visitor address
Leiv Eirikssons vei 39
7040 Trondheim

Tel (+ 47) 73 90 40 00
E-mail ngu@ngu.no
Web www.ngu.no/en-gb/